Major Intrinsic Proteins - Structure, function, interactions

KIRSCHT, ANDREAS

2016

Document Version:
Other version

Major Intrinsic Proteins

Structure, function, interactions

Andreas Kirscht

Division of Biochemistry and Structural Biology

Department of Chemistry

Lund University, Sweden

2016

Front page: Electron densities of *At*TIP2;1. View on the selectivity filter with its histidines in the front (purple) and arginine in the back (dark blue). Three waters in the centre mark the beginning of the pore, while two waters (dark blue) can be seen behind the right histidine and under loop C – the beginning of the side pore…

Major intrinsic proteins
Structure, function, interactions

Printed in Sweden by Media-Tryck AB, Lund, 2016

Division of Biochemistry and Structural Biology
Department of Chemistry
Lund University
PO Box 124
221 00 Lund
ISBN (printed version) 978-91-7422-480-1

ISBN (digital version) 978-91-7422-481-8

Major intrinsic proteins

Structure, function, interactions

Andreas Kirscht

DOCTORAL DISSERTATION
Division of Biochemistry and Structural Biology

Lund University 2016

LUND
UNIVERSITY

by due permission of the Faculty of Science, Lund University, Sweden

To be defended at Lund University, 3rd of November 2016, 9.15 am in lecture hall C, Kemicentrum, Naturvetarvägen 14.

Faculty opponent

Prof. Dr. Eric Beitz

Organization
LUND UNIVERSITY

Department of Biochemistry and Structural Biology
Lund University
PO Box 124
221 00 Lund

Document name
DOCTORAL DISSERTATION

Date of issue
10th of October 2016

Author: Andreas Kirscht

Sponsoring organization

Title and subtitle: Major intrinsic proteins – Structure, function, interactions

Abstract

Major intrinsic proteins, also referred to as aquaporins (AQPs) are localized in membranes of all domains of life to increase the permeability to water or other small, polar molecules. Several monophyletic groups can be discerned in this large and divergent protein superfamily. Members within these subfamilies commonly show a similar substrate selectivity established by conserved filters. Comparison of structurally known selectivity filters have elucidated some of the mechanisms underlying substrate profiles. However, the physiological function of these diverse and abundant proteins can only be fully appreciated in combination with an understanding of their regulatory properties.

This work provides the first molecular view on a tonoplastic protein, *At*TIP2;1, which is situated in the membrane of the plant vacuole and permeable to water, ammonia, but not glycerol. The novel selectivity filter with a fifth residue in direct contact to substrates is compared to structures of other subfamilies to explain the present selectivity. The mechanism of permeation is investigated with mutations, stopped-flow and by growth assays. The animal AQP8s, which have similar substrate profiles, are modeled on the plant protein and their expected functions are discussed in the light of their structures. Furthermore, protein interactions and interactions with small molecules are analyzed to develop a better understanding of potential regulatory features.

Key words: Aquaporin, membrane protein, crystallography, stopped-flow, molecular dynamics, structure modeling,

Classification system and/or index terms (if any)

Supplementary bibliographical information

Language English

ISSN and key title

ISBN
978-91-7422-480-1

Recipient's notes

Number of pages

Price

Security classification

Abstract

Major intrinsic proteins, also referred to as aquaporins (AQPs), are localized in membranes of all domains of life to increase the permeability to water or other small, polar molecules. Several monophyletic groups can be discerned in this large and divergent protein superfamily. Members within these subfamilies commonly show a similar substrate selectivity established by conserved filters. Comparison of structurally known selectivity filters have elucidated some of the mechanisms underlying substrate profiles. However, the physiological function of these diverse and abundant proteins can only be fully appreciated in combination with an understanding of their regulatory properties.

This work provides the first molecular view on a tonoplastic protein, *At*TIP2;1, which is situated in the membrane of the plant vacuole and permeable to water, ammonia, but not glycerol. The novel selectivity filter with a fifth residue in direct contact to substrates is compared to structures of other subfamilies to explain the present selectivity. The mechanism of permeation is investigated with mutations, stopped-flow and by growth assays. The animal AQP8s, which have similar substrate profiles, are modeled on the plant protein and their expected functions are discussed in the light of their structures. Furthermore, protein interactions and interactions with small molecules are analyzed to develop a better understanding of potential regulatory features.

List of Publications

This doctoral thesis is compiled cumulative and includes four manuscripts, which follow an introduction to the field. In this introduction, manuscripts will be referred to by their Roman numbers (I-IV).

I. **Crystal Structure of an Ammonia-Permeable Aquaporin**
Kirscht A, Kaptan SS, Bienert GP, Chaumont F, Nissen P, de Groot BL, Kjellbom P, Gourdon P, Johanson U (2016)
PLoS Biol 14(3): e1002411. doi: 10.1371/journal.pbio.1002411

II. **Homology models of seven vertebrate AQP8s, a preview based on the structure of an ammonia permeable plant aquaporin**
Kirscht A, Sonntag Y, Johanson U
Manuscript

III. **Heterologously expressed plant aquaporins *So*PIP1;2 and *So*PIP2;1 form stable and functional heteromers**
Kirscht A, Kjellbom P, Johanson U
Manuscript

IV. **Increased Permeability of the Aquaporin *So*PIP2;1 by Mercury and Mutations in Loop A**
Kirscht A, Survery S, Kjellbom P, Johanson U
Front. Plant Sci. 7:1249 (2016) doi: 10.3389/fpls.2016.01249

Publications and manuscripts not included in this thesis:

The Aquaporin Splice Variant *Nb*XIP1;1 α Is Permeable to Boric Acid and Is Phosphorylated in the N-terminal Domain
Ampah-Korsah H, Anderberg HI, Engfors A, Kirscht A, Norden K, Kjellstrom S, Kjellbom P, Johanson U
Front. Plant Sci. 7:862 (2016) doi: 10.3389/fpls.2016.00862

Single amino acid substitutions in the selectivity filter render *Nb*XIP1;1 α aquaporin water permeable
Ampah-Korsah H, Sonntag Y, Engfors A, Kirscht A, Kjellbom P, Johanson U
Manuscript

Overexpression and purification of *Arabidopsis thaliana* NIP1;1 & NIP5;1 aquaporins
Ampah-Korsah H, Kirscht A, Engfors A., Leavy S, Kjellbom P, Johanson U
Manuscript

Contribution to the Papers

The author of this thesis, Andreas Kirscht (AK), contributed to the included papers in the following way.

I. AK performed protein overproduction, purification, stopped-flow assays, and crystallization. AK participated in conceiving and designing the study, as well as determining and analyzing the structure. AK contributed in drafting and finalizing the manuscript.

II. AK conceived the study and chose sequences and modeling methods. AK performed the modeling and constructed the hybrid structures. AK drafted the manuscript except for the validation part. AK contributed to finalize the manuscript.

III. AK contributed in designing the study. AK performed all experiments and analyzed the data. AK drafted and contributed in finalizing the manuscript.

IV. AK contributed in designing the study. AK performed stopped-flow and tryptophan fluorescence experiments. AK drafted the result section and contributed to the rest of the manuscript. AK participated in finalizing the manuscript.

Contents

Abbreviations

AQP	Aquaporin, Animal MIP
CAM	Crassulacean Acid Metabolism
GIP	GlpF-like Intrinsic Protein
GlpF	*Escherichia coli* glycerol facilitator
HIP	Hybrid Intrinsic Protein
kg	kilogram
L	Liter = 0.001 m^3
MD	Molecular Dynamics
MIP	Major Intrinsic Protein
NDI	Nephrogenic Diabetes Insipidus
NIP	Noduline 26-like Intrinsic Protein
PAGE	PolyAcrylamide Gel Electrophoresis
PDB ID	Protein Data Base IDentifier
PIP	Plasma membrane Intrinsic Protein
SDS	Sodium Dodecyl Sulfate
SIP	Small basic Intrinsic Protein
TIP	Tonoplast Intrinsic Protein
XIP	X Intrinsic Protein

Glossary

Substrate is a molecule that participates in a chemical process. In enzymology it is a reaction partner of an enzyme and converted to a product. Here the term is used interchangeable with permeate – a molecule, whose permeation through the membrane is facilitated by a certain MIP.

Aquaporins channel water through the membrane. Commonly used to group either all MIPs, all animal MIPs, or water specific animal MIPs (with or without AQP8). For clarity this term is avoided in the main body of this thesis.

Stopped-flow is an experimental set-up for measurements of relaxation kinetics. Two solutions are mixed and recordings are triggered, when a pre-defined volume is reached.

Molecular dynamics simulations calculate the movement of all molecules within narrow time-steps in a self-contained space, using a certain force field and defined molecular parameters. Can be performed unbiased or by applying an external force.

Preface

This thesis is written to attain a degree as Doctor of Philosophy. I wonder how to start it, just as I wondered why I should do research in this field. According to Plato, this is the only way to start something. Socrates says in Plato´s Theaetetus (section 155d) "For this feeling of wonder shows that you are a philosopher, since wonder is the only beginning of philosophy, …". One interpretation is that a prerequisite for knowledge is to wonder about an observation. The motivation is the interest to "look behind things", which is nowadays called curiosity. The psychologist Berlyne named four reasons to be curious [1], an emotion that is not limited to philosophers, but just human: A situation that awakes curiosity is novel, complex, uncertain or conflicting. So, to motivate you to read this thesis, I want to mention these aspects of my work; and I will start to do so right in the following introduction. Before I begin, I can assure you that there will be enough complex and conflicting results. On one of our manuscripts we got the comment that the uncertainty of findings published in this field is too high to relate our results to aspects of general interest. What the reviewer meant was that we could be wrong about how we (and other peer-reviewed papers) relate these findings, and we cannot disprove this. The reason for this uncertainty in our case, which is commonly stated, is the complexity of the field. Nevertheless, to keep my viewpoint and for curiosity reasons, I will present the bigger picture anyway, and you are asked to draw your own conclusions. It is intrinsic to science that the more is known, the more questions are uncovered. If we can construct a simple system that still answers our question, we feel safe and certain – no matter how virtual this certainty may be. I devised this thesis simple, with the aim not to stress the correctness of statements too much. How novel a piece of information is, depends on the connection to already known knowledge that is considered, or not. As this turns out to be rather subjective, I don´t dare to qualify the underlying thesis in this respect. However, my supervisors and I have been surprised on several occasions. These moments are the most fun part of research and I hope some of this will be transferred to you – enjoy reading!

Introduction

Multi-cellular organisms can be described as collections of organs containing various tissues. These tissues can be distinguished because of the intrinsic properties of their cells. And even within cells, compartments fulfill their distinct function, such as the nucleus keeping the genetic material and the mitochondria, which serve as power plants of the cell. This is achieved by their specific properties, including structure, protein content, and membrane permeability. The latter is dependent on lipid and protein composition. To modulate membrane permeabilities, cells can vary the abundance of integral membrane transporters and channels. These proteins have evolved to allow for passage of certain molecules, while others are prohibited. In case of channels this is achieved by a selectivity filter. Therefore, to be able to understand cellular function, it is fundamental to elucidate the structures of these proteins and correlate them to their function. The resolution required to analyze selectivity filters is at least at the level of amino acid residues. For novel membrane structures this is a major hurdle, as success chances are fairly low and investments are significant. Alternatively – if related structures are available – new structures can be modeled based on their similarity to already known ones. Both strategies are used to collect data, eventually summarized to a bigger picture, the physiology of a cell. However, even a certain cell has to adapt to changing environmental conditions. Therefore, the final goal is to understand the concerted action and regulation of several proteins on a metabolic pathway. This is not straight forward, as diversity and redundancy of utilized channels make conclusions rather difficult. Still, structural insights into regulation and interaction of proteins are a prerequisite for being able to modify pathways by genetic engineering (e.g. transgenic plants) or by design of drugs (e.g. medical treatment).

The proteins that have been structural and functional characterized in this thesis are expressed in plants and vertebrates and are known to facilitate the permeation of water and ammonia. Consequently, these proteins are related to water homeostasis

and nitrogen metabolism, which will be introduced in the next chapter. Water specific channels have been used to construct biomimetic membranes, suitable to produce ultra-pure water. A patent is based on results which were gathered in the progress of these doctoral studies. In plants, modifying the expression of members from this protein family has been shown to increase crop yield [2-4], growth rate [5], or resulted in more stress tolerant species [6, 7]. In animals, drugs that modulate activity or abundance of water channels have the potential to alleviate several harmful conditions, including injuries, intoxications and disease [8], albeit their development faces intrinsic hurdles [9].

The subsequent chapters prelude the attached manuscripts, starting with a wide view on the field of this thesis, which is followed by an introduction to the protein family studied. The main part will end with a short résumé of the papers and relate the findings to published literature.

Basic molecules

In biology we constantly aim to establish systems. In order to understand these systems, they are separated in parts that we try to collect as much information about as possible to describe these systems adequately. The function of a certain part is included, if it describes the system better. Thereby, function is very much dependent on the definition of a given system. In biology, the systems have a tendency to be too complex to know all the details. There are two ways out of this. One way is the phenomenological description. Here, differences in details can be pointed out that lead to a certain change – or phenotype. This is of practical use, without claiming to understand the whole system. The other way is reductionism, which means to ask simpler questions – for example "what does this do?" or "how does this look?". One can analyze a function of a single part of a larger system without knowing, if there will be enough information at the end to answer a question of physiological relevance. The present work provides insights into molecular mechanisms of water and ammonia permeability. The concluded properties of featured proteins are discussed in the light of predefined systems including water homeostasis and nitrogen metabolism in cells. Due to the fundamental nature of the research, no experimental evidence regarding physiological relevance is provided. Nevertheless, the opportunity is given to briefly summarize which cellular functionality this work touches upon.

2.1. Water as solvent of life

Lawrence Henderson elaborated on the properties of water and its importance for the inhabitability of earth [10]. Regardless if life is possible in an alternative solvent, water is for many reasons fundamental to life on earth. On a global scale, water pleases with its great abundance on the surface, its heat capacity, ice density, melting- and evaporation point, to name a few. Thereby water has a tremendous impact on the climate and continuously provides a suitable solvent for chemical reactions. The physical properties of water underlying these features are its polarity, its dissociation constant and the unique hydrogen bond density in its liquid phase. The strong

interactions provided by hydrogen bonds even throughout liquid water leads to cohesion and counters the enthalpy of protein internal hydrogen bonds. This compensation allows for flexible proteins, which are able to rearrange during folding and to change their conformation.

Because of the polar – or hydrophilic – nature of water, cells and compartments are separated from the environment by hydrophobic membranes. This insulation results in intrinsically low exchange rates for polar molecules, some of which are necessary for cellular function. In the 1950s it was suspected that cells need to facilitate the permeation of water to adapt to osmolarity changes in the environment [11]. Most cells contain a lot of water and are dependent on preserving a minimum content. Multicellular organisms have developed a variety of solutions to cope with changing conditions. Plants and animals have ways to transport aqueous solutions and have measures to reduce loss of water, but their tissues and cell properties vary enough to justify a separate introduction.

2.1.1. Water cycle in terrestrial plants

Plants can be schematically separated in roots and shoot. While roots take up water and ions, the shoot utilizes green cells for photosynthesis, oxidizing water to build sugars from CO_2. Synthesized sugars (assimilates) are transported from the green plant cells to other areas of the plant (e.g. roots) through living cells comprising the tissue phloem. Water is taken up by the roots and is, together with nutrients, transported passively, vertically via the xylem. In wooden plants the exterior of cells in this tissue can be strongly lignified. In tree stems this is so pronounced that this dead cells form stiff capillaries. The pressure for the transport is partially achieved by transpiration of the leaves, which creates a tension in the capillary xylem vessels, due to the cohesive properties of water (the cohesion-tension-theory [12] reviewed in [13]). The surface area of the leaves available for evaporation is increased by spongy mesophyl cells. Gas exchange through closable openings (stomata), which are situated in the lower epidermis of leaves. A stoma is formed by a pair of specialized guard cells – in plants with two embryonic leaves (dicotyledons) these are kidney bean shaped cells with a heterogeneous cell wall (Figure 1). Stoma opening is achieved by pumping potassium from neighboring cells into the vacuole to create inward-directed water potential. Osmotic driven water potential can be measured as internal pressure,

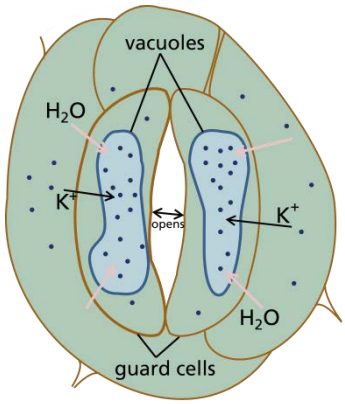

Figure 1: Stoma opening. Potassium is pumped into the vacuoles of guard cells. Increasing turgor pressure results in bending of the asymmetrical build cells.

called turgor. Because of the heterogeneity of the guard cell walls, increasing turgor bends these, which leads to opening of the stoma. The vacuolar membrane (tonoplast) is about 100 times more permeable to water than the plasma membrane [14]. This is achievd by a dense display of highly water permeable proteins belonging to the tonoplast intrinsic proteins (TIPs; one isoform of this subfamily is characterized in **paper I**). Uncontrolled water loss is reduced by a hydrophobic coating of the leave surface (cuticula), so much of the water that is lost evaporates through stomata; despite these losses, stomatal gas exchange during the day is necessary to increase photosynthetic efficiency by uptake of CO_2. It is commonly found that C_3 plants lose up to 700-1300 mol water per mol of assimilated CO_2 ([15], chapter 8.1). C_4 plants reduce this loss by a factor of 2 ([15], chapter 8.4) through higher compartmentalization of the processes and local enrichment of CO_2. As effective adaptation to arid environments, CAM plants separate gas exchange and photosynthesis even in time: CO_2 is taken up at night and stored as carbonic acids until utilization in sugar synthesis during the day. The efficient regulation of stomata function is of particular importance under water shortage conditions, as increased tension in the xylem can lead to air seeding (cavitation) followed by vessel dysfunction (embolism). Additional to prevention of drying, xylem refilling from the roots is necessary. In addition to transpiration, some plants can supply the shoot with water by actively transporting ions over root membranes, creating a so-called root pressure. The way water is taken up by the root and transported through different tissues before it evaporates from a leave requires a complex regulation of water permeabilities. Lateral transport of water in a plant is realized in three ways. Water can move hydraulically outside the cells in the cell walls and through the xylem, which is called the apoplastic pathway. Transcellular flow of water is selectively facilitated by MIPs and driven by osmotic pressure. When water has entered the cell, it can be routed to neighboring cells via plasmodesmata, which are connections of the cytoplasms. On this symplastic pathway no further permeation of hydrophobic membranes is needed. Dependent on plant anatomy, water use these

pathways to reach the vascular tissue, containing the xylem, which is surrounded by an endodermis. The spaces between endodermal cells have deposits of the hydrophobic substance suberine, which assemble the Casparian strip, preventing water to leave the central cylinder by an uncontrolled apoplastic pathway. As water has to permeate inner and outer cell membrane to cross this hydrophobic barrier, the flux can be regulated. This is done by controlling the abundance and activity of plasma membrane localized MIPs. Some regulatory properties of two protein isoforms belonging to this protein family are studied in **paper III** and **IV**.

Osmotic pressure can be used for more than to open and close stomata. Some plants – like *Samanea saman* – can regulate the turgor in specialized motor cells to lift leaves and leaflets [16]. Likewise in *Mimosa pudica*, TIP- facilitated water flux through the tonoplast, resulting in rapid turgor loss, participates in motor cell function [17]. Leaf movements in tobacco involve fast cell elongation, a process that was shown to depend on a water channel, a PIP1 situated in the plasma membrane [18].

2.1.2. Osmoregulation in vertebrates

Dynamic stability of biological systems is a fundamental concept summarized under the term of homeostasis. All organisms must maintain solute concentrations within species-typical boundaries in order to function. To be able to survive greater environmental fluctuations, animals have developed numerous compensatory mechanisms. All mechanisms are more or less dependent on water content and thereby on transport properties through the membrane. Osmoregulation and nitrogen excretion are two examples of compensatory processes in animals that will be further described.

Loss of water is a major challenge for most terrestrial animals. Water loss can be due to evaporation as well as excretion of water together with excessive ions and nitrogen compounds. In vertebrates homeostasis is controlled to a large extend by the kidneys. In order to detoxify extracellular fluid, the blood passes the kidneys through the renal arteries. To decrease water loss during excretion, blood is filtered in several steps established by specialized compartments of the nephrons. In the first step, filtration takes place in the renal corpuscle, separating plasma from cells and proteins. The filtrate entering the Bowman´s capsule results in highly concentrated urine which will exit the body. It demonstrates an efficient reabsorption of water together with ions,

glucose, and proteins. Water reflux is enhanced by the countercurrent organization of the tubules employing a variety of semi-permeable membranes, which enable passive and active transport. Reabsorption of water in the collecting duct is positively regulated by the antidiuretic hormone vasopressin that is released in the hyperthalamus. After separating toxic compounds from the blood, the highly salt-concentrated and nitrogenous solution exits the body.

Most vertebrates are osmoregulators, keeping their internal osmotic concentration constant. Fish have developed measures to cope with osmotic gradients in addition to regulating their excretion. Atlantic salmon for example, also inhabiting freshwater, can take up salts from the dilute environment over the gills [19]. A reversed ion flow is actively achieved in seawater fish [20, 21], accompanied by an adapted water permeability through the apical membrane of epithelial cells [22, 23]. Additionally, the glomerular filtration rate is lowered to reduce water loss to the hypertonic environment [24].

2.2. Nitrogen metabolism

Nitrogen is an essential element for biological macromolecules, such as proteins and nucleic acids. Atmospheric nitrogen is mainly found in its biological inactive form N_2. For nitrogen being utilized in organic reactions, the triple bond of N_2 must be reduced. The natural process is termed nitrogen fixation, and it is achieved by diazotrophic prokaryotes that commonly live in symbiosis with plants, such as *Fabacaeae* or *Azolla*. Nitrogen is fixated as ammonia. Additionally, about 10^{11} kg of ammonia per year is synthesized by the Harber-Bosch process. This energy demanding process consumes ca. 1.1% of the global energy (Swaminathan and Sukalac (2004) cited in [25]). Most of the ammonia that is synthesized out of atmospheric nitrogen by the Harber-Bosch process is utilized in fertilizers, fostering agricultural output. The way synthetic and natural nitrogen fertilizers are used cause severe environmental problems [26]. Water quality, air quality, soil quality, greenhouse balance, ecosystems and biodiversity; these are the five key societal threats identified by the European Nitrogen Assessment (ENA) [27]. Accordingly, nitrogen usage affects nature and our way of living.

2.2.1. Nitrogen usage in plants

In plants, ammonia is further converted to nitrite and nitrate, all three molecules serving as a nitrogen source for plants. Nitrogen taken up as ammonia by the roots, needs to be distributed throughout the whole plant. Nitrate as an ion can be stored efficiently and serves the plant as a long term nitrogen pool. Nitrate can be reduced by nitrate reductase and further by nitrite reductase to ammonia. But ammonia is usually not translocated to the shoot.

$$\text{ATP} + \text{L-glutamate} + \text{NH}_3 \longleftrightarrow \text{ADP} + \text{P}_i + \text{L-glutamine}$$

$$2\ \text{L-glutamate} + \text{NAD}^+ \longleftrightarrow \text{L-glutamine} + \text{2-oxoglutarate} + \text{NADH} + \text{H}^+$$

Instead, glutamate-ammonia ligase (GS) attaches ammonia to glutamate and, in cycle with glutamate synthase (GOGAT), 2-oxoglutarate is utilized to build up a glutamate pool. Glutamate further serves as base for the synthesis of various amino acids and the treatment of plant roots with ammonia upregulates GOGAT in rice seedlings [28].

Ammonia with a pK_a of 9.25 mainly occurs as ammonium ions in the cell. While ammonia can permeate the plasma membrane fairly easy, ammonium cannot. Ammonia flux across the plasma membrane is further enhanced by proteins belonging to the family of ammonium transporters (Amt). The relatively high pK_a of ammonia and the high permeability of ammonia result in two distinct problems. As most of the ammonia molecules that are taken up from the outside is protonated in the cytosol, they alkalize the internal milieu. This may be the reason why ammonia concentration in the cell is always kept low, although it serves as a fundamental chemical group for the synthesis of biomolecules. In fact, most plants show growth defects if their roots are challenged by ammonia concentrations of > 0.1 mM [29]. While rice, being dependent on ammonia as a nitrogen source during soil flooding, can tolerate higher concentrations of ammonia, barley is negatively affected, potentially caused by energy demanding excretion of ammonia leading to futile cycling [30]. This problem is acute, when a lot of ammonia is taken up by the roots. Another ammonia related problem involves the movement out from the plant. Ammonia concentration in the atmosphere varies between 1 and 20 nmol per mol air. As the partial pressure of ammonia in the cytosol of leaves is typically higher, nitrogen loss of agricultural fields to the atmosphere can be up to 70 kg per km^2 and

season [31]. If ammonia enters a cell, it can be converted by GS or permeate further. At atmospheric ammonia concentrations below a rarely reached limit (compensation point), there is a net loss by ammonia permeating outer membranes [32]. At higher concentrations ammonia can be uptaken by leafs [33]. As for water, the kinetics of this can be lowered by minimizing the surface and coating epidermal cells. However, it is a potential leakage, where gas needs to be exchanged, such as for the stomatal uptake of CO_2 for photosynthetic carbon fixation. Both problems can be reduced by utilizing a compartment that can take up ammonia in a comparable speed or even faster than the plasma membrane. If ammonia permeation is not actively driven, the pure permeation into another compartment would not help, as the diffusion back is just as fast. The compartment needs be able to accumulate ammonia, and the fastest way of conversion is its protonation to ammonium. The conversion to other molecules, such as nitrate or glutamate, is feasible, but happens on a different time scale. Both accumulation and protonation of ammonia is achieved, if the pH in the compartment is lower than in the cytosol. This requires a highly buffered milieu, preferably insensitive to higher ammonium concentrations. Fortunately, such a compartment is available in higher plants – the vacuole. The central vacuole is the compartment that can fill out up to 95% of the intracellular volume. Additionally, its internal pH is stabilized by proton pumps to 5.5 and its membrane – the tonoplast – potentially has a larger surface than the plasma membrane. To improve the permeability to ammonia even further, an ammonia permeable MIP is present in the tonoplast. This integral membrane protein is in high abundance in the vacuolar membrane named tonoplast intrinsic protein (TIP) [34].

In summary, nitrogen is taken up by the roots, mainly as ammonia or nitrate. While the latter can be stored or translocated, ammonia is processed before further distribution throughout the plant. Plants have evolved in various ways to utilize different nitrogen sources and to be able to compartmentalize their nitrogen-containing compounds (reviewed in [35]).

2.2.2. Nitrogen metabolism in animals

Animals take up nitrogen mainly in the form of proteins. The available 21 amino acids, which are used to synthesize proteins, can alternatively be oxidized to urea and CO_2. Most amino acids in human cells are taken up with food. The pancreas releases

proteases and peptidases, which digest proteins to amino acids in the intestines. Amino acids and small peptides can leave the intestines by channels and transporters. The necessary gradient for various Na^+-dependent amino acid transporters is sustained by ATP driven Na^+/K^+ antiporters. The amino acids are distributed throughout the body via the blood stream. Thereby, nitrogen compounds cycle between liver, kidney and peripheral tissues (e.g. skeletal muscles). Skeletal muscles with a high energy demand produce pyruvate by glycolysis. Then, the amino group from glutamate is transferred to pyruvate by alanine transaminase, producing alanine and α-ketoglutarate. Alanine is transported to the liver, thereby removing excessive amino acids from the muscle cells. Alanine is converted back in the liver by gluconeogenesis. The product glucose is transported to the muscle cells, thus closing the so-called glucose-alanine cycle.

Ammonia is the direct product of the oxidation of amino acids. Ammonia accumulates therefore under conditions, where protein degradation is enhanced or amino acids are used as energy source (during fastening). Despite the central metabolic role of ammonia, concentrations in the blood serum are as low as 20-40 µM. Elevated concentrations above 0.4 mM are toxic to cells, increasing intracellular pH and thereby causing alkalosis. As a result, a disturbance of ammonia conversion leads to an accumulation of ammonia in the blood, which has been connected to hepatic encephalopathy [36]. This emphasizes the importance of ammonia removal from the cytosol. In case of neurons, fast help comes from astrocytes, which can take up excessive ammonia and glutamate [37]. In the brain, GS plays a major role in the regulation of glutamate concentrations and thereby ammonia detoxification. Further, how is excessive nitrogen removed from an organism? In animals, 80% is excreted as urea, which is produced in the liver. In this process, named the urea cycle, two ammonia molecules are attached to ornithine. Notably, while one ammonia molecule enters the cycle in the mitochondrion, the second ammonia group comes from aspartate, situated in the cytoplasm. Therefore, the efficiency of urea production is dependent on the mitochondrial ammonia concentration. One source of ammonium is glutamate, which is converted to α-ketoglutarate by glutamate dehydrogenase (GDH) in the mitochondrial matrix. As a consequence, internal ammonia concentration and therefore urea production is influenced by the permeability of the inner mitochondrial membrane. This

permeability is dependent on the abundance of ammonia permeable proteins [38, 39] such as AQP8. The mechanism of this facilitation has not been described yet, due to the lack of structural information. Therefore, several vertebrate AQP8s were modeled in **paper II**.

In ureotelic organisms, which include vertebrates except for *Diapsida,* urea is removed from the blood by the kidney (see chapter 2.1.2). In contrast, all living *Sauropsida* but turtles, together with terrestrial arthropods are uricotelic and excrete uric acid, which requires only a fraction of the water to excrete. Most aquatic animals use their liquid habitat to alternatively directly excrete ammonia to the environment (ammoniotelic). In freshwater fish, the kidney even dilutes the urine for excretion. These animals mainly utilize the gills to release excessive nitrogen [40].

Major Intrinsic Proteins

Major Intrinsic proteins (MIPs) form a large superfamily of integral membrane proteins named after their first recognized members dominating certain biological membranes. The founding member of this superfamily was identified in the extraction of bovine eye lenses (MIP1 later renamed AQP0) [41]. MIPs are found in various membranes, where they facilitate the passive diffusion of small polar molecules, such as water and ammonia, over the lipid bilayer.

This chapter gives an overview over this superfamily; a phylogenetic background is necessary in order to introduce some subfamilies as foundation for the later discussed functional properties. The chapter is separating phylogeny, structure, and function rather than the more common presentation of various subfamilies for easier indication of certain differences between various isoforms.

3.1. Phylogeny

MIPs are commonly found in all domains of life (archaea, bacteria and eukaryota) [42-44]. This indicates their ancient origin dating about 2.5 to 3 billion years ago [42, 43]. Proteins of this superfamily have diverged and today form several distinct monophyletic groups (Figure 2). Thirteen major groups have been discerned, but their phylogeny stays unresolved [45]. Members of some subfamilies can be related by primary amino acid sequence similarity, such as “super aquaporins” from plants and animals, whereas for other clusters, which share similar function, it is more difficult to find support for a merge based on sequence similarity, e.g. plant TIPs and animal AQP8s or plant PIPs and so-called “true aquaporins” from animals. Members of a subfamily share a high degree of conservation i.e., amino acid identity. After more and more genome sequences have become available, phylogenetic trees of MIPs have been built for several species. The human genome codes for 13 MIPs (AQP0 – AQP12), belonging to four different groups. Six human isoforms group together as

"true aquaporins" and are known to be specifically permeable to water, four are glycerol-facilitator-like proteins (GLPs), one is AQP8 and two cluster as "super-aquaporins". This name reflects the great phylogenetic distance of its family members to other MIPs [46], not only in animals, but also in plants. Plant MIPs are more diverged, presenting seven monopheletic groups in land plants, but not all groups are found in higher plants. Generally, seed plants have fewer MIP families, but express many more isoforms. Whole-genome analysis identified 35 MIPs in *Arabidopsis thaliana* [47], 33 in rice [48], 47 in tomato [3, 49], and 31 in maize [50]. Utilizing the information of structural conserved features allowed the identification of more subfamilies in mosses [51] and algae [52]. To standardize the nomenclature of plant MIPs, all subfamilies are abbreviated by three letters, the last two being always "IP" for intrinsic proteins. Most subfamilies can then be divided further into distinct monophyletic groups, which are marked by a digit following the three letter family abbreviation. Members of a certain subgroup are then numbered, with a second digit separated by a semicolon. The subfamily of plant plasma membrane intrinsic proteins (PIPs) is highly conserved and forms two distinct groups [53], which can be found as early as in bryophytes [51] and remained separated throughout higher land plants. While earlier plants are commonly found to present many MIP subfamilies, higher land plants in general evolved more isoforms but maintained less subfamilies. This could be interpreted as adaptation to the number of tissues and developmental stages, each requiring a certain expression pattern. Of the plant MIP subfamilies comprising many isoforms, Nodulin-26-like intrinsic proteins (NIPs) [54] present the most diverged subfamily. In Arabidopsis seven NIP groups are present, but this separation is only applicable when comparing closely related plant species. Employing a less stringent grouping introduced for rice and maize allows clustering NIPs of distant plant species. Within another subfamily of Arabidopsis MIPs – the tonoplast intrinsic proteins (TIPs) – five groups can be distinguished [47]. From these groups TIP1s and TIP3s are closer related than the rest, but show distinct structural differences, which are addressed in chapter 4.2. Overall, the TIP subfamily is less diverse than NIPs, but not as homogeneous as PIPs. Hybrid intrinsic proteins (HIPs) have their name from sharing similarities with PIPs and TIPs. The small and basic intrinsic protein family (SIPs) cluster together with AQP11 and AQP12 from animals and has the largest phylogenetic distance to the rest of the superfamily – presenting unusual NPA motifs and uncommon selectivity filters. These "super aquaporin" are even more separated

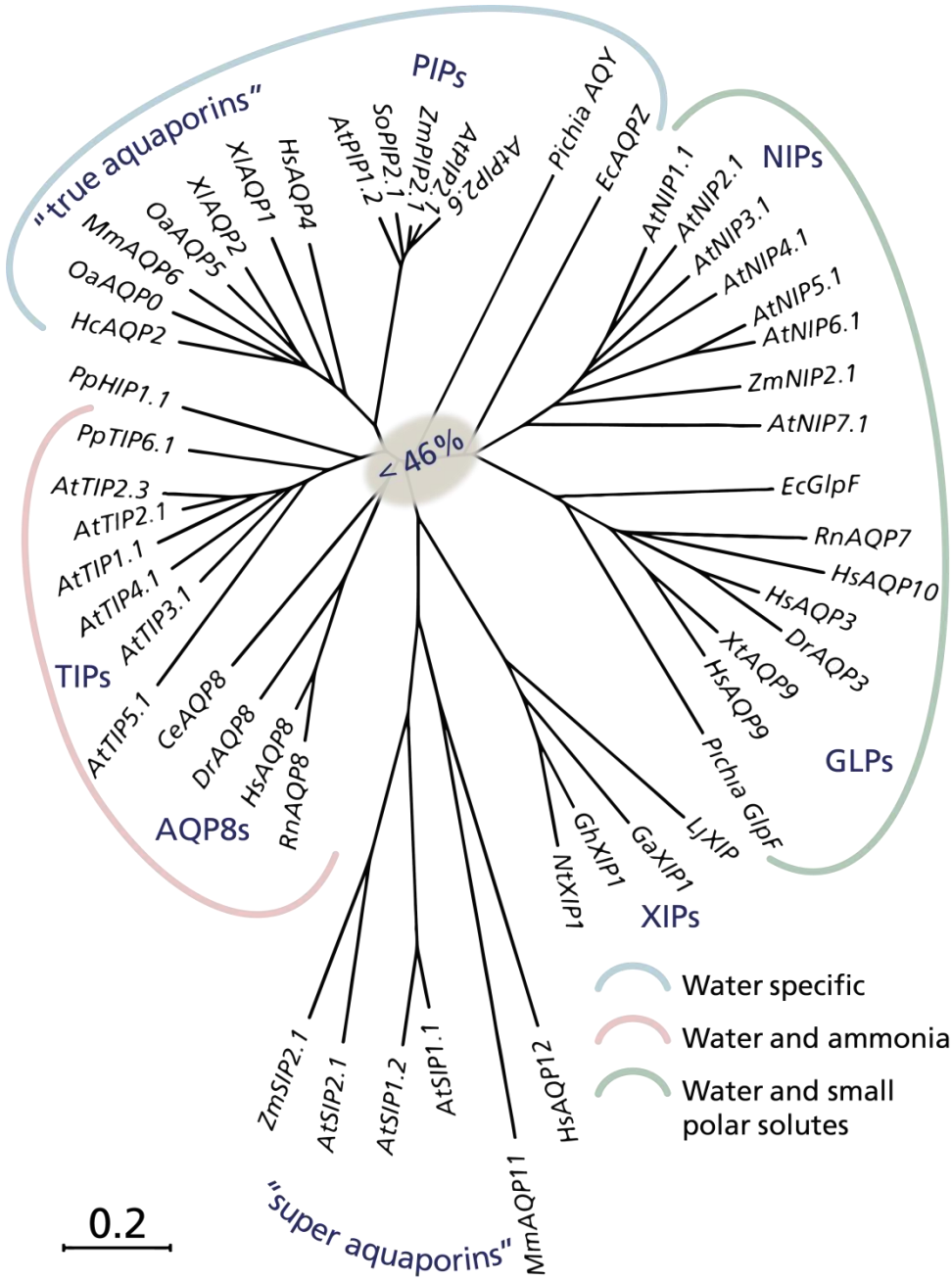

Figure 2: Phylogenetic tree of Major intrinsic proteins. 52 representative MIPs were selected to construct this neighbor-joining tree, which excludes algal and archaeal proteins. The legend informs about the substrate profiles. Gray shading is used to hide uncertain clustering, determined by bootstrap method.

than X intrinsic proteins (XIPs), where X stands for unknown function and localization. XIPs have a relatively low similarity to other MIPs (about 30% amino acid identity), are common in dicots and early land plants, but are missing in monocots and Arabidopsis [51], which is why they have been less investigated yet. GlpF-like intrinsic proteins (GIPs) have only been detected in mosses and group together with GLPs from animals [55]. In algae seven subfamilies were found [52], of which two – PIPs and GIPs – are known from higher plants, five subfamilies cannot be joined with other MIP subfamilies and are therefore termed MIPA to MIPE. Finding PIPs and GIPs in algae suggests that these subfamilies have emerged before the evolution of terrestrial plants.

3.2. Function

MIPs are channels, facilitating passive diffusion of water and small uncharged, polar solutes. Thereby MIPs accelerate the equilibration of their specific substrates over the membrane. Dependent on the compound and its gradient, this leads to faster replenishing, dilution or change of physical cell parameters. The physiological relevance for a given function is dependent on MIP expression levels, localization and regulation of the protein. This will be summarized in chapter 5. Many reported functions of MIPs have been difficult to prove by phenotyping, which may be caused by redundant expression, an intrinsically high permeability of the membranes to some compounds, and – above all – the ability of organisms to adapt to new situations. This chapter focuses on permeability rates reported for natural occurring substrates.

All tested MIPs have in common that they exclude protons from permeating. This is important, as organisms sustain a proton gradient over most of their membranes. Leakage of protons would diminish this gradient and result in energy loss. Overall, members of this superfamily channel water and small polar solutes, while permeability rates to certain substrates can vary a lot between different isoforms. Due to the high conservation within MIP subfamiles, substrate specificity can be addressed to specific subfamilies and even groups. The plant subfamily of PIPs and some animal AQPs (AQP0, 1, 2, 4, 5, and 6) are referred to as water specific, as their substrate profiles do not include much more than water. Despite the high degree of conservation among isoforms of the same subfamily and within groups, they seem to fulfill various functions in cells. While PIP2s have proven to be good water channels

[56] (**paper III and IV**), oocytes expressing PIP1s displayed a much lower permeability rate. The difference in membrane conductivity might originate from different targeting to the oocyte cell membrane [57]. In addition to water, PIPs have been reported to conduct CO_2 [2, 58, 59] and hydrogen peroxide [60-62]. TIPs and AQP8s are not only excellent water channels, but have also been shown to facilitate the permeation of ammonia [39, 63, 64] (**paper I**), urea [65, 66], and even glycerol [67, 68]. Furthermore, two TIP1s and human AQP8 were reported to permeate H_2O_2 [60]. Among structurally described MIPs, GLPs have the widest pore [69] (Figure 6). A member from *Escherichia coli* (GlpF) was known to transport glycerol [70] decades before the identification of the MIP superfamily. GLPs are known to be permeable to water and urea. Additionally, GlpF [71] as well as AQP7 and AQP9 [72, 73]were reported to conduct arsenic and antimony compounds. Some of the MIP subfamilies still await functional investigation. The subfamily of XIPs, which can be found in mosses and higher plants, is one of these. However, other metalloids – namely boron and silicon – have been added to the list of substrates permeating NIPs [74-76]. Interestingly, one of the NIPs has been shown to channel larger molecules such as urea and glycerol, but not to increase water permeability when localized to the *Xenopus laevis* oocytes membrane [77]. It will be very exciting to analyze the structural basis for this phenomenon. What is known about the mechanisms of substrate specificity is addressed in the next chapters.

3.3. Structure

More than 50 released structures of MIPs can be found in the protein databank RCSB (**paper II**). Table 1 lists examples of MIP structures. Only the structure with the highest resolution is referred to if several are available belonging to the same protein. Remarkably, while most of the proteins for which structures are available can be found multiple times in the database, referring to different isoforms or mutants, only a few groups are represented. Most of the structures describe water specific MIPs. The comparison of these with the structures available for GLPs dominated the field for a long time. The separation of MIPs in just two groups – aquaporins and aquaglyceroporins is still common. The publication of an archaeal AqpM placed the structure in-between these two groups. Retrospectively, after a TIP- structure is available, *Mm*AqpM can be viewed as a protein, sharing water specific MIP, GLP and TIP features, which will be pointed out in chapter 4.1.

Table 1: Selected 3d structures of Major Intrinsic Proteins.

Protein	Res.	Reference	PDB ID	Selectivity	Remark
*Bt*AQP0	2.2	[78]	1YMG	Water specific	1
*Bt*AQP1	2.2	[79]	1J4N	Water specific	1
*Hs*AQP2	2.75	[80]	4NEF	Water specific	
*Hs*AQP4	1.8	[81]	3GD8	Water specific	1, 2
*Hs*AQP5	2.0	[82]	3D9S	Water specific	
*So*PIP2;1	2.1	[83]	1Z98	Water specific	1, 2, 3
*Pp*AQY1	0.88	[84]	3ZOJ	Water specific	2, 3, 4
*Ec*AqpZ	2.5	[85]	1RC2	Water specific	1, 2, 3
*Ec*GlpF	2.2	[69]	1FX8	GLP	2
*Pf*AQP	2.05	[86]	3CO2	GLP	
*Mm*AqpM	1.68	[87]	2F2B	AqpM	1
*At*TIP2;1	1.18	**paper I**	5I32	Water + ammonia	

1 Structures from other organisms or at lower resolution available

2 Structures with mutations available

3 Structures at different pH or with ligands available

4 Pore blocked by Y31

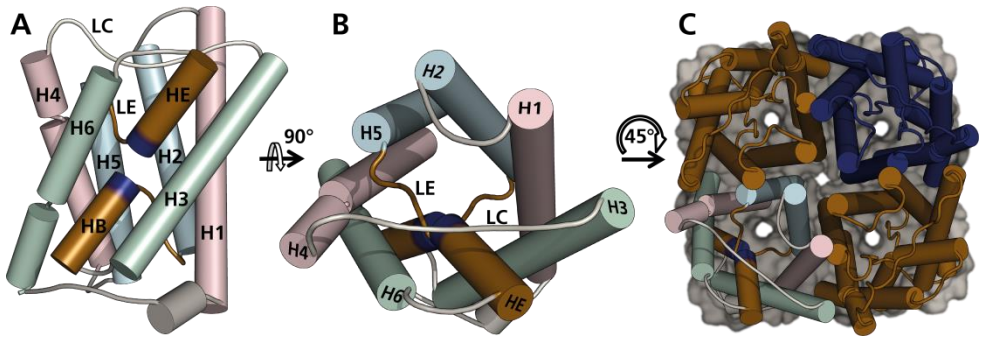

Figure 3: Stuctural overview of MIPs. A *At*TIP2;1 monomer is shown in side view. The colors represent equivalent helices that result from a direct repeat in the sequence. This repeat results in a pseudo 2-fold symmetry. **B** Topview of A (non-cytosolic side). **C** MIPs are found as tetramers.

All structures were solved as homotetramers (**paper I**), where each monomer comprises a functional unit. The major contribution to the energy of intermonomeric

binding comes from hydrophobic interactions at their interfaces. As a result, some proteins of this superfamily are not resolved completely as monomer when separated by SDS PAGE [88-93]. This can be used to reveal the strength of interactions between different monomers (**paper III**). For *At*TIP2;1 the binding strength is so high that the tetramer is the main (virtually only) band on an SDS polyacrylamide gel (Figure 4). This is in line with the unusually high temperature stability, which was measured to be 86°C, even when solubilized in detergent (a nonyl glucoside). From a physical point of view it is interesting to note that the high temperature stability correlates with SDS resistance. This indicates a correlation of intermonomeric interactions within oligomers and thermal stability of each monomer. This is supported by observations on unfolding of GlpF, which disassembles into monomers before further unfolding [94]. To achieve these strong interactions, MIPs must have evolved in such a way that their interfaces are complementary to each other. This gives rise for co-evolution of certain residues, which slows down the change, as several mutations must occur simultaneously and match each other. This becomes even less likely for heteromeric interactions, which influence the selection of different gene products, hence constraining certain parts of the proteins and conserving their sequence. The details of interactions between mostly hydrophobic residues at the interfaces can be seen in crystal structures with atomic resolution (< 2 Å). However, when modeling structures as monomers, refined rotamers of interface residues are solely based on the interaction within their own monomer, of course. It can be challenging to match their conformation after assembling a tetramer, which is dependent on the difference between the initial and the final position (**paper II**). The assembly is using a 4-fold symmetry commonly found for MIP structures. This assumption may be right, considering the homogenous nature of a homotetramer, but excludes – in crystal structures and models – the possibility of pair wise interactions. Such interactions were suggested for cysteines of neighboring monomers [95], stabilizing the tetramer. Further experiments revealed that these cysteines form disulfide bridges, which can be broken by reducing agents, changing their oligomerization pattern on an SDS gel ([96], **paper IV**). Compared to other subfamilies, the high degree of conservation in both PIP groups is suggesting a functional role, which remains puzzling, as the function is carried out by each monomer. This is further discussed in chapter 5.2 and **paper III**.

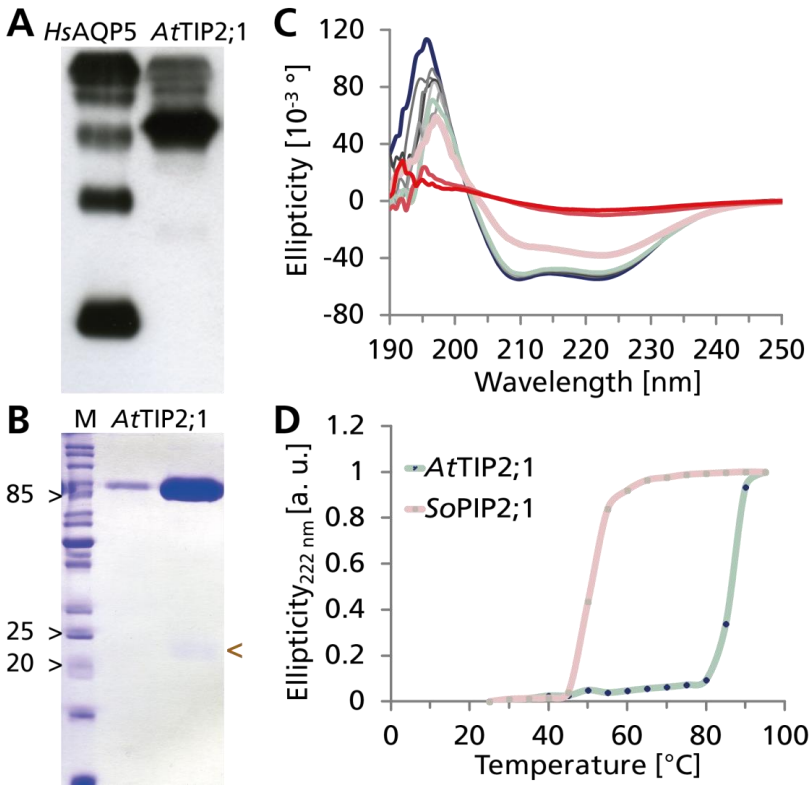

Figure 4: Stability of *At*TIP2;1. A and **B** show the extraordinary SDS stability of MIPs. **A** Western blot displays human AQP5 presenting not only monomers, but various oligomers. The main band of *At*TIP2;1 is the tetramer running fast at around 90 kDa. This becomes clearer in an SDS PAGE (**B**), where a large amount of purified protein is loaded on the right lane and only a small fraction separates as monomer (brown arrow). **C** and **D** demonstrate the high temperature stability of MIPs in detergent solution. **C** Circular dichroism is used to observe unfolding of the helices depending on temperature. Denaturation plot in **D** yields a melting temperature of 51°C for *So*PIP2;1 and 86°C for *At*TIP2;1.

The pore in monomers is formed by six membrane spanning helices (H1 – H6) connected by five loops (LA – LE). Both, C- and N-terminus, are on the cytosolic side. In some isoforms the termini are known to participate in the regulation of membrane trafficking and permeability (see chapter 5). Depending on the isoform, loop A is found in various lengths and has been seen in crystal structures to fold over neighboring monomers, which may contribute to tetrameric stability. The longest loop, loop C, connects H3 and H4 on the non-cytosolic side. The beginning of this loop is less conserved, and some longer versions form short helices. One residue of

this loop is located close to the pore (see chapter 5), and carbonyl groups before this position contribute to keep the loop close to the helices. The C terminal part of loop C is structurally more conserved and forms a small peripheral loop. The length of loop D is also variable between subfamilies, and structures of *So*PIP2;1 presented this loop in different conformations, which is further described in chapter 5. Two of the loops (loop B on the cytosolic side and loop E on the opposing side) fold half way through the membrane and form shorter helices (HB and HE) on their way back. The N-terminal ends of these helices, pointing towards each other in the center of the membrane, each possess a conserved amino acid motif, the NPA box [97]. This focuses the positive partial charge of the macro dipoles formed by the helices on the amide group of asparagine, which leads to electrostatic repulsion of protons [98-100]. The positive charge re-orients dipolar molecules like water [101] and ammonia (video of **paper I**) close to the pore-center, which was formerly believed to prevent a potential proton transfer via a Grotthuss mechanism [102]. The bipolar orientation of water can be excluded as a major contribution to the energy barrier for protons (elaborated in [103]). Instead, the NPA boxes have been shown to be the place of cation exclusion [104] and [105]. The diameter of the pore is such that seven to eight water molecules can be seen as single file in static structures. Permeating water molecules are hydrogen bonded to carbonyls from loop B and loop E and to asparagines from NPA boxes lining the pore (Figure 5). Thereby the carbonyls compensate the polar substrates for the loss of hydrogen bonds to bulk waters (**paper I**). Additionally, pore waters in crystallographic structures orient in such a way to hydrogen bond to each other, as the rest of the pore is lined with hydrophobic residues. Both ends of the pore widen to the surface, forming vestibules and resembling the pore roughly in a shape of an hour glass [97]. Underneath the vestibule on the non-cytosolic side the narrowest part of the pore is situated, at least in all solved structures except *At*TIP2;1 (**paper I**). As it comprises the highest energy barrier for solutes, it has a major impact

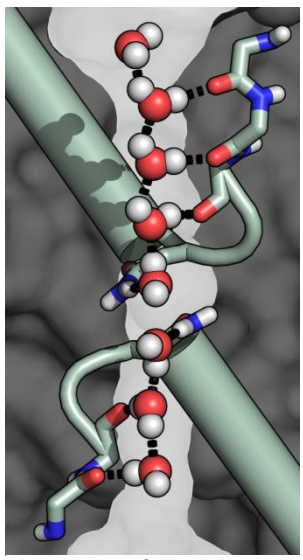

Figure 5: Schematic pore representation. Helixes B and E form dipoles with the positive ends at the asparagines of the NPA boxes. This orients waters in the pore. Carbonyls lining the pore serve as hydrogen bond (black dashes) acceptors.

on the permeability. In some isoforms the energy barrier for a substrate molecule to pass is significantly lower than for the native membrane, while in other isoforms the thresholds in these regions for the same molecule are so high that permeation can be practically excluded. Therefore, only this region – 5 Å long and approximately 7.5 Å away from the pore center – is here termed selectivity filter. The name aromatic arginine filter, which has been commonly used (**paper I**), is avoided in order to be valid also for isoforms that do not have an arginine at this position. As this region defines the substrate profile, participating residues are functionally constrained and widely conserved within the subfamilies (**paper I** and **II**). Therefore, many subfamilies can be functionally categorized based on the amino acid residues defining the selectivity filter. The next chapter attempts to introduce these categories.

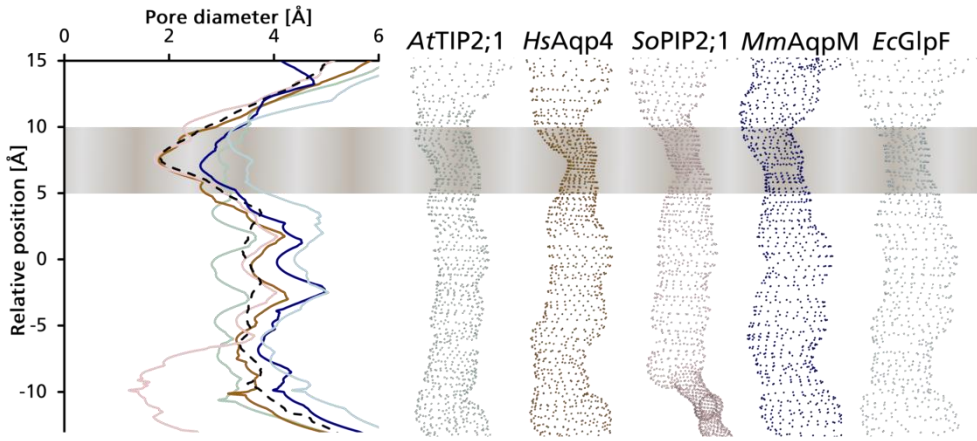

Figure 6: Pore diameters determined with HOLE [106]. Graph displays diameters of largest possible spheres along the pore. Curves colored as dotted representation of the circumferences of these spheres. Dashed line presents an average diameter of water specific pores. Gray shaded area marks the selectivity filter. The constriction is not as pronounced in *At*TIP2;1. Channels permeable to glycerol present an overall wider pore, while *At*TIP2;1 is more narrow than other MIPs around the NPA box (relative position 0 Å).

Selectivity filter

Before high resolution structural information about MIPs was available, five positions (P1 – P5) in sequence alignments where meant to be responsible for selectivity, as the corresponding amino acid residues clustered with known substrate specificities [107]. After the structures of *Hs*AQP1 and *Ec*GlpF had been solved, it became clear that these residues would not directly interact with molecules in the pore.

As the name suggests, the selectivity filter in MIPs is the region in the pore that defines the substrate specificity (summarized in [108]). It generally establishes the highest energy barrier for permeating molecules, thereby limits their flow rate and has evolved to efficiently exclude protons from permeation [109]. The functional constrains of preventing certain molecules to permeate, while maximizing the facilitation of others, results in evolutionary conservation. This connects structural features to the substrate specificity conserved in subfamilies and groups of MIPs. This chapter defines features of the selectivity filter in structurally known MIPs by pointing out participating amino acid residues and their interactions. The filter comprises five positions which are named according to their location in their secondary structures. All described selectivity filters include amino acid residues, which interact directly with substrates in helix 2 ($H2^{p}$), helix 5 ($H5^{p}$), and helix E (HE^{p}). Additionally, one carbonyl positioned in loop E (LE^{p}) serves as hydrogen bond acceptor. A fifth amino acid residue situated in loop C (LC^{p}) has an intrinsic effect on the permeability, although not interacting with substrates in all isoforms (**paper I**).

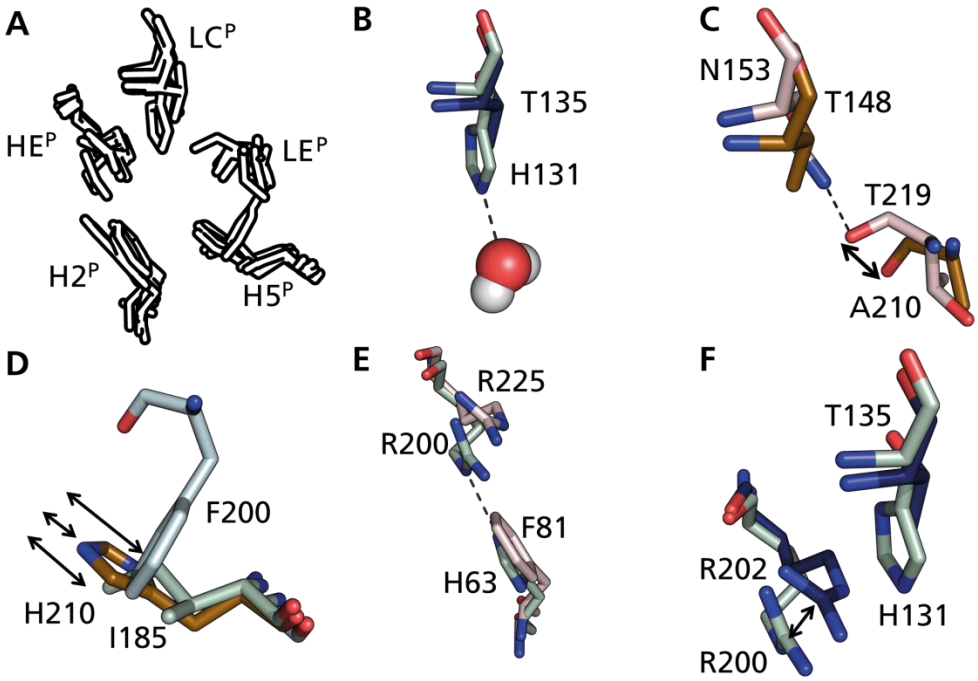

Figure 7: View from the non-cytosolic side on the five positions that contribute to the constriction region of the pore and are named according to the secondary structural element they reside in. **A Selectivity filter** overview of the five positions each individually depicted in B-F. **B** LC^P can be interacting with pore molecules, such as in TIPs. **C** LE^P carbonyl orients in one of two ways depending on a possible hydrogen bond donor at LC^P, as common in water specific channels (exception *Hs*AQP4). **D** H5^P is a conserved histidine in water specific MIPs. Aquaglyceroporins contribute with a phenylalanine (residue from LE^P). In contrast, isoleucines, as found in TIPs, AQP8s, and AqpM, are also hydrophobic but closer to the pore centre. **E** Aromatic residues in H2^P are spatially very conserved. TIP2s have histidine, which hydrogen bonds to HE^P arginine. **F** HE^P is a highly conserved arginine. In water specific channels and aquaglyceroporines the residue orients with the secondary ketimine towards the pore centre. In proteins with large residues in LC^P, arginine is shifted towards H2^P. *At*TIP2;1- pale blue; *Mm*AqpM – dark blue; *So*PIP2;1 – salmon; *Hs*AQP4 – bronze.

There are mainly three ways to increase the energy potential for a molecule at a position in the pore. Electrostatic repulsion is specific for charges of the same type and increases the threshold for applicable molecules significantly. Beside the charge specificity, pH dependence might be a limitation for this selection. While the imidazole rings of histidines are double protonated and positively charged at acidic pH, they lose this property in at neutral pH. Sterical hindrance of a molecule is an intuitive way to block a passage. Here, the distances that can be derived from crystal

structures give an impression of the upper size limits for a substrate. One has to keep in mind that the hindrance must be viewed in a dynamic way and at a physiological temperature. The minimum energy based positioning of residues in a crystal structure measured at 100K may not represent the dominating state *in vivo*. Molecular dynamics (MD) simulations provide a tool to elucidate dynamic behavior at room temperature (**paper I**). The limitations of sterical means to establish selectivity are obvious. For spherical molecules only a maximum property is defined – the radius. All molecules with similar or smaller size can penetrate. How would MIPs be water specific and not allow for ammonia permeation, given the similar size of the molecules? There must be an additional way of selection for uncharged molecules. In aqueous solution an immediate consequence of a confined space is the loss of hydrogen bonds to bulk waters. While entropy is rising in cases where hydrophobic surfaces of the protein are occupied by hydrophobic molecules, there is a cost in enthalpy when polar molecules have to break their hydrogen bonds while moving through the pore. This leads to a pore presenting hydrophobic patches as well as hydrogen bond partners all along, but especially constrained in the selectivity filter. The energy gain of a hydrogen bond is dependent on the distance between donor and acceptor as well as on their mutual orientation. Keeping these properties in mind, the following description will compare selectivity filters of three structurally known MIP types: water specific MIPs, aquaglyceroporins, as well as water and ammonia permeable MIPs.

4.1. Common ground

One of the hydrogen acceptors is present in all MIPs – the carbonyl located in loop E (LE^P). This carbonyl can hydrogen bond to a neighboring residue situated in loop C (LC^P), which is the case for most water specific MIPs. The LE^P carbonyl is dragged towards LC^P and is thereby oriented towards the center of the pore – a location defined as group II. This leads to a contorted backbone of loop E, N-terminal to LE^P (Fig. 8). The counterpart of this contortion is enabled by the carbonyl two residues before LE^P, which hydrogen bonds to LC^P and the amide after this residue. The energy demanding contortion is underlining the uniqueness of water specific MIPs.

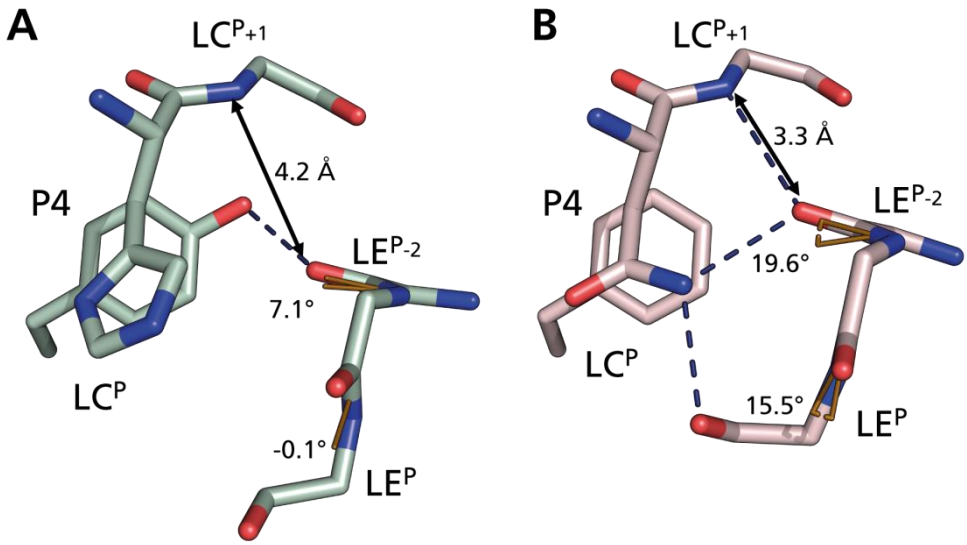

Figure 8: Position 4 close-up of structures **A** *At*TIP2;1 and **B** *So*PIP2;1. Residue in "Position 4" correlates with carbonyl orientation at the site two residues before LE^{P}. This carbonyl commonly hydrogen bonds (blue dashes) to amide after LC^{P} in water specific MIPs. If it also binds to LC^{P} together with LE^{P} carbonyl (group II orientation), as in *So*PIP2;1, the backbone is contorted. In proteins with LE^{P} carbonyl in group I, such as *At*TIP2;1, "Position 4" residue can hydrogen bond to the carbonyl belonging to the amino acid situated two residues before LE^{P}, which allows it to have a greater distance to loop C.

The evolutionary conservation of LC^{P} is a result of structural constrains, which reach further away and have impact on the amino acid located in position P4. In solved structures of *At*TIP2;1, *Hs*AQP4 and *Mm*AqpM the amino acid in P4 is tyrosine, which forms a hydrogen bond to the carbonyl two amino acid residues before LE^{P}. This leaves the backbone of loop E in a more relaxed state with greater distance to loop C. LC^{P} carbonyls of all water unspecific MIPs adapt a more flexible conformation (defined as group I), increasing the pore diameter and compensating for the lack of hydrogen bonds donated by residues in helix 5 (H5^{P}). Thereby, P4 serves as an example for functional demands leading to the conservation of structural features, which cannot be derived from a single structure, but can be suggested from sequence alignments. While LC^{P} is always a hydrogen-bonding amino acid residue in water specific MIPs, the functionality of this position across the superfamily is diverse and hardly understood. In GLPs, LC^{P} residues are small and hydrogen bond to a hydroxyl group of the amino acid residues after HE^{P} arginine. Like in water specific

MIPs, the residue at LC^P of GLPs does not interact with pore molecules, which is the reason why earlier it was not included in the definition of the selectivity filter. However, in TIP2s a histidine is stabilized in space by hydrogen bonding with the δ-nitrogen as acceptor to Ser 201 (**paper I**). The ε-nitrogen of the imidazole ring is pointing towards the pore center and serves as hydrogen donator. TIP3s, which are also ammonia permeable MIPs, replace histidine with phenylalanine. The functional relation and identical residues on all other selectivity filter positions lead to alignment of phenylalanine at position LC^P for vertebrate AQP8s for the modeling in **paper II**. As a result, phenylalanine occupies a similar space as histidine in *At*TIP2;1. Additional to the direct interaction with pore waters, both residues are able to push the neighboring residue at position HE^P away.

Position HE^P resides a highly conserved arginine, which contributes with its positive charge to the repulsion of protons and other cations. In all solved structures, arginine interacts with loop C either directly or – in *At*TIP2;1 – via water molecules. These hydrogen bonds keep loop C in close vicinity and orients the guanidinium group such that the secondary ketimine is exposed. In water specific MIPs and GLPs this nitrogen is oriented towards the pore center and offers hydrogen bonds to substrates. Bulky residues like histidine or phenylalanine in LC^P are able to reorient HE^P arginine towards $H2^P$. All observed $H2^P$ residues are aromatic and occupy the same space, orienting tangential to the pore. While phenylalanines in water specific MIPs and tryptophans in GLPs render $H2^P$ hydrophobic, animal AQP8s and most TIPs have instead a histidine at this position. This residue or a less common glutamine can stabilize arginine in the alternative position by accepting a hydrogen bond from arginine and donating one to a backbone carbonyl at the same phase of helix 2. In addition, hydrogen bonds can be provided to pore molecules. In this aspect $H2^P$ histidines compensate for the lack of histidine at $H5^P$, which is present in water specific filters. All TIPs and AQP8s have a hydrophobic isoleucine at $H5^P$, which also increases the pore diameter. Still, without the hydrogen bond acceptor provided by the more flexible LE^P, water transport is diminished. Therefore, the results of mutational studies presented in **paper I** confirm previous conclusions that water is not selected over ammonia by size [110]. This highlights the importance of hydrogen bond compensation. The possibility of solutes to maintain hydrogen bonds to waters decreases rapidly at the filter and further upon entering the single file pore. Figure 6a

in **paper I** displays the energy landscape and the number of hydrogen bonds of an ammonia molecule along the pore of *At*TIP2;1. The negative correlation between energy barrier and number of hydrogen bonds is most prominent between NPA region and selectivity filter region. This elucidates the need for a continuous hydrogen bonding network throughout the pore. Not only hydrophobicity is increasing the energy a molecule needs to pass the filter, also sterical hindrance can block the path. In line with this, MIPs, which are permeable to larger molecules, present a wider selectivity filter. To establish this, GLPs have glycine at $H5^{P}$. This leaves enough space for a phenylalanine – actually the residue of LE^{P} – to orient tangential to the pore, leaving the pore even wider than an isoleucine at this location (Figure 7D), which is conserved in all AQP8s and TIPs in this position. Isoleuine leaves more space than a histidine – present in water specific MIPs – without providing a hydrogen bond to permeating molecules. The importance of hydrogen bond formation is highlighted when looking at a mutational study presented in **paper I**. When exchanging $H5^{P}$ histidine in water specific *Hs*AQP1 to isoleucine, ammonia permeability was gained. Although the diameter of the pore is larger in the mutant, water permeation is prohibited. This can be explained by the required energy, removing a polar and hydrogen bonding molecule from aqueous solution, which is higher for a water molecule than for ammonia. Together with a small residue at LC^{P} and a relaxed LE^{P} carbonyl, GLPs form as expected the most spacious filter. Maybe surprisingly, filter in AQP8s and TIP2s are of comparable diameter, and although they share identical filter, they are reported to have different permeabilities to glycerol and urea. Looking at the significantly wider pore of GLPs around the NPA box, the selection of these large molecules in other MIPs could be arranged at different places than the selectivity filter, as discussed in **paper II**. One should keep in mind that evolution is based on functional selection. That means that the selectivity filter can only evolve independently to allow or prohibit a certain molecule, if the energy barrier for this molecule is nowhere higher and if there is a selection pressure, meaning a physiological relevance to be permeable. Physiological relevance is reasonably questioned, where membrane permeabilities are significantly higher.

As if the picture with three different filter types was not complex enough, there is a structure available that features properties of all three. *Mm*AqpM $H2^{P}$ phenylalanine and HE^{P} arginine are positioned as in water specific MIPs. On the other side it

resembles an aquaglyceroporins, as LC^P is a threonine, which neither hydrogen bonds to LE^P carbonyls nor pushes HE^P arginine away. It presents an isoleucine at $H5^P$ like TIPs. Therefore, it has a selectivity filter, which is slightly more narrow than aquaglyceroporins, but of comparable hydrophobicity. In this way, it represents a configuration that was not achieved in the mutational studies in **paper I**. $H5^P$ was exchanged to isoleucine in this experiment, which resulted in exclusive ammonia permeability. A conclusion is difficult, as the mutation of LE^P residue to a small glycine was necessary to return water permeability. It appears that a small residue is needed in LE^P to allow the carbonyl to be in the relaxed "group I" position. In AqpM, which is a relatively poor water channel [44], LE^P serine is small enough to find the carbonyl belonging to group I. In conclusion, LC^P histidine in TIP2s – although bigger than asparagine or threonine – increases the water permeability specifically and still allows for ammonia conductivity.

4.2. Outlook

The investigation of structure-function relationships of three MIP types provides a basic understanding of selectivity in these channels. Considering how many subfamilies that are structurally unknown and especially the diversity of their substrate profiles, there is still a lot to learn. Selectivity filters evolved to realize permeability to certain substrates. The selection for a certain amino acid residue is based on the permeability for several molecules – substrates and excluded species. There are cases when it is more crucial to prevent certain molecules from permeation than increasing permeability for others. As a result, the selectivity profiles together with the expression pattern may provide physiological insights on subcellular compartments. Additionally, these differences in selectivity carry fundamental knowledge about the physical features of the selectivity filter, which may be valuable when trying to reproduce a certain specificity in artificial systems. As a motivation to look forward to the coming structures, the end of this chapter gives some examples of what is not known about MIP selectivity filters.

TIP3s probably have a similar filter to AQP8, which are modeled in **paper II** and would thereby show a similar substrate profile. Evolutionary closely related TIP1s have also phenylalanine at LC^P, but lack an arginine at HE^P. The replacing valine should render the filter wide and hydrophobic. Unclear is the functionality of $H2^P$

histidine in this subfamily. There is no obvious reason to assume a different position than in all other MIPs, but the absence of arginine could mean an ordinary pK_a for the imidazole nitrogens. In acidic vacuoles – at a pH 5.5 – the histidine may provide enough positive charge to repel protons. HIPs got their name for having a sequence similar to PIPs and TIPs. For the selectivity filter this means that three histidines assemble around the arginine, which is likely to cause a narrow passage. *Pt*XIP2 was modeled with isoleucine at $H2^p$ and $H5^p$ [111]. In another study [112], XIP1s from tobacco were alternatively aligned with threonine at $H5^p$, which is a conserved amino acid residue three positions C-terminal of the isoleucine. Considering the hydrophobic nature of XIPs, which demonstrated no or little water permeability, one would expect a hydrophobic residue. There is a third alternative with phenylalanine, which is immediately N-terminal of the isoleucine. This fairly conserved residue is replaced by tyrosine in *Pt*XIP3.2 and *Pt*XIP3.3. The latter is the only XIP of the study with an NPI motif that presented some water facilitation (2.5-fold of control). This does not explain, why XIP2;1 also showed the same water permeability. To refer to the ordinary – and more polar – NPA motif would contradict with the theory that the highest energy barrier almost completely defines the permeability. Another special feature of XIPs awaits structural verification. Alignments put a completely conserved cysteine at LC^p. This residue can potentially serve as hydrogen donor for LE^p carbonyl, but has on the opposing side a second cysteine behind HE^p arginine to form a disulphide bridge [51]. Therefore, the carbonyl grouping will depend on this unknown structure.

NIPs have been modeled using multiple template procedures, based on water specific MIPs and *E.coli* GlpF [113] or employing Phyre2 [76]. LE^p carbonyls in these models show an orientation as water specific MIPs. HE^p arginine is displayed in the orientation towards the pore centre. This is not the only possibility, especially considering glutamine in $H2^p$ that is able to hydrogen bond to arginine. In regard to their wider substrate profile and in light of newly available structural information (**paper I**, this chapter), the selectivity filters may have been modeled wider as they actually are.

MIP regulation

Considering the number of water specific MIPs in multicellular organisms, it can be expected that physiological diversity connected to water permeation is achieved by regulation of functional properties of the membrane, including their inserted proteins. As mentioned earlier, due to instrinsic permeabilities and redundant expression, it has proven to be difficult to find phenotypes for many MIP mutants. Thanks to tremendous efforts in the field, several physiological effects have been connected to MIP function. The diversity is not only a result of specific substrate profiles, but a variety of different regulation mechanisms on various levels of cell organization. These levels include – not exclusively – transcriptional and translational control as well as directing localization to regulate protein amounts. The latter can be influenced by posttranslational modifications that are also utilized to gate the pore, which is realized by conformational changes. The probabilities of conformations are modulated by environmental conditions and further augmented for different posttranslational modifications and even oligomerization states. The complexity of the described features does not uncommonly lead to controversial observations and conclusions, which keep being debated. Still, some reported physiological roles of MIPs are presented at the end of this chapter.

5.1. The right expression

Some functional features demand stable proteins and a suitable turnover time. Membrane proteins are commonly found to be fairly stable. So are MIPs, which can be easily suggested looking at the overall helical structure. This fold results in high temperature stability. The structural features related to molecular integrity of this type of membrane proteins are introduced in chapter 3.3. These structural properties may be a prerequisite for achieving a high protein density in native membranes. TIPs were reported to comprise 40% of the tonoplastic proteins [114], while PIP homologs in spinach plasma membranes represent around 20% of the integrated proteins [115]. This high expression levels are extraordinary and only representative

for some isoform. Many isoforms are expressed in specific tissues at certain developmental stages, so correlation between different isoforms can indicate their physiological role.

Members of the MIP superfamily are found to be co-expressed when comparing multiple developmental stages and various organs of Arabidopsis [116]. Cell development is not the only process to be controlled by transcription factors. Thorough analysis of transcription levels of PIPs and TIPs in Arabidopsis has demonstrated expression correlation between different isoforms upon drought stress [117, 118]. The highest correlation coefficients were calculated for PIP1;1/PIP2;1 and TIP2;1/TIP1;2. Another example for a stress response has been reported for rats, where expression of AQP9 in the liver increased during starvation [119]. Considering the variety of membrane properties, it is expected that protein expression levels of MIPs are not only triggered by environmental conditions. Expression patterns of several MIPs have been investigated – comparing different cells, developmental stages, or subcellular compartments. Six different fluorescent labeled TIPs have been mapped in Arabidopsis roots [120]. While some isoforms are broadly expressed, others can be localized to certain cells – such as *At*TIP2;1, which was exclusively visualized in primordial cells of lateral roots. TIP1s are reported to be highly expressed in expanding cells [121-123]. Expression analysis of TIPs in Arabidopsis seeds elucidated tissue- and development-specific distributions [124].

Not only transcriptional regulation influences protein abundance in a cell. Inconsistent mRNA and protein levels of radish PIPs upon hormone treatment suggested additional ways to dynamically modify protein amounts [125]. Simultaneously expressed MIPs may undergo different post-translational regulations resulting in diverse processing or targeting. Biosynthesis happens in the endoplasmic reticulum, and for polytopic membrane proteins a model is described that achieves the final topology by co-translational insertion [126] of the helices at the translocon [127]. For some proteins, this process has proven to be more complex. While human AQP4 is integrated segment wise [128], AQP1 matures from an intermediate 4-helix stage to the final fold [129], requiring a reorientation of helix 3 in the membrane, which includes the passage of loop C [130].

Once the protein is correctly folded, it has to be targeted to its final destination. Ubiquitination of *At*PIP2;1 by E3 ubiquitin ligase has been seen to regulate ER retention and degradation by 26S proteasome in reaction to drought stress [131]. Trafficking from the ER to the final destinations is realized via the Golgi apparatus. Targeting of *At*PIP2;1 is dependent on phosphorylation of particular C-terminal residues, which allows to counteract upon salt stress [132]. Phosphorylation at this site affects the protein amount in endosomes relative to the plasma membrane. Endocytosis is further inhibited by another plant hormone, auxin [133]. Similar trafficking is described for human AQP2 expressed in principal cells of the collecting duct in kidneys. Here, phosphorylation by protein kinase A results in delivery to the apical membrane [134]. Additional mechanisms of trafficking control have been observed for PIP1 and PIP2s. When expressing plant PIPs separately in oocytes, PIP2s were efficiently targeted to the membrane, while PIP1s were retained in the ER. Localization of PIP1 could be improved by co-expression with PIP2 in maize [57] and grapevine [135]. The base for the higher density of PIP1 and PIP2 in the membranes was reported to be direct interactions between these isoforms [57]. These interactions have been investigated and evidence for heteromer formation has been presented, when expressing maize PIPs in oocytes [96, 136] and spinach PIPs in *Pichia pastoris* (**paper III**). Targeting of MIPs to other membranes is well known but not yet understood. MIPs have been reported to reside not only in the plasma membrane and the tonoplast [137], but in plasmolemmasomes [138], in the symbiosome of root nodules [139], in the inner envelope of chloroplasts [59], in the inner mitochondrial membrane [38, 140], and in the endoplasmic reticulum [141, 142]. The heterogeneity of localizations underlines the complexity of physiological effects that may derive from MIP functions.

5.2. In response

Different developmental stages can require adaptation of membrane properties. Regarding development, change in membrane permeabilities can be achieved in a suitable timeframe by adjusting the adequate expression levels. For many physiological processes, this adaptation is too slow. To adjust membrane conductivity for water as a rapid response to shifting external conditions, several mechanisms are available to alter the permeability of MIPs. These mechanisms include reversible conformational changes on the cytosolic side of the protein and are referred to as

"gating". Posttranslational modifications and different cytosolic conditions have been described to trigger gating. Structures of *So*PIP2;1 in an open and in a closed state introduced a molecular mechanism for gating [83] (Figure 9). It involves the conformational change of loop D. When loop D is stabilized in the closed conformation, leucine 197 sits in the pore. The position of leucine 197 is guided by serine 274 of the neighboring monomer that interacts by H-bonds with the backbone nitrogens of proline 199 and leucine 200 of the D-loop. Loop D can be further stabilized by interaction with aspartate 28 and glutamate 31 from the N-terminus and water mediated attachment to loop B. The two negative residues immediately suggest a binding adding a positive charge. The energetic states in the different conformations influence the open probability and thereby the permeability rate. How these interactions are achieved or how they are disturbed, is here described in more detail.

Before any MIP structure was available, it was demonstrated that phosphorylation of an α-TIP increased the water permeability in oocytes [143]. Furthermore, it was known that the same modification of two conserved serines alters the permeability of *So*PIP2;1 [144]. Serine 274 is unphosphorylated in a closed structure, while the C-terminal stretch is ordered between two adjacent monomers. Upon phosphorylation, serine opens the space for leucine 197, which can move out of the pore. Serine 115 is situated in a phosphorylation site in loop B. Although phosphorylation could not directly be shown in *So*PIP2;1, this site was found to be more phosphorylated in maize cells that had an increased water permeability [145]. According to mutational studies including structural analysis, a phosphate at serine 115 may perturb the hydrogen bonding network between the N-terminus and loop D in the closed conformation [146]. Another serine (S188) in *So*PIP2;1 participates in hydrogen bonding within loop D and can potentially be phosphorylated. Mutating this residue to a negative charged glutamate resulted in a permeability increase of 3-fold compared to the wild type. If this modification occurs *in vivo*, the effect is potentially larger than for S115 and S274 together. Mutational studies in maize [147] confirm the importance of the serines in loop B and D, while the N-terminal serine appeared not to be critical in oocytes. A previous mutational study of SoPIP2;1 in oocytes showed that serine 274 clearly influenced the water permeability of the oocyte membrane. MD simulations agree with proposed models of alteration of the open probability by changing the interaction of loop D [83]. In addition to

phosphorylation, low pH and Ca^{2+} were presented to reduce water channel activity [148]. A histidine in loop D was pointed out to cause pH sensitivity [149]. This was explained by the first plant MIP structure (i.e. *So*PIP2;1) at pH 8, which displayed this histidine relatively close to aspartate 28 in the N-terminus [83]. In a closed structure obtained at pH 6 one histidine of the tetramer interacts instead water-mediated with loop B [150] (not displayed in Figure 9). Still, mutational studies in which this negative residue (aspartate 8) is replaced with alanine present a weaker pH effect [151]. Instead of a calcium, a cadmium is seen in the structure to be coordinated by glutamate 31. In MD simulations, loop D is interacting dynamically with the N-terminus in a direct manner or water-mediated. Another metal binding site on the cytosolic side was seen in a crystal grown with mercury and cadmium [152]. The metal is hexagonally coordinated by the hydroxyl group of a threonine in loop D, a backbone carbonyl in the C-terminal stretch, and four water molecules. Although it binds to two sites involved in gating, the effect has not yet been further investigated. From the findings that localization of PIP1 to the membranes of oocytes was dependent on the coexpression with PIP2, it was deduced that physical interaction occurs [57]. As it is known now that PIP1 and PIP2 can form heteromers ([96, 153] and **paper III**), several regulatory features may be addressed. ER retention dependent on the ubiquitination state can be altered, as the targeting to the plasma membrane occurs as tetramers. The same can be true for phosphorylation influencing internalization to endosomes. Ultimately, as the stabilization of loop D in a closed state requires binding of the C-terminus to the neighboring monomer, oligomerization could fine-tune gating properties [154].

Even given a particular posttranslational state and with certain abundance in the membrane, protein facilitated fluxes are variable. Membrane composition is known to modulate the function of integral proteins. Accordingly, AqpZ was reported to have a different stability dependent on the kind and on the number of bound lipids *in vitro*, which included cardiolipin. Furthermore, proteoliposomes lacking this lipid displayed only half of the permeability rate [155]. Other MIPs were reported to change their permeabilities dependent on membrane fluidity. In contrast to *Hs*AQP4, which has a reduced permeability in more rigid membranes [156], *So*PIP2;1 was proposed to be activated by changes in the membrane [152].

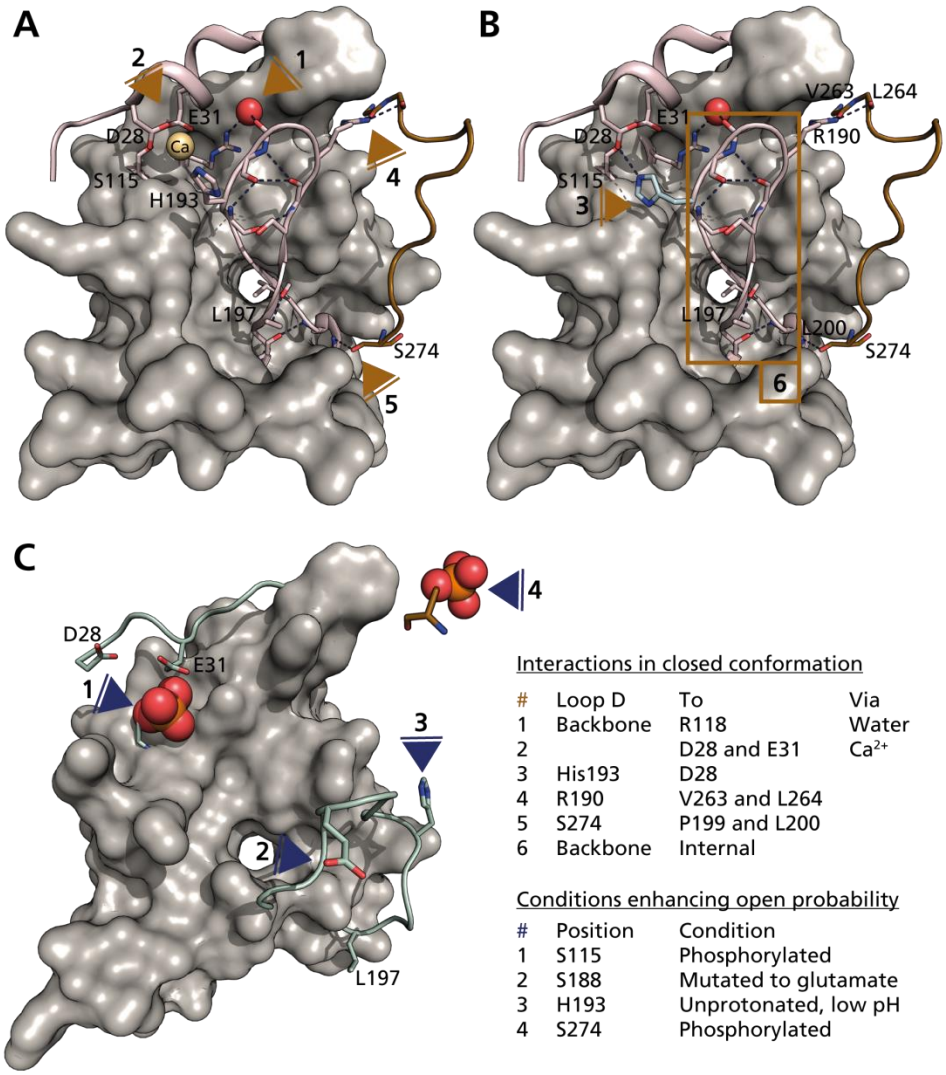

Figure 9: Gating of *So*PIP2;1. Cytosolic view of a monomer in closed (**A** and **B**) and open conformation (**C**). **C** displays loop D in a conformation seen in one protomer of 2B5F, for which L197 is located close to the tetrameric centre. **B** If loop D is anchored over the pore, as in the closed structure 1Z98, L197 is instead blocking the pore. The position of L 197 the in open state is occupied in the closed state by S274, which comes from the C-terminal stretch of the (clock-wise) neighboring monomer. Here, the C-terminus is structured in the intermonomeric interface and bonds to R190. The closed conformation can be further stabilized by negative residues close to the N-terminus either coordinating Ca^{2+} (A, yellow sphere) or bridging to protonated H193 (B), while interactions of loop D with loop B, C- terminus, and internal hydrogen bonds are disturbed by phosphorylation of S115, S188 and S274.

If permeability variations express the evolutionary optimization of the protein to a certain lipid environment, or the possibility to modulate its function by changing membrane composition, needs to be evaluated in each case. However, a mechano-sensitive gating mechanism has been proposed for water channels in rabbit kidney [157], for Aqy1 [158, 159], and for human AQP1 [160].

5.3. Physiology

Regulation of protein amounts by varying transcription, translation, localization, and degradation as well as permeability adjustment in response to cellular conditions, such as Ca^{2+} concentrations, membrane properties, and pH, represents a number of tools to modify MIP-dependent functions. This in combination with a large amount of isoforms with different substrate profiles and located to different compartments, it is not surprising that several MIP functions could be correlated to physiological events. Although not many and rather mild phenotypes have been found, some of these physiological effects will be briefly exemplified.

Phosphorylation of plant proteins has been shown to be dependent on Ca^{2+} concentrations [115]. More directly, calcium-dependent kinases have been used to phosphorylate MIPs [161, 162]. This could relate to cell signaling, which can be triggered by various effectors. Accordingly, altered water flux could be connected to several different stress conditions or developmental stages. *So*PIP2;1 activity was regulated based on extracellular osmolarity [115]. Phosphorylation of a particular serine in soybean Nodulin 26 increases water permeability, a state that can be influenced by senescence, salinity, and water shortage [163]. Dephosphorylation of a MIP in the plasma membrane of tulip petals that leads to pore closure [164], was more specific at 5°C, which was interpreted that the phosphatase serves as chilling sensor [165]. Another relation between temperature and MIP function was described for maize roots, where H_2O_2 dependent MIP regulation was postulated as a response to membrane damage caused by chilling [145]. Another stress for plants is flooding, as it lowers the oxygen level in the roots. Plants can counter this by gating of PIPs, which is a result of the lowered cytosolic pH [149] (protonation of histidine in loop D, Figure 9). However, plants must regulate water fluxes stress-independently as mentioned in chapter 2.1.1. Membrane water permeabilities affect the cellular level – such as release of turgor pressure – as well as whole plant transport of assimilates.

Accordingly, transcript levels of TIPs in sunflower were correlated to the opening of stomata [166]. Similarly, elevated expression levels of tonoplastic protein together with a proton pump were connected to the development of pulvini motor cells [17]. In Arabidopsis, *PIP1;2* was found under the control of a promoter, which is induced by blue light. This promoter is temporally active, when increased water permeability is needed, e.g. in the elongation zones of the root, in the guard cells of stomata and in vascular bundle sheath cells [167].

A well-studied process is the water permeability adjustment of membranes in the kidney in response to homeostatic needs, briefed in chapter 2.1.2. A major part of the water entering the kidney is reabsorbed in the proximal tubules and in the loop of Henle, which involves the function of water specific AQP1. In the distal nephrons urine is further concentrated dependent on the osmoregulator vasopressin. Here, AQP3 and AQP4 are expressed in epithelial cells of the collecting duct [168, 169] to assure high flow rates over the basolateral membrane (facing the blood). In contrast, a vasopressin receptor on this side triggers protein kinase A via cAMP releasing adenylate cyclase. This amplified signal leads to phosphorylation dependent trafficking of endosomal AQP2 to the apical plasma membrane (facing urine). A persistently high concentration of the antidiuretic hormone vasopressin additionally affects the expression levels of AQP2 [170], which entails the control of water retention in a complex manner. While AQP3 and AQP4 deficient animals show reduced ability to concentrate urine, individuals with disturbed AQP2 activity [171] or abundance [172] even suffer from nephrogenic diabetes insipidus (NDI).

Future perspective

Regarding the *At*TIP2;1 project, the new structure opened the door for a different view on MIP selectivity. However, most of it is not fully understood yet. Solving structures of other MIPs with different selectivity filters and substrate profiles will eventually lead step-by-step to a clearer picture. Recently a high resolution structure was solved of a MIP from *Hydrangea macrophylla* belonging to the group of TIP1s (T. Ito *et al*, unpublished). Furthermore, MD simulations, like umbrella sampling, provide a useful tool to investigate the energy profiles of the pores. Interesting targets would include TIP1s, which could show a different way to achieve specificity, as it would resemble the first structure without arginine at HE^{P}. *At*TIP1;1 was expressed and purified in small amounts to allow for functional characterization. Water and ammonia permeability was confirmed (Figure 10), but further investigations need to be done to elucidate specificity and heteromerization experiments could be done as established for **paper IV**.

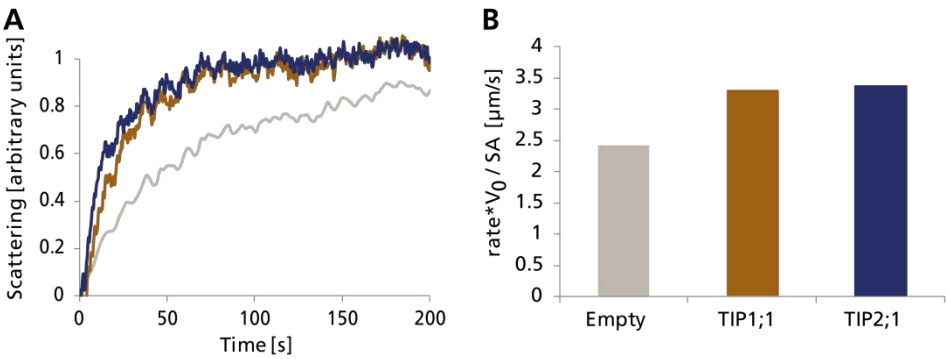

Figure 10: TIP function. *At*TIP1;1 and *At*TIP2;1 show water (**A**) and ammonia (**B**) permeability. Graphs in A are color-coded as in B.

Substrate specificities of XIPs and NIPs are still not complete and these isoforms need to be further investigated. Structural knowledge about these proteins potentially allows for industrial and agricultural application. HIPs are far from characterized in the sense that the static filter modeled using the same C_{α} positions are too narrow for

any water to pass. Either the filter is sufficiently wide or the flexibility of the two histidines in LC^{P} and $H5^{P}$ allow water for passage. Functional and structural data needs to be acquired to elucidate permeation mechanisms.

Considering the high thermal stability of 86°C, the high salt stability and SDS resistance, one could further investigate how this is achieved in *At*TIP2;1. On the other hand, with the stability and the high expression rate of 240 mg purified protein per L culture, this protein should be possible to investigate further. Given the good diffracting crystals and many crystal conditions without optimization, this could be neutron crystallography. As crystals of a size bigger than 0.5 mm^3 are needed, this will be a challenging project, but also the gain will be tremendous. A neutron structure would allow seeing the protons of pore waters interacting with each other and with the protein.

The functional characterization of NIPs and XIPs is far from finished, and novel functions await their discovery. To understand biology of already fairly well investigated substrate permeabilities e.g. for water and ammonia, regulation and localization of the proteins must be described in more detail. For the latter a challenge needs to be overcome: Confidence about the subcellular localization of MIPs requires a strict risk assessment of contaminants. By combining regulation, membrane abundance, and permeability rates, systems biology approaches may be applied by simulating whole metabolic pathways. The results in return could suggest experimental set-ups, which may increase the chance of finding phenotypes. Either way, by computational methods covering complex systems or by classical reductionism by i.e. deploying knock-out approaches and creating phenotypes that could potentially resolve questions related to function

Contribution to the field

This chapter briefly summarizes the scientific outcome of the projects, which is outlined in the appended manuscripts. The goal is to give an overview of the novelties achieved and to position these relative to their value for the scientific community. All papers use structural findings to describe functional properties, such as activity and regulatory aspects. Figure 11 lists water and ammonia as substrates as well as seven aspects of structure-function relation and refers to the papers concerning this aspects. The language is consciously chosen to be more direct, which opens up for discussion.

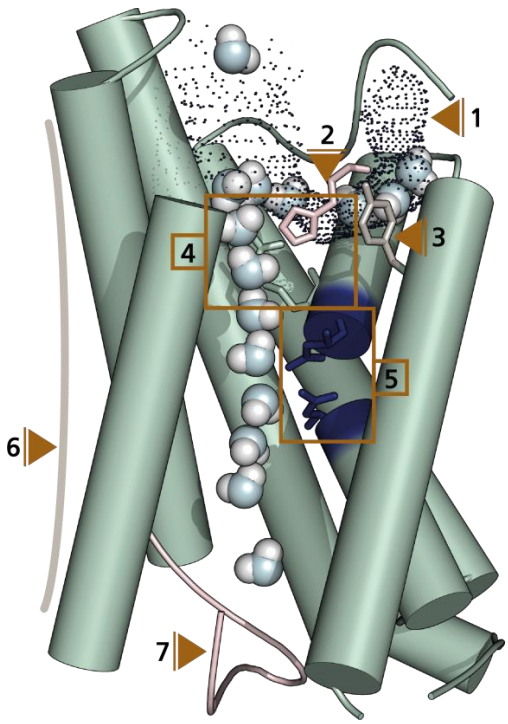

Water

Ammonia

#	Aspect	Paper
1	Side pore	I
2	Proton shuttle	I
3	Position 4	I
4	Selectivity filter	I, II
5	NPA motifs	II
6	Monomer interaction	II, III
7	Gating	III, IV

Figure 11: Contribution to the field. Schematic inside view without H4, LB, and LE. Different aspects of MIP structures are numbered and referred to the papers that discuss related results. Ammonia permeable MIPs are presented in paper I and II, while all MIPs included in this thesis facilitate water permeation.

Paper I presents a high resolution structure of *At*TIP2;1. This provides the first structure of a protein, which is neither water specific nor does it belonging to the subfamily of aquaglyceroporines. TIP2;1 from Arabidopsis was homology modeled together with other isoforms [173] as well as TIP2;1 from wheat in a separate attempt [174], but due to an error in the alignments, the selectivity filter was not correctly defined. Our functional assays confirmed the already known water [175] and ammonia [64, 174, 176] permeability. Additionally, TIPs have been shown to be localized to the tonoplast [175, 177]. The implications of an ammonia permeability increase of the membrane separating the vacuole are elucidated in chapter 2.2.1. Together, TIPs can play a role in the nitrogen cycle (see chapter 2.2) and therefore, fundamental insights into their function are interesting in many aspects.

After *Vigna radiata* H^+-PPase (PDB ID 4A01), *At*TIP2;1 structure provides the second look onto a tonoplast membrane protein. As for the structure of the H^+-PPase, a related plasma membrane localized protein (e.g. *So*PIP2;1), is available for *At*TIP2;1. Thus, we compared the surface electrostatics of these two isoforms. The non-cytosolic side of the tonoplast intrinsic protein is significantly more electronegative as compared to the plasma membrane protein *So*PIP2;1. It could be discussed, if this large distribution increases the protein stability in the environment of the vacuole with a pH of 5.5.

The main topic of the paper is the selectivity filter, which presents various novel features (chapter 4). Briefly, the conserved HE^p arginine is in a position, which has not been seen in previous structures of 17 MIP isoforms. It displays hydrogen bonds to $H2^p$ histidine, which has in turn a shifted pK_a. The arginine is pushed away by LC^p histidine, which is the first amino acid residue from loop C to be seen interacting with pore molecules. Additionally, the comparison with already published structures revealed a clustering of LE^p carbonyls in two confined spaces. A correlation between this grouping of carbonyl locations and substrate profile is discussed. As this grouping is dependent on the availability of a hydrogen bond donor in LC^p, the amino acid at this position is called the fifth selectivity filter residue, and it is suggested to be relevant for all MIPs. To relate the structure to water and ammonia permeability, mutational studies on human AQP1 are used to study key residues. Here, no mutations were done to block the pore or make it unnaturally wide, due to the uncertainty of putative alignments. On the contrary, a gain-of-function strategy was

applied. There is no ammonia facilitating residue, as one might have expected. Instead, there are constellations that allow for ammonia and water permeation, where other amino acids of the selectivity filter suggest other substrates. In a nutshell: $H5^{P}$ isoleucine enlarges the pore diameter, but cannot hydrogen bond to substrates. All AQP1 H180I mutants (that show no function) have increased ammonia permeability, but only the quadruple mutant that allows the repositioning of LE^{P} carbonyl (to group I) show water permeability. The N127H single mutant is still water specific. A double mutant with C189G is needed to compare to the quadruple mutant to separate the effect of the LE^{P} carbonyl grouping in TIP2s. To elucidate ammonia permeation mechanism further, we have employed MD simulations. Four aspects were investigated: The ammonia permeability of *At*TIP2;1 was verified by calculating the energy barrier based on umbrella sampling, and spontaneous permeation of ammonia was observed in unbiased simulations. Furthermore, ammonium ion accumulation on the protein surface was mapped and – not surprisingly – could be correlated to negatively charged residues. The energy profile for ammonia permeation was compared to hydrogen bond densities along the pore. The formation of hydrogen bonds compensates for the desolvation energy when a substrate molecule enters the pore and correlates well with the energy profile. Interestingly, there are two pore positions between the selectivity filter and the NPA region, where higher density of hydrogen bonding can be seen. This is not further discussed, but could be related to the constraints of water molecules in hydrogen bonding distance, which are located at the selectivity filter and the NPA boxes. Beside the novel orientation of HE^{P} arginine, the most striking feature found in the structure is a higher position of loop C. In result, arginine is not directly stabilized by loop C but via mediating waters. In fact, the structure presents waters from the pore underneath loop C and up to the vacuolar surface, which is therefore termed side pore. This is caused by the shortness of loop C between H3 and LC^{P} and the positioning of the histidine residue at this site. This and structural waters binding to the amide before LC^{P} lead to an omega angle of more than 20°. What could be the selection pressure that evolutionary leads to this structural phenomenon? We describe a mechanism of ammonium deprotonation that involves the sidepore and proton shuttling by the LC^{P} histidine to potentially enhance ammonia permeation (Figure 12).

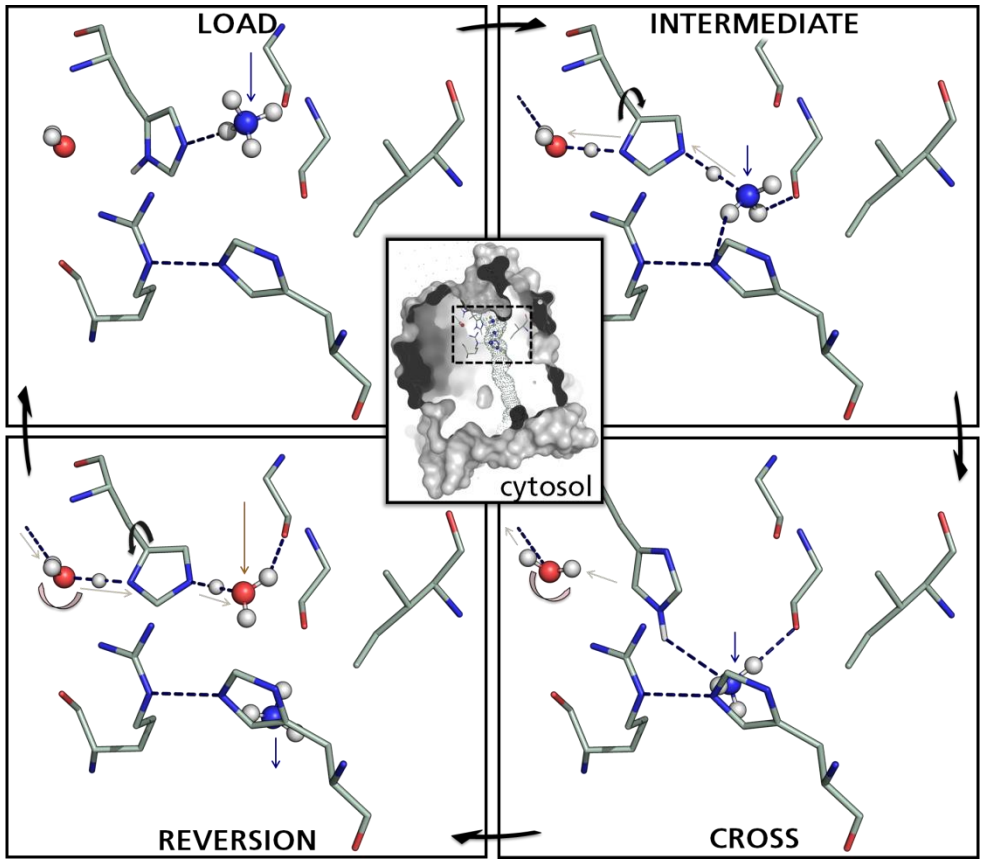

Figure 12: Speculative ammonia permeation mechanism in case of ammonium deprotonation. Ammonium enters the pore from the vacuolar side. Histidine at LC^P takes up a proton from ammonium and releases at the same time a proton to the water in the side pore. The proton is transported along the side pore via Grotthus mechanism. Histidine can flip to keep hydrogen bonded to ammonia. The histidine is regenerated releasing the Nε hydrogen to bulk water in the pore.

To be clear, we do not propose facilitation in just one direction under equilibrium conditions – that is against thermodynamical principles; we just describe the mechanism in one direction. Unfortunately, we do not have the experimental set-up to easily show pH dependent permeation. Lowering the pH decreases the ammonia gradient accordingly and thereby lowers the exchange rates. Compensatory effects and other time-dependent errors may make an accurate measurement difficult. Another unanswered question is, if this mechanism needs a pH gradient over the membrane, as available in case of the tonoplast. This can be established during patch-clamp experiments, but not in stopped-flow. Instead, we checked if necessary requirements

for this mechanism are met. MD simulations present a continuously water-filled side pore, and the histidine can flip between two major conformations, which is also seen in the provided video. Furthermore, as expected from the vicinity of the positively charged arginine, protonated histidine is more flexible to reach side pore waters. As there is an ongoing debate, whether local substrate accumulation can enhance membrane permeation or not, NH_4^+ distribution was summed up over simulation time and found to be elevated near negatively charged residues (aspartates). If expecting an effect by such an accumulation, as seen in Fig 4A in **paper I**, one could also consider the intermolecular energy (binding strength) between substrate and amino acid residue reflecting this behavior. However, to transfer the proton from ammonium, it needs to come close to LC^p histidine and thereby to the repelling arginine. The frequency of this event has not been calculated.

Outlook

Once a suitable experiment is available to test pH-dependent permeation, a number of mutants could potentially verify parts of our suggested mechanism. Ammonium contribution should be negated for the mutant H131F, as no proton shuttle is available. Conclusion about relative rates should be avoided without structural information, as the replacing phenylalanine may not be in the selectivity filter. This would increase the permeability at the cost of specificity, a biological relevant parameter that is often not addressed in studies. Furthermore, proton transfer via the Grotthus mechanism would probably not take place in the mutant A205F, if the replacing phenylalanine blocks the side pore. Finally, proton accumulation on the surface can be reduced by mutating aspartates on the vacuolar surface. An immediate candidate is aspartate 210, as it is situated at the cytosolic entrance of the side pore. As for all the mutants, structural integrity should be verified before any conclusions are drawn.

The structure published in **paper I** served as a template for modeling of various AQP8 models. There is no experimental structure available for this isoforms. *At*TIP2;1 served as a better template for modeling and revealed information for better alignment of loop C. Therefore, the new models presented in **paper II** provide probably a stronger base for further investigations of AQP8s.

Paper II and paper III is unpublished work.

Paper IV ends with two topics concerning water channels, which both have been continuously investigated in the last decade. One is regarding the center of the tetramer and its speculated function as an additional pore. The other topic is the complex mechanism of gating. The project started with mutational studies of *So*PIP2;1, proving involvement of disulfide bridges in the oligomerization pattern as seen in SDS-PAGE gels.

Functional assays were performed to measure the effects on the permeability caused by the mutation of bridging cysteines in the tetrameric center. Surprisingly, water permeability increased for both mutants. To test if water could permeate on a different path than the four main pores, a general inhibitor for MIPs was used to block it – mercury. Wildtype and mutants showed about two-fold increase of activity. Structural investigations followed, namely CD and tryptophan fluorescence upon mercury binding. Reversible activation and significant structural changes in micelles indicated a binding close to loop D. About that time, the authors of this paper were encouraged by noticing that another group found the same kinetic effects and suggested binding to the same cysteine (Maria Nybloms PhD thesis, page 48). Although the story changed over time, the published structure complemented our findings and helped to discuss observed features.

Three main results can be summarized: Since not all MIPs are inhibited by mercury (also seen for AQP6 [178]), functional studies that use mercury on complex systems need to be handled with care. There may be water leakage through a central pore of heterologously expressed and delipidized proteins, at least if central disulfide bridges are removed. Furthermore, artificially produced proteoliposomes may not represent kinetic values comparable to that of *in vivo* conditions, as different post-translational modification states may occur. The latter was already shown by mutations (e.g. S188E) that increased the open probability of loop D for the presumably "open" *So*PIP2;1 [146].

Summary

Water is fundamental to life on earth. Nitrogen is an element found in every protein and every piece of DNA. Coping with variations of accessibility of these substrates, all life forms have their ways to influence uptake and release of substrates. To realize this in a specific manner, certain proteins form channels in the cell membranes. Malfunctions of these channels are known to cause defects in humans and other organisms. Plants may be genetically modified to be functionally improved. Therefore, research of this kind of proteins bears the potential to find drugs against related diseases and to improve the performance of agriculturally important crops. Biotechnological advances have already been used to create biomimetic membranes capable of producing pure water. Another goal is to create salt-water filters that operate much more energy efficient than conventional filters.

Here, we produced our proteins of interest in yeast, purified and analyzed them. Functional studies were performed in artificial biomimetic membranes. Protein crystals were grown and put into X-ray beams to reveal a close-up of the protein structure. This worldwide first high resolution structure of this type of channel – permeable to water and ammonia – represents one piece of the puzzle of nitrogen usage in plants. It also founds the base to model related vertebrate (including human) proteins. These proteins are permeable to urea and are therefore connected to a disease called hepatic encephalopathy. This thesis closes with functional results of well-known plant proteins, which were used to shed light on the regulatory properties of plant as well as animal aquaporins.

Populärvetenskaplig sammanfattning

Denna avhandling behandlar två essentiella ting, vatten som är grundläggande för allt liv på jorden och kväve, vilket är ett grundämne som återfinns i varje protein och DNA. Liksom allt annat, måste dessa ämnen hålla en lagom nivå i cellen. För att klara variationer i tillgänglighet av dessa ämnen, har alla livsformer hittat sätt att påverka upptag och frisättning av dem. För att realisera detta på ett specifikt sätt, bildar vissa proteiner kanaler i cellmembranen. Mutationer i dessa kanaler är kända för att orsaka defekter i människor och andra djur, medan växter har modifieras genetiskt med dessa kanaler för att växa bättre. Forskning på denna typ av proteiner har potential att identifiera läkemedel mot sjukdomar relaterade till dessa kanaler, samt att spara gödningsmedel inom jordbruket. Biotekniska framsteg har redan gjorts för att med hjälp av dessa kanaler skapa biomimetiska membraner kapabla att producera ultrarent vatten. Ett annat mål är att skapa saltvattenfilter som fungerar mycket mer energieffektivt än konventionella filter.

Vi har producerat de proteiner vi forskar på i jäst, varefter de har renats upp och analyserats. Funktionella studier utfördes i artificiella biomembraner. Vi lyckades få ett protein att bilda kristaller vilka sattes i en röntgenstråle för att avslöja en atomärbild av proteinstrukturen. Detta resulterade i en högupplöst struktur, vilken är den första i världen för denna typ av kanal - genomsläpplig för vatten och ammoniak - och utgör en viktig pusselbit i förståelsen av kväveanvändningen i växter. Strukturen utgör också basen för de modeller vi har byggt av relaterade proteiner från djur (inklusive människa). Dessa former deltar i produktion av urea och är t.ex. relevanta för en sjukdom som kallas hepatisk encefalopati. Dessutom har strukturella och funktionella egenskaper hos två närbesläktade proteiner vilka är specifika för vatten studerats för att förstå vilka regleringsmöjligheter det finns i växter.

Zusammenfassung

Um Leben aufrecht zu erhalten, müssen Lebewesen stetig Stoffe aufnehmen und abgeben. Damit dies kontrolliert werden kann, gestalten Zellen ihre Membranen den Anforderungen entsprechend. Dazu gehört die Verwendung von spezifischen Kanälen, deren Menge und Funktion beeinflusst werden kann. Die hier vorliegende Arbeit befasst sich mit Kanälen, die spezifisch für Wassermoleküle sind oder zudem auch Ammoniak passieren lassen. Während Wasser in allen Zellen benötigt wird, um Stoffwechselvorgänge aufrecht zu halten, ist Ammoniak elementar für die Herstellung von DNS und Proteinen. Einige Krankheiten sind bekannt, die ihren Ursprung in Veränderungen an diesen Kanälen haben. Auf der anderen Seite konnten Gene solcher Kanäle in Pflanzen derart modifiziert werden, dass die Pflanzen z.B schneller wuchsen. Zu verstehen, wie diese Kanäle ihre Funktionen erfüllen, kann dazu führen, dass Medikamente gegen bestimmte Krankheiten entwickelt werden können oder Pflanzen weniger gedüngt werden müssen. Anwendung findet sich auch in künstlichen Membranen, die in der Lage sind, Flüssigkeiten sehr spezifisch zu filtern.

Um die Funktion dieser Kanäle zu analysieren, wurden diese in Hefepilzen produziert und extrahiert. In reiner Form wurden sie in künstliche Membranen konstituiert, um ihre Fähigkeit zu messen, Wasser und Ammoniak zu leiten. Zusätzlich wurden Kristalle aus einem Kanal gezüchtet, die dazu dienten, mithilfe von Röntgenlicht dessen Aufbau zu ermitteln. Diese weltweit erste Struktur eines Kanals, der Wasser und Ammoniak leitet, dient dazu, diese Funktionen zu erklären und insbesondere Mechanismen der Ammoniakleitung zu ergründen. Da eine Struktur mit dieser Auflösung nicht immer experimentell ermittelt werden kann, wurden ähnlich anmutende Kanäle auf den neugewonnenen Informationen basierend modelliert. Diese Modelle von Kanälen, wie es sie in Menschen und anderen Tieren gibt, liefern womöglich ein kleines Puzzleteil zum Verständnis unseres Harnstoffstoffwechsels. Abschließend stellen funktionelle Untersuchungen an zwei weiteren pflanzlichen Kanälen Details über Regulationsmöglichkeiten dieser Kanäle bereit.

Acknowledgements

First I want to express my gratitude to **Urban** for being such a great mentor. I talked to many people about supervision and therefore I know that I was very lucky to become your student. Your empathy allows you to treat every student individually. You spend an exceptional amount of effort on each student. Your cool and perfect analytical thinking let you encounter every problem I confronted you with; no matter how confused I have been, you could clarify the situation. We had a long time together re-re-writing our manuscript. It was not cumbersome, but fun and I learned a lot. You always say that writing is a process. I always thought the text is processed, but now I know, I got processed as well. Thanks for guiding this transformation.

In particular I thank you for all the "small" chats we had about everything. I enjoyed so much the conversations about Science theory and Evolution. Thank you for sharing your experiences of your hobby.

Thank you **Per** for everything you provided during these years; and thank you for commenting on this thesis and thereby improving it so much.

Dear **Aquaporin group**: You were my colleagues. Thank you for creating an atmosphere I enjoyed to work in. I liked to come to work, where I could discuss results or give advice. We had an open environment, where we could freely share ideas and easily collaborate. I wish you all the luck you need for successful experiments and the patience to succeed in the potentially troublesome field of membrane protein biochemistry. Remember: "If it was easy, everybody would do it".

Special thanks I want to give to **Sabeen**, who managed to stay with me in the office for all these years. We had nice conversations about family, religion, politics, and cultural differences. Thank you for teaching me some words in Urdu.

Anders, you were my PhD idol. All my knowledge I have about tube amplifiers comes from you. Thanks for always sharing your ideas on cooking. I enjoyed our

discussions about movies and EU politics. Most importantly, thank you for being a friend.

Jan Kvassmann for all the nice discussions on stopped-flow and liposome preparation.

CMPS can be a crowded place, full of brainiacs running through the corridors from one experiment to the other. Thanks for all the "Hej" that made our society so open. Especially thankful I am for all of you that had time for a chat. **Ingemar** about Arsenal (Good luck in the coming years) or publishing, **Maria** about career and language issues, **Eva** (football), **Evelina**, **Robert** (about RP), **Roberto** (about job application), **Kristoffer**, **Janina** (about dancing and crystallography – not at the same time), …

All the footballer, innebandy, and especially badminton **players** that let me chase the ball/shuffle cock.

Adorno and Lingneng will always be grateful to be kept alive. Thanks to the **DnD party** for all the fun, fighting and dying side by side.

Kamil for the nice trip to Monte Erice.

Oskar, **Erik**, and **Alak**: Thank you for representing a good outcome from teaching.

Alak, your smile, your heart (and your voice ;-)) is so great to fill the whole department. Every department should have someone to raise the spirit. As you are unique, I am happy that you are with us.

Michael, was soll ich sagen? Du hast mich so oft unterstützt. Wir hatten gewinnbringende wissenschaftliche Diskussionen und ich durfte bei dir in Aarhus sein. Ich hab manchmal immer noch das Gefühl, dir einen Kaffeekocher zu schulden. Vielen Dank auch für die netten Mittagessen und die vielen Fussballspiele, die wir gemeinsam erlebt haben.

References

1. BERLYNE, D.E., *A theory of human curiosity.* Br J Psychol, 1954. **45**(3): p. 180-191.
2. Uehlein, N., et al., *The tobacco aquaporin NtAQP1 is a membrane CO2 pore with physiological functions.* Nature, 2003. **425**(6959): p. 734 - 737.
3. Sade, N., et al., *Improving plant stress tolerance and yield production: is the tonoplast aquaporin SlTIP2;2 a key to isohydric to anisohydric conversion?* New Phytologist, 2009. **181**(3): p. 651-661.
4. Sade, N., et al., *The Role of Tobacco Aquaporin1 in Improving Water Use Efficiency, Hydraulic Conductivity, and Yield Production Under Salt Stress.* Plant Physiology, 2010. **152**(1): p. 245-254.
5. Aharon, R., et al., *Overexpression of a plasma membrane aquaporin in transgenic tobacco improves plant vigor under favorable growth conditions but not under drought or salt stress.* Plant Cell, 2003. **15**(2): p. 439-47.
6. Pang, Y., et al., *Overexpression of the tonoplast aquaporin AtTIP5;1 conferred tolerance to boron toxicity in Arabidopsis.* Journal of Genetics and Genomics, 2010. **37**(6): p. 389-397.
7. Peng, Y., et al., *Overexpression of a Panax ginseng tonoplast aquaporin alters salt tolerance, drought tolerance and cold acclimation ability in transgenic Arabidopsis plants.* Planta, 2007. **226**(3): p. 729-740.
8. Ishibashi, K., S. Hara, and S. Kondo, *Aquaporin water channels in mammals.* Clinical and Experimental Nephrology, 2009. **13**(2): p. 107-117.
9. Verkman, A.S., M.O. Anderson, and M.C. Papadopoulos, *Aquaporins: important but elusive drug targets.* Nat Rev Drug Discov, 2014. **13**(4): p. 259-277.
10. Henderson, L.J., *The Fitness of the Environment, an Inquiry Into the Biological Significance of the Properties of Matter.* The American Naturalist, 1913. **47**(554): p. 105-115.
11. Stein, W.D. and J.F. Danielli, *Structure and function in red cell permeability.* Discussions of the Faraday Society, 1956. **21**(0): p. 238-251.
12. Böhm, J., *Capillarität und Saftsteigen.* Ber Dtsch Bot Ges, 1893. **11**: p. 203–212.

13. Steudle, E., *The Cohesion-Tension Mechanism and the Acquisition of Water by Plant Roots.* Annu Rev Plant Physiol Plant Mol Biol, 2001. **52**: p. 847-875.
14. Maurel, C., et al., *Purified vesicles of tobacco cell vacuolar and plasma membranes exhibit dramatically different water permeability and water channel activity.* Proceedings of the National Academy of Sciences of the United States of America, 1997. **94**(13): p. 7103-7108.
15. Heldt, H.-W. and F. Heldt. *Plant biochemistry.* 2005; Available from: http://site.ebrary.com/id/10169848.
16. Satter, R.L., et al., *Potassium Flux and Leaf Movement in Samanea saman : I. Rhythmic Movement.* The Journal of General Physiology, 1974. **64**(4): p. 413-430.
17. Fleurat-Lessard, P., et al., *Increased Expression of Vacuolar Aquaporin and H+-ATPase Related to Motor Cell Function in Mimosa pudica L.* Plant Physiology, 1997. **114**(3): p. 827-834.
18. Siefritz, F., et al., *The plasma membrane aquaporin NtAQP1 is a key component of the leaf unfolding mechanism in tobacco.* Plant J, 2004. **37**(2): p. 147-55.
19. Evans, D.H., P.M. Piermarini, and K.P. Choe, *The Multifunctional Fish Gill: Dominant Site of Gas Exchange, Osmoregulation, Acid-Base Regulation, and Excretion of Nitrogenous Waste.* Physiological Reviews, 2005. **85**(1): p. 97-177.
20. Karnaky, K.J., *STRUCTURE AND FUNCTION OF THE CHLORIDE CELL OF FUNDULUS-HETEROCLITUS AND OTHER TELEOSTS.* American Zoologist, 1986. **26**(1): p. 209-224.
21. Tipsmark, C.K., et al., *Branchial expression patterns of claudin isoforms in Atlantic salmon during seawater acclimation and smoltification.* American Journal of Physiology - Regulatory, Integrative and Comparative Physiology, 2008. **294**(5): p. R1563-R1574.
22. Aoki, M., et al., *Intestinal water absorption through aquaporin 1 expressed in the apical membrane of mucosal epithelial cells in seawater-adapted Japanese eel.* Journal of Experimental Biology, 2003. **206**(19): p. 3495-3505.
23. Tipsmark, C.K., K.J. Sørensen, and S.S. Madsen, *Aquaporin expression dynamics in osmoregulatory tissues of Atlantic salmon during smoltification and seawater acclimation.* The Journal of Experimental Biology, 2010. **213**(3): p. 368-379.
24. Brown, J.A., et al., *Single nephron filtration rates (SNGFR) in the trout,Salmo gairdneri.* Pflügers Archiv, 1978. **377**(1): p. 101-108.
25. Metz B., D.O.R., Bosch P.R., Dave R., Meyer L.A., *Contribution of Working Group III to the Fourth Assessment Report of the Intergovernmental Panel on*

Climate Change. Cambridge University Press, Cambridge, United Kingdom and New York, NY, USA, 2007.
26. Sutton, M.A., et al., *Too much of a good thing.* Nature, 2011. **472**(7342): p. 159-161.
27. Sutton, M.A. and H. van Grinsven, *The European Nitrogen Assessment - Sources, Effects and Policy Perspectives.* 2011.
28. Yamaya, T., et al., *A Supply of Nitrogen Causes Increase in the Level of NADH-Dependent Glutamate Synthase Protein and in the Activity of the Enzyme in Roots of Rice Seedlings.* Plant and Cell Physiology, 1995. **36**(7): p. 1197-1204.
29. Schenk, M. and J. Wehrmann, *The influence of ammonia in nutrient solution on growth and metabolism of cucumber plants.* Plant and Soil, 1979. **53**(3): p. 403-414.
30. Britto, D.T., et al., *Futile transmembrane NH4+ cycling: A cellular hypothesis to explain ammonium toxicity in plants.* Proceedings of the National Academy of Sciences, 2001. **98**(7): p. 4255-4258.
31. Sutton, M.A., et al., *Assessment of the magnitude of ammonia emissions in the United Kingdom.* Atmospheric Environment, 1995. **29**(12): p. 1393-1411.
32. Graham D., F., et al., *On the Gaseous Exchange of Ammonia between Leaves and the Environment: Determination of the Ammonia Compensation Point.* Plant Physiol., 1980. **66**(4): p. 710–714.
33. Silva, L.C.R., et al., *Carbon dioxide level and form of soil nitrogen regulate assimilation of atmospheric ammonia in young trees.* Scientific Reports, 2015. **5**: p. 13141.
34. Johnson, K.D., H. Höfte, and M.J. Chrispeels, *An intrinsic tonoplast protein of protein storage vacuoles in seeds is structurally related to a bacterial solute transporter (GIpF).* Plant Cell, 1990. **2**(6): p. 525-532.
35. Tobin, A.K. and T. Yamaya, *Cellular compartmentation of ammonium assimilation in rice and barley.* Journal of Experimental Botany, 2001. **52**(356): p. 591-604.
36. Soria, L.R., et al., *Ammonia detoxification via ureagenesis in rat hepatocytes involves mitochondrial aquaporin-8 channels.* Hepatology, 2013. **57**(5): p. 2061-2071.
37. Suárez, I., G. Bodega, and B. Fernández, *Glutamine synthetase in brain: effect of ammonia.* Neurochemistry International, 2002. **41**(2–3): p. 123-142.
38. Calamita, G., et al., *The Inner Mitochondrial Membrane Has Aquaporin-8 Water Channels and Is Highly Permeable to Water.* Journal of Biological Chemistry, 2005. **280**(17): p. 17149-17153.

39. Saparov, S.M., et al., *Fast and Selective Ammonia Transport by Aquaporin-8.* Journal of Biological Chemistry, 2007. **282**(8): p. 5296-5301.
40. Smith, H.W., *THE EXCRETION OF AMMONIA AND UREA BY THE GILLS OF FISH.* Journal of Biological Chemistry, 1929. **81**(3): p. 727-742.
41. Gorin, M.B., et al., *The major intrinsic protein (MIP) of the bovine lens fiber membrane: Characterization and structure based on cDNA cloning.* Cell, 1984. **39**(1): p. 49-59.
42. Pao, G.M., et al., *Evolution of the MIP family of integral membrane transport proteins.* Mol Microbiol, 1991. **5**(1): p. 33-7.
43. Park, J.H. and M.H. Saier, Jr., *Phylogenetic characterization of the MIP family of transmembrane channel proteins.* J Membr Biol, 1996. **153**(3): p. 171-80.
44. Kozono, D., et al., *Functional Expression and Characterization of an Archaeal Aquaporin: AqpM FROM METHANOTHERMOBACTER MARBURGENSIS.* Journal of Biological Chemistry, 2003. **278**(12): p. 10649-10656.
45. Danielson, J. and U. Johanson, *Phylogeny of major intrinsic proteins.* Adv Exp Med Biol, 2010(679): p. 19-31.
46. Morishita, Y., et al., *Molecular Mechanisms and Drug Development in Aquaporin Water Channel Diseases: Aquaporin Superfamily (Superaquaporins): Expansion of Aquaporins Restricted to Multicellular Organisms.* Journal of Pharmacological Sciences, 2004. **96**(3): p. 276-279.
47. Johanson, U., et al., *The complete set of genes encoding major intrinsic proteins in Arabidopsis provides a framework for a new nomenclature for major intrinsic proteins in plants.* Plant Physiol, 2001. **126**(4): p. 1358-69.
48. Sakurai, J., et al., *Identification of 33 rice aquaporin genes and analysis of their expression and function.* Plant Cell Physiol, 2005. **46**(9): p. 1568-77.
49. Reuscher, S., et al., *Genome-Wide Identification and Expression Analysis of Aquaporins in Tomato.* PLoS ONE, 2013. **8**(11): p. e79052.
50. Chaumont, F., et al., *Aquaporins constitute a large and highly divergent protein family in maize.* Plant Physiol, 2001. **125**(3): p. 1206-15.
51. Danielson, J. and U. Johanson, *Unexpected complexity of the Aquaporin gene family in the moss Physcomitrella patens.* BMC Plant Biology, 2008. **8**(1): p. 45.
52. Anderberg, H., J. Danielson, and U. Johanson, *Algal MIPs, high diversity and conserved motifs.* BMC Evolutionary Biology, 2011. **11**(1): p. 110.
53. Kammerloher, W., et al., *Water channels in the plant plasma membrane cloned by immunoselection from a mammalian expression system.* Plant J, 1994. **6**(2): p. 187-99.

54. Heymann, J. and A. Engel, *Aquaporins: Phylogeny, Structure, and Physiology of Water Channels.* News Physiol Sci, 1999. **14**: p. 187 - 193.
55. Gustavsson, S., et al., *A Novel Plant Major Intrinsic Protein in Physcomitrella patens Most Similar to Bacterial Glycerol Channels.* Plant Physiology, 2005. **139**(1): p. 287-295.
56. Moshelion, M., et al., *Plasma membrane aquaporins in the motor cells of Samanea saman: diurnal and circadian regulation.* Plant Cell, 2002. **14**(3): p. 727-39.
57. Fetter, K., et al., *Interactions between plasma membrane aquaporins modulate their water channel activity.* Plant Cell, 2004. **16**(1): p. 215-28.
58. Hanba, Y.T., et al., *Overexpression of the barley aquaporin HvPIP2;1 increases internal CO(2) conductance and CO(2) assimilation in the leaves of transgenic rice plants.* Plant Cell Physiol, 2004. **45**(5): p. 521-9.
59. Uehlein, N., et al., *Function of Nicotiana tabacum Aquaporins as Chloroplast Gas Pores Challenges the Concept of Membrane CO2 Permeability.* The Plant Cell Online, 2008. **20**(3): p. 648-657.
60. Bienert, G.P., et al., *Specific Aquaporins Facilitate the Diffusion of Hydrogen Peroxide across Membranes.* Journal of Biological Chemistry, 2007. **282**(2): p. 1183-1192.
61. Dynowski, M., et al., *Plant plasma membrane water channels conduct the signalling molecule H2O2.* Biochem J, 2008. **414**(1): p. 53-61.
62. Hooijmaijers, C., et al., *Hydrogen peroxide permeability of plasma membrane aquaporins of Arabidopsis thaliana.* Journal of Plant Research, 2012. **125**(1): p. 147-153.
63. Klebl, F., M. Wolf, and N. Sauer, *A defect in the yeast plasma membrane urea transporter Dur3p is complemented by CpNIP1, a Nod26-like protein from zucchini (Cucurbita pepo L.), and by Arabidopsis thaliana delta-TIP or gamma-TIP.* FEBS Lett, 2003. **547**(1-3): p. 69-74.
64. Loque, D., et al., *Tonoplast intrinsic proteins AtTIP2;1 and AtTIP2;3 facilitate NH3 transport into the vacuole.* Plant Physiol, 2005. **137**(2): p. 671 - 680.
65. Gerbeau, P., et al., *Aquaporin Nt-TIPa can account for the high permeability of tobacco cell vacuolar membrane to small neutral solutes.* The Plant Journal, 1999. **18**(6): p. 577-587.
66. Liu, L.H., et al., *Urea transport by nitrogen-regulated tonoplast intrinsic proteins in Arabidopsis.* Plant Physiol, 2003. **133**(3): p. 1220-8.
67. Li, G.-W., et al., *Transport functions and expression analysis of vacuolar membrane aquaporins in response to various stresses in rice.* Journal of Plant Physiology, 2008. **165**(18): p. 1879-1888.

68. Engelund, M.B., et al., *Differential expression and novel permeability properties of three aquaporin 8 paralogs from seawater-challenged Atlantic salmon smolts.* The Journal of Experimental Biology, 2013. **216**(20): p. 3873-3885.
69. Fu, D., et al., *Structure of a glycerol-conducting channel and the basis for its selectivity.* Science, 2000. **290**(5491): p. 481-6.
70. Richey, D.P. and E.C.C. Lin, *Importance of Facilitated Diffusion for Effective Utilization of Glycerol by Escherichia coli.* Journal of Bacteriology, 1972. **112**(2): p. 784-790.
71. Meng, Y.L., Z. Liu, and B.P. Rosen, *As(III) and Sb(III) Uptake by GlpF and Efflux by ArsB in Escherichia coli.* Journal of Biological Chemistry, 2004. **279**(18): p. 18334-18341.
72. Liu, Z., et al., *Arsenite transport by mammalian aquaglyceroporins AQP7 and AQP9.* Proceedings of the National Academy of Sciences of the United States of America, 2002. **99**(9): p. 6053-6058.
73. Liu, Z., et al., *Arsenic trioxide uptake by human and rat aquaglyceroporins.* Biochemical and Biophysical Research Communications, 2004. **316**(4): p. 1178-1185.
74. Takano, J., et al., *The Arabidopsis major intrinsic protein NIP5;1 is essential for efficient boron uptake and plant development under boron limitation.* Plant Cell, 2006. **18**(6): p. 1498 - 1509.
75. Ma, J.F., et al., *A silicon transporter in rice.* Nature, 2006. **440**(7084): p. 688-91.
76. Deshmukh, R., et al., *Identification and functional characterization of silicon transporters in soybean using comparative genomics of major intrinsic proteins in Arabidopsis and rice.* Plant Molecular Biology, 2013. **83**(4-5): p. 303-315.
77. Wallace, I. and D. Roberts, *Distinct transport selectivity of two structural subclasses of the nodulin-like intrinsic protein family of plant aquaglyceroporin channels.* Biochemistry, 2005. **44**(51): p. 16826 - 16834.
78. Harries, W.E., et al., *The channel architecture of aquaporin 0 at a 2.2-A resolution.* Proc Natl Acad Sci U S A, 2004. **101**(39): p. 14045-50.
79. Sui, H., et al., *Structural basis of water-specific transport through the AQP1 water channel.* Nature, 2001. **414**(6866): p. 872-8.
80. Frick, A., et al., *X-ray structure of human aquaporin 2 and its implications for nephrogenic diabetes insipidus and trafficking.* Proceedings of the National Academy of Sciences, 2014. **111**(17): p. 6305-6310.
81. Ho, J.D., et al., *Crystal structure of human aquaporin 4 at 1.8 Å and its mechanism of conductance.* Proceedings of the National Academy of Sciences, 2009. **106**(18): p. 7437-7442.

82. Horsefield, R., et al., *High-resolution x-ray structure of human aquaporin 5.* Proceedings of the National Academy of Sciences, 2008. **105**(36): p. 13327-13332.
83. Tornroth-Horsefield, S., et al., *Structural mechanism of plant aquaporin gating.* Nature, 2006. **439**(7077): p. 688-94.
84. Kosinska Eriksson, U., et al., *Subangstrom Resolution X-Ray Structure Details Aquaporin-Water Interactions.* Science, 2013. **340**(6138): p. 1346-1349.
85. Savage, D.F., et al., *Architecture and selectivity in aquaporins: 2.5 a X-ray structure of aquaporin Z.* PLoS Biol, 2003. **1**(3): p. E72.
86. Newby, Z.E.R., et al., *Crystal structure of the aquaglyceroporin PfAQP from the malarial parasite Plasmodium falciparum.* Nat Struct Mol Biol, 2008. **15**(6): p. 619-625.
87. Lee, J.K., et al., *Structural basis for conductance by the archaeal aquaporin AqpM at 1.68 A.* Proc Natl Acad Sci U S A, 2005. **102**(52): p. 18932-7.
88. Plasencia, I., et al., *Structure and Stability of the Spinach Aquaporin SoPIP2;1 in Detergent Micelles and Lipid Membranes.* PLoS ONE, 2011. **6**(2): p. e14674.
89. König, N., G.A. Zampighi, and P.J.G. Butler, *Characterisation of the major intrinsic protein (MIP) from bovine lens fibre membranes by electron microscopy and hydrodynamics.* Journal of Molecular Biology, 1997. **265**(5): p. 590-602.
90. Smith, B.L. and P. Agre, *Erythrocyte Mr 28,000 transmembrane protein exists as a multisubunit oligomer similar to channel proteins.* Journal of Biological Chemistry, 1991. **266**(10): p. 6407-6415.
91. Aerts, T., et al., *Hydrodynamic characterization of the major intrinsic protein from the bovine lens fiber membranes. Extraction in n-octyl-beta-D-glucopyranoside and evidence for a tetrameric structure.* Journal of Biological Chemistry, 1990. **265**(15): p. 8675-8680.
92. Verbavatz, J.M., et al., *Tetrameric assembly of CHIP28 water channels in liposomes and cell membranes: a freeze-fracture study.* The Journal of Cell Biology, 1993. **123**(3): p. 605-618.
93. Borgnia, M.J., et al., *Functional reconstitution and characterization of AqpZ, the E. coli water channel protein.* Journal of Molecular Biology, 1999. **291**(5): p. 1169-1179.
94. Veerappan, A., et al., *The Tetrameric α-Helical Membrane Protein GlpF Unfolds via a Dimeric Folding Intermediate.* Biochemistry, 2011. **50**(47): p. 10223-10230.
95. Kukulski, W., et al., *The 5A structure of heterologously expressed plant aquaporin SoPIP2;1.* J Mol Biol, 2005. **350**(4): p. 611-6.

96. Bienert, G.P., et al., *A conserved cysteine residue is involved in disulfide bond formation between plant plasma membrane aquaporin monomers.* Biochemical Journal, 2012. **445**(1): p. 101-111.
97. Jung, J.S., et al., *Molecular structure of the water channel through aquaporin CHIP. The hourglass model.* J Biol Chem, 1994. **269**(20): p. 14648-54.
98. de Groot, B.L., et al., *The Mechanism of Proton Exclusion in the Aquaporin-1 Water Channel.* Journal of Molecular Biology, 2003. **333**(2): p. 279-293.
99. Chakrabarti, N., et al., *Molecular basis of proton blockage in aquaporins.* Structure (Camb), 2004. **12**(1): p. 65-74.
100. Chakrabarti, N., B. Roux, and R. Pomès, *Structural Determinants of Proton Blockage in Aquaporins.* Journal of Molecular Biology, 2004. **343**(2): p. 493-510.
101. Tajkhorshid, E., et al., *Control of the selectivity of the aquaporin water channel family by global orientational tuning.* Science, 2002. **296**(5567): p. 525-30.
102. Cukierman, S., *Et tu, Grotthuss! and other unfinished stories.* Biochimica et Biophysica Acta (BBA) - Bioenergetics, 2006. **1757**(8): p. 876-885.
103. de Groot, B.L. and H. Grubmüller, *The dynamics and energetics of water permeation and proton exclusion in aquaporins.* Current Opinion in Structural Biology, 2005. **15**(2): p. 176-183.
104. Wu, B., et al., *Concerted action of two cation filters in the aquaporin water channel.* The EMBO Journal, 2009. **28**(15): p. 2188-2194.
105. Wree, D., et al., *Requirement for asparagine in the aquaporin NPA sequence signature motifs for cation exclusion.* FEBS Journal, 2011. **278**(5): p. 740-748.
106. O.S. Smart, J.M.G., B.A. Wallace, *The Pore Dimensions of Gramicidin A* Biophysical Journal, 1993(65): p. 2455-2460.
107. Froger, A., et al., *Prediction of functional residues in water channels and related proteins.* Protein Sci, 1998. **7**(6): p. 1458-68.
108. Beitz, E., et al., *In Vitro Analysis and Modification of Aquaporin Pore Selectivity*, in *Aquaporins*, E. Beitz, Editor. 2009, Springer Berlin Heidelberg: Berlin, Heidelberg. p. 77-92.
109. Li, H., et al., *Enhancement of Proton Conductance by Mutations of the Selectivity Filter of Aquaporin-1.* Journal of Molecular Biology, 2011. **407**(4): p. 607-620.
110. Beitz, E., et al., *Point mutations in the aromatic/arginine region in aquaporin 1 allow passage of urea, glycerol, ammonia, and protons.* Proc Natl Acad Sci USA, 2006. **103**(2): p. 269 - 274.
111. Gupta, A. and R. Sankararamakrishnan, *Genome-wide analysis of major intrinsic proteins in the tree plant Populus trichocarpa: Characterization of XIP*

subfamily of aquaporins from evolutionary perspective. BMC Plant Biology, 2009. **9**(1): p. 134.
112. Bienert, G.P., et al., *Solanaceae XIPs are plasma membrane aquaporins that facilitate the transport of many uncharged substrates.* The Plant Journal, 2011. **66**(2): p. 306-317.
113. Bansal, A. and R. Sankararamakrishnan, *Homology modeling of major intrinsic proteins in rice, maize and Arabidopsis: comparative analysis of transmembrane helix association and aromatic/arginine selectivity filters.* BMC Structural Biology, 2007. 7(1): p. 27.
114. Maeshima, M., *TONOPLAST TRANSPORTERS: Organization and Function.* Annual Review of Plant Physiology and Plant Molecular Biology, 2001. **52**(1): p. 469-497.
115. Johansson, I., et al., *The major integral proteins of spinach leaf plasma membranes are putative aquaporins and are phosphorylated in response to Ca2+ and apoplastic water potential.* Plant Cell, 1996. **8**(7): p. 1181-91.
116. Schmid, M., et al., *A gene expression map of Arabidopsis thaliana development.* Nat Genet, 2005. **37**(5): p. 501-6.
117. Alexandersson, E., et al., *Transcriptional regulation of aquaporins in accessions of Arabidopsis in response to drought stress.* The Plant Journal, 2010. **61**(4): p. 650-660.
118. Alexandersson, E., et al., *Whole gene family expression and drought stress regulation of aquaporins.* Plant Mol Biol, 2005. **59**(3): p. 469 - 484.
119. Carbrey, J.M., et al., *Aquaglyceroporin AQP9: Solute permeation and metabolic control of expression in liver.* Proceedings of the National Academy of Sciences, 2003. **100**(5): p. 2945-2950.
120. Gattolin, S., et al., *In vivo imaging of the tonoplast intrinsic protein family in Arabidopsis roots.* BMC Plant Biology, 2009. **9**(1): p. 133.
121. Ludevid, D., et al., *The Expression Pattern of the Tonoplast Intrinsic Protein gamma-TIP in Arabidopsis thaliana Is Correlated with Cell Enlargement.* Plant Physiol, 1992. **100**: p. 1633 - 1639.
122. Chaumont, F., et al., *Characterization of a maize tonoplast aquaporin expressed in zones of cell division and elongation.* Plant Physiol, 1998. **117**: p. 1143 - 1152.
123. Higuchi, T., et al., *Molecular Cloning, Water Channel Activity and Tissue Specific Expression of Two Isoforms of Radish Vacuolar Aquaporin1.* Plant and Cell Physiology, 1998. **39**(9): p. 905-913.
124. Gattolin, S., M. Sorieul, and L. Frigerio, *Mapping of Tonoplast Intrinsic Proteins in Maturing and Germinating Arabidopsis Seeds Reveals Dual*

Localization of Embryonic TIPs to the Tonoplast and Plasma Membrane. Molecular Plant, 2011. **4**(1): p. 180-189.
125. Suga, S., S. Komatsu, and M. Maeshima, *Aquaporin isoforms responsive to salt and water stresses and phytohormones in radish seedlings.* Plant Cell Physiol, 2002. **43**(10): p. 1229-37.
126. Blobel, G., *Intracellular protein topogenesis.* Proceedings of the National Academy of Sciences, 1980. **77**(3): p. 1496-1500.
127. Simon, S.M. and G. Blobel, *A protein-conducting channel in the endoplasmic reticulum.* Cell, 1991. **65**(3): p. 371-380.
128. Shi, L.-b., et al., *Distinct biogenesis mechanisms for the water channels MIWC and CHIP28 at the endoplasmic reticulum.* Biochemistry, 1995. **34**(26): p. 8250-8256.
129. Skach, W.R., et al., *Biogenesis and transmembrane topology of the CHIP28 water channel at the endoplasmic reticulum.* The Journal of Cell Biology, 1994. **125**(4): p. 803-815.
130. Virkki, M.T., et al., *Folding of Aquaporin 1: Multiple evidence that helix 3 can shift out of the membrane core.* Protein Science, 2014: p. n/a-n/a.
131. Lee, H.K., et al., *Drought Stress-Induced Rma1H1, a RING Membrane-Anchor E3 Ubiquitin Ligase Homolog, Regulates Aquaporin Levels via Ubiquitination in Transgenic Arabidopsis Plants.* The Plant Cell Online, 2009. **21**(2): p. 622-641.
132. Prak, S., et al., *Multiple Phosphorylations in the C-terminal Tail of Plant Plasma Membrane Aquaporins: Role in Subcellular Trafficking of AtPIP2;1 in Response to Salt Stress.* Molecular & Cellular Proteomics, 2008. **7**(6): p. 1019-1030.
133. Paciorek, T., et al., *Auxin inhibits endocytosis and promotes its own efflux from cells.* Nature, 2005. **435**(7046): p. 1251-1256.
134. Fushimi, K., S. Sasaki, and F. Marumo, *Phosphorylation of Serine 256 Is Required for cAMP-dependent Regulatory Exocytosis of the Aquaporin-2 Water Channel.* Journal of Biological Chemistry, 1997. **272**(23): p. 14800-14804.
135. Vandeleur, R.K., et al., *The Role of Plasma Membrane Intrinsic Protein Aquaporins in Water Transport through Roots: Diurnal and Drought Stress Responses Reveal Different Strategies between Isohydric and Anisohydric Cultivars of Grapevine.* Plant Physiology, 2009. **149**(1): p. 445-460.
136. Zelazny, E., et al., *FRET imaging in living maize cells reveals that plasma membrane aquaporins interact to regulate their subcellular localization.* Proceedings of the National Academy of Sciences, 2007. **104**(30): p. 12359-12364.

137. Hofte, H., et al., *Vegetative and Seed-Specific Forms of Tonoplast Intrinsic Protein in the Vacuolar Membrane of Arabidopsis thaliana.* Plant Physiol, 1992. **99**(2): p. 561-570.
138. Robinson, D.G., et al., *PIP1 Aquaporins Are Concentrated in Plasmalemmasomes of Arabidopsis thaliana Mesophyll.* Plant Physiol, 1996. **111**(2): p. 645-649.
139. Fortin, M.G., N.A. Morrison, and D.P. Verma, *Nodulin-26, a peribacteroid membrane nodulin is expressed independently of the development of the peribacteroid compartment.* Nucleic Acids Res, 1987. **15**(2): p. 813-24.
140. Amiry-Moghaddam, M., et al., *Brain mitochondria contain aquaporin water channels: evidence for the expression of a short AQP9 isoform in the inner mitochondrial membrane.* The FASEB Journal, 2005. **19**(11): p. 1459-1467.
141. Ishikawa, F., et al., *Novel type aquaporin SIPs are mainly localized to the ER membrane and show cell-specific expression in Arabidopsis thaliana.* FEBS Lett, 2005. **579**(25): p. 5814-20.
142. Mizutani, M., et al., *Aquaporin NIP2;1 is Mainly Localized to the ER Membrane and Shows Root-Specific Accumulation in Arabidopsis thaliana.* Plant and Cell Physiology, 2006. **47**(10): p. 1420-1426.
143. Maurel, C., et al., *Phosphorylation regulates the water channel activity of the seed-specific aquaporin alpha-TIP.* Embo J, 1995. **14**(13): p. 3028-35.
144. Johansson, I., et al., *Water transport activity of the plasma membrane aquaporin PM28A is regulated by phosphorylation.* Plant Cell, 1998. **10**(3): p. 451-9.
145. Aroca, R., et al., *The role of aquaporins and membrane damage in chilling and hydrogen peroxide induced changes in the hydraulic conductance of maize roots.* Plant Physiol, 2005. **137**(1): p. 341-53.
146. Nyblom, M., et al., *Structural and Functional Analysis of SoPIP2;1 Mutants Adds Insight into Plant Aquaporin Gating.* Journal of Molecular Biology, 2009. **387**(3): p. 653-668.
147. Van Wilder, V., et al., *Maize Plasma Membrane Aquaporins Belonging to the PIP1 and PIP2 Subgroups are in vivo Phosphorylated.* Plant and Cell Physiology, 2008. **49**(9): p. 1364-1377.
148. Gerbeau, P., et al., *The water permeability of Arabidopsis plasma membrane is regulated by divalent cations and pH.* Plant J, 2002. **30**(1): p. 71-81.
149. Tournaire-Roux, C., et al., *Cytosolic pH regulates root water transport during anoxic stress through gating of aquaporins.* Nature, 2003. **425**(6956): p. 393-7.
150. Frick, A., M. Järvå, and S. Törnroth-Horsefield, *Structural basis for pH gating of plant aquaporins.* FEBS Letters, 2013. **587**(7): p. 989-993.

151. Verdoucq, L., A. Grondin, and C. Maurel, *Structure-function analysis of plant aquaporin AtPIP2;1 gating by divalent cations and protons.* Biochem J, 2008. **415**(3): p. 409-16.
152. Frick, A., et al., *Mercury increases water permeability of a plant aquaporin through a non-cysteine-related mechanism.* Biochemical Journal, 2013. **454**(3): p. 491-499.
153. Zelazny, E., et al., *An N-terminal diacidic motif is required for the trafficking of maize aquaporins ZmPIP2;4 and ZmPIP2;5 to the plasma membrane.* The Plant Journal, 2009. **57**(2): p. 346-355.
154. Bellati, J., et al., *Intracellular pH sensing is altered by plasma membrane PIP aquaporin co-expression.* Plant Molecular Biology, 2010. **74**(1): p. 105-118.
155. Laganowsky, A., et al., *Membrane proteins bind lipids selectively to modulate their structure and function.* Nature, 2014. **510**(7503): p. 172-175.
156. Tong, J., Margaret M. Briggs, and Thomas J. McIntosh, *Water Permeability of Aquaporin-4 Channel Depends on Bilayer Composition, Thickness, and Elasticity.* Biophysical Journal, 2012. **103**(9): p. 1899-1908.
157. Soveral, G., R.I. Macey, and T.F. Moura, *Membrane stress causes inhibition of water channels in brush border membrane vesicles from kidney proximal tubule.* Biology of the Cell, 1997. **89**(5-6): p. 275-282.
158. Fischer, G., et al., *Crystal Structure of a Yeast Aquaporin at 1.15 Å Reveals a Novel Gating Mechanism.* PLoS Biol, 2009. **7**(6): p. e1000130.
159. Soveral, G., et al., *Membrane tension regulates water transport in yeast.* Biochimica et Biophysica Acta (BBA) - Biomembranes, 2008. **1778**(11): p. 2573-2579.
160. Ozu, M., et al., *Human AQP1 Is a Constitutively Open Channel that Closes by a Membrane-Tension-Mediated Mechanism.* Biophysical Journal, 2013. **104**(1): p. 85-95.
161. Johnson, K.D. and M.J. Chrispeels, *Tonoplast-Bound Protein Kinase Phosphorylates Tonoplast Intrinsic Protein.* Plant Physiology, 1992. **100**(4): p. 1787-1795.
162. Sjovall-Larsen, S., et al., *Purification and characterization of two protein kinases acting on the aquaporin SoPIP2;1.* Biochim Biophys Acta, 2006. **1758**(8): p. 1157-64.
163. Guenther, J.F., et al., *Phosphorylation of soybean nodulin 26 on serine 262 enhances water permeability and is regulated developmentally and by osmotic signals.* Plant Cell, 2003. **15**(4): p. 981-91.
164. Azad, A.K., et al., *Phosphorylation of plasma membrane aquaporin regulates temperature-dependent opening of tulip petals.* Plant Cell Physiol, 2004. **45**(5): p. 608-17.

165. Azad, A.K., et al., *Characterization of protein phosphatase 2A acting on phosphorylated plasma membrane aquaporin of tulip petals.* Biosci Biotechnol Biochem, 2004. **68**(5): p. 1170-4.
166. Sarda, X., et al., *Two TIP-like genes encoding aquaporins are expressed in sunflower guard cells.* Plant J, 1997. **12**(5): p. 1103-11.
167. Kaldenhoff, R., et al., *The blue light-responsive AthH2 gene of Arabidopsis thaliana is primarily expressed in expanding as well as in differentiating cells and encodes a putative channel protein of the plasmalemma.* Plant J, 1995. 7(1): p. 87-95.
168. Ecelbarger, C., et al., *Aquaporin-3 water channel localization and regulation in rat kidney.* Am J Physiol., 1995. **269**(5 Pt 2): p. F663-72.
169. Terris, J., et al., *Distribution of aquaporin-4 water channel expression within rat kidney.* Vol. 269. 1995. F775-F785.
170. DiGiovanni, S.R., et al., *Regulation of collecting duct water channel expression by vasopressin in Brattleboro rat.* Proceedings of the National Academy of Sciences, 1994. **91**(19): p. 8984-8988.
171. Deen, P., et al., *Requirement of human renal water channel aquaporin-2 for vasopressin-dependent concentration of urine.* Science, 1994. **264**(5155): p. 92-95.
172. Marples, D., et al., *Lithium-induced downregulation of aquaporin-2 water channel expression in rat kidney medulla.* The Journal of Clinical Investigation, 1995. **95**(4): p. 1838-1845.
173. Wallace, I.S. and D.M. Roberts, *Homology modeling of representative subfamilies of Arabidopsis major intrinsic proteins. Classification based on the aromatic/arginine selectivity filter.* Plant Physiol, 2004. **135**(2): p. 1059-68.
174. Jahn, T.P., et al., *Aquaporin homologues in plants and mammals transport ammonia.* FEBS Lett, 2004. **574**(1-3): p. 31-6.
175. Daniels, M.J., et al., *Characterization of a new vacuolar membrane aquaporin sensitive to mercury at a unique site.* Plant Cell, 1996. **8**(4): p. 587-99.
176. Holm, L., et al., *NH3 and NH 4 + permeability in aquaporin-expressing Xenopus oocytes.* Pflügers Archiv, 2005. **450**(6): p. 415-428.
177. Karlsson, M., et al., *An abundant TIP expressed in mature highly vacuolated cells.* Plant J, 2000. **21**(1): p. 83-90.
178. Ma, T., et al., *cDNA Cloning and Gene Structure of a Novel Water Channel Expressed Exclusively in Human Kidney: Evidence for a Gene Cluster of Aquaporins at Chromosome Locus 12q13.* Genomics, 1996. **35**(3): p. 543-550.

PLOS | BIOLOGY

RESEARCH ARTICLE

Crystal Structure of an Ammonia-Permeable Aquaporin

Andreas Kirscht[1], Shreyas S. Kaptan[2], Gerd Patrick Bienert[3,4], François Chaumont[3], Poul Nissen[5], Bert L. de Groot[2], Per Kjellbom[1], Pontus Gourdon[5¤]*, Urban Johanson[1]*

1 Department of Biochemistry and Structural Biology, Center for Molecular Protein Science, Lund University, Lund, Sweden, **2** The Max Planck Institute for Biophysical Chemistry, Computational Biomolecular Dynamics Group, Göttingen, Germany, **3** Institut des Sciences de la Vie, Université catholique de Louvain, Louvain-la-Neuve, Belgium, **4** IPK—Leibniz Institute of Plant Genetics and Crop Plant Research Department of Physiology and Cell Biology, Gatersleben, Germany, **5** Danish Research Institute of Translational Neuroscience–DANDRITE, Nordic-EMBL Partnership for Molecular Medicine, Department of Molecular Biology and Genetics, Aarhus University, Aarhus C, Denmark

¤ Current address: Department of Biomedical Sciences, University of Copenhagen, Blegdamsvej 3B, DK-2200 Copenhagen, Denmark, and Department of Experimental Medical Science, Lund University, Sölvegatan 19, SE-221 84 Lund, Sweden.
* urban.johanson@biochemistry.lu.se (UJ); pontus@sund.ku.dk (PG)

Citation: Kirscht A, Kaptan SS, Bienert GP, Chaumont F, Nissen P, de Groot BL, et al. (2016) Crystal Structure of an Ammonia-Permeable Aquaporin. PLoS Biol 14(3): e1002411. doi:10.1371/journal.pbio.1002411

Academic Editor: Raimund Dutzler, University of Zurich, SWITZERLAND

Received: November 17, 2015

Accepted: February 19, 2016

Published: March 30, 2016

Data Availability Statement: The refined structure and structure factor amplitudes have been deposited in the Protein Data Bank, www.pdb.org, with accession code 5I32. All other relevant data are within the paper and its Supporting Information files.

Funding: Financial support from the Swedish Research Council (VR) UJ, PK; Formas, the Research School of Pharmaceutical Sciences (FLÄK) PK; the Belgian National Fund for Scientific Research (FNRS), the Interuniversity Attraction Poles Programme–Belgian Science Policy, and the "Communauté française de Belgique–Actions de Recherches Concertées" are gratefully

Abstract

Aquaporins of the TIP subfamily (Tonoplast Intrinsic Proteins) have been suggested to facilitate permeation of water and ammonia across the vacuolar membrane of plants, allowing the vacuole to efficiently sequester ammonium ions and counteract cytosolic fluctuations of ammonia. Here, we report the structure determined at 1.18 Å resolution from twinned crystals of *Arabidopsis thaliana* aquaporin *At*TIP2;1 and confirm water and ammonia permeability of the purified protein reconstituted in proteoliposomes as further substantiated by molecular dynamics simulations. The structure of *At*TIP2;1 reveals an extended selectivity filter with the conserved arginine of the filter adopting a unique unpredicted position. The relatively wide pore and the polar nature of the selectivity filter clarify the ammonia permeability. By mutational studies, we show that the identified determinants in the extended selectivity filter region are sufficient to convert a strictly water-specific human aquaporin into an *At*TIP2;1-like ammonia channel. A flexible histidine and a novel water-filled side pore are speculated to deprotonate ammonium ions, thereby possibly increasing permeation of ammonia. The molecular understanding of how aquaporins facilitate ammonia flux across membranes could potentially be used to modulate ammonia losses over the plasma membrane to the atmosphere, e.g., during photorespiration, and thereby to modify the nitrogen use efficiency of plants.

Author Summary

Ammonia is a central molecule in nitrogen metabolism. Aquaporins are integral membrane proteins that form channels that accelerate the passive permeation of small polar uncharged molecules, like water and ammonia, across lipid membranes of the cell.

acknowledged FC; GPB was an FNRS Postdoctoral Researcher and is currently supported by an Emmy Noether grant 1668/1-1 from the Deutsche Forschungsgemeinschaft. PN was supported by an advanced research grant (Biomemos) of the European Research Council. Access to synchrotron sources was supported by the Danscatt program of the Danish Council of Independent Research, and by BioStruct-X contract 860. The funders had no role in study design, data collection and analysis, decision to publish, or preparation of the manuscript.

Competing Interests: The authors have declared that no competing interests exist.

Abbreviations: AQP, aquaporin; MD, molecular dynamics; NPA, Asn-Pro-Ala; OG, n-octyl-β-D-glucoside; PIP, plasma membrane intrinsic protein; PMF, potential mean force; POPC, 1-Palmitoyl-2-oleoylphosphatidylcholine; TIP, Tonoplast Intrinsic Protein.

Structural information of ammonia-permeable aquaporins has been lacking. Here, we report a high-resolution structure of the ammonia-permeable aquaporin *At*TIP2;1 and explore it by functional assays of mutants and by molecular dynamics simulations. Our data uncover unexpected features of the substrate selectivity filter, including a conserved arginine in a new orientation that is stabilized by interactions to a histidine that is linked to ammonia specificity. An additional histidine in a different part of *At*TIP2;1 fortifies the position of the arginine and interacts directly with the substrate in the channel. This histidine is therefore included in an extended selectivity filter, which should prompt a reinterpretation of the determinants of specificity in all types of aquaporins. We speculate that an intriguing water-filled side pore, next to the substrate-binding histidine, participates in deprotonating ammonium ions, which could increase the net permeation of ammonia. Understanding the principles of ammonia permeability may, in the future, allow us to modulate the passage of ammonia and generate crops with higher nitrogen-use efficiency.

Introduction

Nitrogen is a macronutrient that is often limiting for plant growth. Hence, efficient channeling and storage of ammonia, a central molecule in nitrogen metabolism, is of fundamental importance. Tonoplast Intrinsic Proteins (TIPs) belonging to the Major Intrinsic Protein family, also known as the aquaporin (AQP) superfamily, have been shown to conduct both water [1] and ammonia [2–4]. TIPs are present in all land plants, but whereas primitive plants like mosses only have one type of TIP (TIP6), five specialized subgroups (TIP1–5) have evolved in higher plants [5]. TIPs may constitute up to 40% of the protein in the vacuolar membrane, i.e., the tonoplast [6], and have been suggested to enhance nitrogen uptake efficiency and detoxification by acid entrapment of ammonium ions in vacuoles [3]. Furthermore, TIP-mediated increase of ammonia permeability was proposed to play a role in remobilization of vacuolar ammonia during nitrogen starvation [2] and in reallocation of nitrogen at senescence [7]. Recently, TIPs were included in a revised model of futile cycling under high ammonia conditions [8]. Sequence similarities to TIPs are observed in mammalian AQP8s [9], which are also ammonia-permeable [10] and have been implicated in pathological conditions like hyperammonemia and hepatic encephalopathy [11].

Crystal structures have established that AQPs are homotetramers, where each of the monomers holds a functional pore created by six membrane-spanning helices (helix 1–helix 6), five connecting loops (loop A–loop E), and two shorter helices (helix B and helix E; Fig 1), both displaying the AQP-signature motif Asn-Pro-Ala (NPA) [12–16]. Helices B and E connect at the NPA motifs in the middle of the membrane, thus forming a bipartite transmembrane segment. Different AQP isoforms facilitate permeation of a variety of small uncharged polar molecules, while protons are efficiently excluded from the pore in part by the positive charge, which is focused at the NPA region by the macro dipoles of the short helices [17]. Substrate specificity is thought to be achieved by the aromatic/arginine selectivity filter [18], which has been defined as four residues located at the noncytosolic end of the pore [19]. Of these residues, an arginine is conserved in the short helix E of most AQPs and contributes to the exclusion of protons [20], whereas a histidine in helix 5 is associated with water specificity [13]. AQPs permeable to ammonia and water called aquaammoniaporins, including the human *Hs*AQP8, typically lack the histidine in helix 5 but instead have a histidine in helix 2 [2–4]. However, all previously published AQP structures represent either water-specific channels (true AQPs) or the water- and glycerol-conducting aquaglyceroporins, so a further understanding of the structural

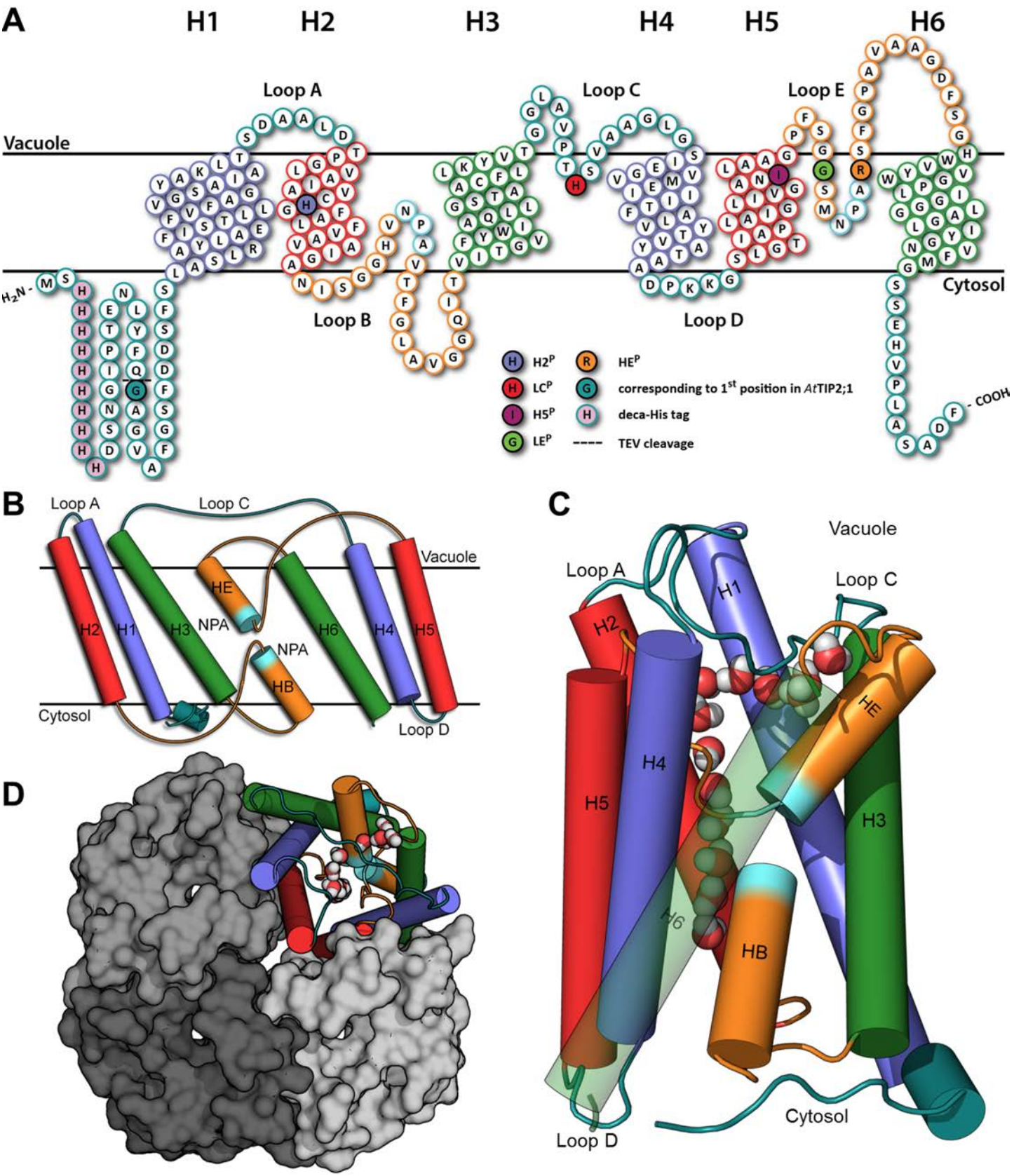
A
H1
H2
H3
H4
H5
H6
Loop A
Loop B
Loop C
Loop D
Loop E
Vacuole
Cytosol
H2P
LCP
H5P
LEP
HEP
corresponding to 1st position in AtTIP2;1
deca-His tag
TEV cleavage
B
Loop A
Loop C
Vacuole
HE
NPA
NPA
HB
H2
H1
H3
H6
H4
H5
Cytosol
Loop D
C
Vacuole
Loop A
Loop C
H1
H2
HE
H4
H5
H3
H6
HB
Cytosol
Loop D
D

Fig 1. Topology and structure of *At*TIP2;1. (A) Topology plot showing membrane-spanning helices (H1–H6) and intervening loops (A–E). Homologous regions in the internal repeat are indicated by colors. The five positions of an extended selectivity filter are marked according to the key within the figure. The glycine (Gly 1) corresponding to the initiator methionine in *At*TIP2;1 is shaded in dark cyan next to a dashed line representing the TEV cleavage site, and the N-terminal deca-His tag is shaded in purple. (B) Two short helices (HB and HE) in loop B and E, connected via conserved NPA-motifs, form a seventh transmembrane segment. All membrane-spanning segments are tilted in the membrane, but it is most accentuated in helices H3, H6, HB, and HE facing the lipid bilayer. (C) Eight water molecules form a single file in the main pore of the monomer, connecting the cytosolic and vacuolar vestibules. At the top right, five additional water molecules are seen in a side pore underneath loop C. (D) *At*TIP2;1 tetramer viewed from the vacuolar side. Monomers are shown in surface representation and in the cartoon representation used in (B) and (C).

doi:10.1371/journal.pbio.1002411.g001

features that confer ammonia selectivity has been missing. To close this gap in knowledge, we set out to crystallize the aquaammoniaporin *At*TIP2;1 from *A. thaliana*. Here, we present the crystal structure of *At*TIP2;1 determined at atomic resolution (1.18 Å with partial twinning). Combined with molecular dynamics (MD) simulations and functional studies of mutants, the structure provides new insight into the molecular basis of substrate selectivity in the AQP superfamily.

Results

Overall Structure of *At*TIP2;1

Heterologously expressed *At*TIP2;1 yielded up to 1.1 mg of purified and concentrated protein per g of wet *Pichia pastoris* cells. Purified *At*TIP2;1 was verified as a functional water channel, inhibited by mercury, and also permeable to ammonia (Fig 2). *At*TIP2;1, solubilized by n-octyl-β-D-glucoside, was crystallized at pH 5.0 and the structure determined at 1.18 Å resolution (Table 1). In the reported structure, 238 amino acid residues are resolved, and only the N-terminal tag and 12 native residues at the C-terminus are not included in the model. In contrast to other AQPs (e.g., *So*PIP2;1 [14], *Hs*AQP5 [15]), neither loops nor the resolved parts of terminal regions overlap with neighboring monomers in the tetramer. Loop A and loop D fold back on their own subunit and the N- and C-terminal regions meet at the outer edge of the cytoplasmic vestibule without restricting the pore (Fig 1C and 1D). Accordingly, the structure of *At*TIP2;1 constitutes an open channel where the cytosolic and vacuolar vestibules are connected by a pore lining eight water molecules in a single file.

An Extended Selectivity Filter

Interestingly, the pore diameter of *At*TIP2;1 at the NPA region is smaller than in other AQPs, and it remains constant at around 3 Å throughout the pore (Fig 3A and 3B). This is unusual, since in other structures of open AQPs, the aromatic/arginine selectivity filter constitutes the narrowest part of the pore. As mentioned earlier, amino acid residues at the four positions of the pore selectivity filter in helix 2, helix 5, loop E, and helix E (specifically denoted $H2^P$, $H5^P$, LE^P, and HE^P) are thought to determine the substrate specificity (Figs 1A and 3C). In line with this, TIP2s deviate from other AQPs (Fig 3D), and as expected from mutational studies and modeling [2,22], the wider selectivity filter is mainly due to an isoleucine (Ile 185) at position $H5^P$ in helix 5, replacing a histidine that is conserved in the water-specific AQPs. However, the most striking feature of the *At*TIP2;1 selectivity filter arises from an unpredicted positioning of the arginine at HE^P in helix E (Arg 200), a conserved residue in nearly all AQPs. In *At*TIP2;1, the arginine side chain is pushed to the side of the pore by a histidine located in loop C (His 131), which now appears as a fifth residue (LC^P) of an extended selectivity filter. The novel position of the arginine is further stabilized by a hydrogen bond to the histidine (His 63) at position $H2^P$ in helix 2, which occupies essentially the same space as corresponding aromatic residues of water and glycerol channels (e.g., Phe 81 in *So*PIP2;1 [14], Trp 48 in *Ec*GlpF [12]) without direct effects on the pore aperture. The close interaction with Arg 200 at position HE^P

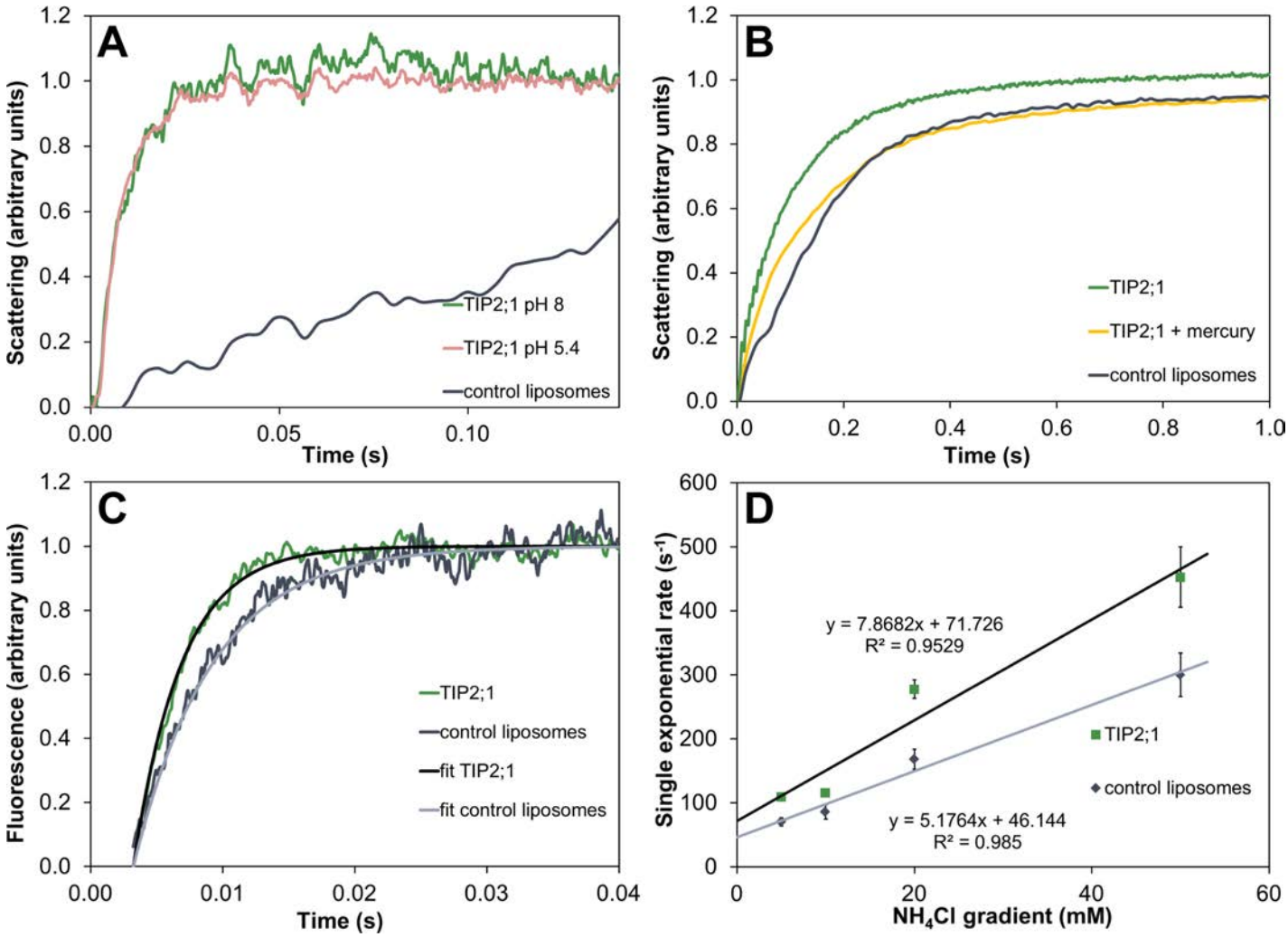

Fig 2. Functional assays. (A) Water permeability of liposomes with and without inserted *At*TIP2;1 measured at different pH values. Stopped-flow experiments with 100 mM hyperosmolar shift present high protein-facilitated conductivities at cytosolic and vacuolar pH. Relative single exponential rate constants of ca. 110 s^{-1} at LPR 30 demonstrate the ability to sustain a highly water-permeable vacuole. (B) Water permeability of purified *At*TIP2;1 (LPR 50) is inhibited by mercury as previously shown in oocytes [21]. (C) Ammonia uptake monitored by increased internal fluorescence after exchange of 20 mM NaCl with 20 mM NH_4Cl, corresponding to an initial NH_3 gradient of 4.5 μM. Proteoliposomes with *At*TIP2;1 (green) show higher permeability than equally-sized control liposomes (grey). Fitted curves yielding single exponential rates are also shown. (D) Summary of rates at different ammonia gradients. Equations and correlation coefficients are given for linear fitting of averaged single exponential rates as a function of total initial concentration gradient of NH_3/NH_4^+. Error bars represent the standard deviation of the rate within a set of approximately ten stopped-flow recordings per liposome sample. The underlying data of panels A–D can be found in S1 Data.

doi:10.1371/journal.pbio.1002411.g002

in helix E suggests a shift in the pK_a of His 63 at position $H2^P$, which is likely to stay unprotonated also in the acidic environment of the vacuole. In contrast to His 63, the additional His 131 at position LC^P in loop C points to the center of the pore and forms a hydrogen bond to a pore-water (Wat 2; Fig 3B). Hence, *At*TIP2;1 represents the first AQP structure where a residue in loop C (His 131) directly participates in interactions with the substrate in the selectivity region, defining an extended selectivity filter with five positions. The histidine residue at position $H2^P$ in helix 2 is conserved in all TIPs, whereas the histidine at position LC^P in loop C is only maintained in some types of TIPs, including the TIP2 isoforms, and appears to have been replaced by phenylalanine in a common ancestor of TIP1s and TIP3s (Fig 3D) [5]. A phenylalanine at position LC^P in loop C is also capable of sterically directing the arginine at position

Table 1. Crystallographic data and refinement statistics.

Data collection	
Space group	*I* 4
Cell dimensions	
a, *b*, *c* (Å) / *a*, *b*, *γ* (°)	89.3, 89.3, 82.5 / 90, 90, 90
Resolution (Å)	44.6–1.18 (1.22–1.18)*
R_{merge} (%)	7.46 (117)*
I/σ_I	12.65 (1.63)*
$CC_{1/2}$	1.00 (0.35)*
Completeness (%)/Redundancy	99.8 (98.0) / 13.2 (10.8)*
Refinement	
Resolution (Å)	44.6–1.18 (1.21–1.18)*
No. reflections	106,000 (10,267)*
Twin operator/Twin fraction (%)	k, h, -l / 40.7
R_{work} / R_{free} (%)	10.2 / 11.2
No. atoms	3,511
Protein (nonhydrogen)/Water	1,688 / 131
B-factors (Å^2)	16.1
Protein / Water	15.0 / 29.6
R.m.s. deviations	
Bond lengths (Å) / angles (°)	0.011 / 1.36
Ramachandran outliers (%)	0.4
Ramachandran favored (%)	98.0
Clashscore	0.00

*Highest resolution shell is shown in parenthesis.

doi:10.1371/journal.pbio.1002411.t001

HE^P in helix E to the side of the pore, but provides a more hydrophobic environment at the selectivity filter. Worth noting, similar to TIP3s, the mammalian AQP8s [9,10] also possess a histidine at position $H2^P$ in helix 2, lack a conserved histidine in loop C, and can be aligned with a phenylalanine at position LC^P in loop C (Fig 3D). Thus, a histidine at position $H2^P$ in helix 2 and an aromatic residue at position LC^P in loop C seem to be a common feature among ammonia-permeable AQPs both in plants and animals. This suggests that the derived phenylalanine at LC^P in loop C of some plant TIPs, which supports ammonia permeability without the ability to form hydrogen bonds to the substrate, reflects an adaptation to a different milieu, e.g., regarding pH or alternatively altered requirements on permeation rate and selectivity.

General Importance of Loop C in AQPs

Measurements of absolute water permeabilities [23] and relative permeabilities to other substrates [24] reveal large variations among water-specific AQPs. For example, mammalian AQP4 has a 4-fold higher single channel water permeability compared to AQP1, although they share identical or similar residues at the four canonical positions of the selectivity filter. Our structure led us to re-examine the amino acid residue at position LE^P in loop E, which contributes with its carbonyl to the selectivity region. Comparison of *At*TIP2;1 with other AQP structures identifies two spatial groups (I and II) of the carbonyls from residues at position LE^P in loop E as illustrated in Supporting Information (S1 Fig; top view in Fig 3C). *At*TIP2;1 groups together with aquaglyceroporins and the water-permeable human AQP4 (group I), whereas the majority of water-specific AQPs constitutes group II due to an asparagine at position LC^P

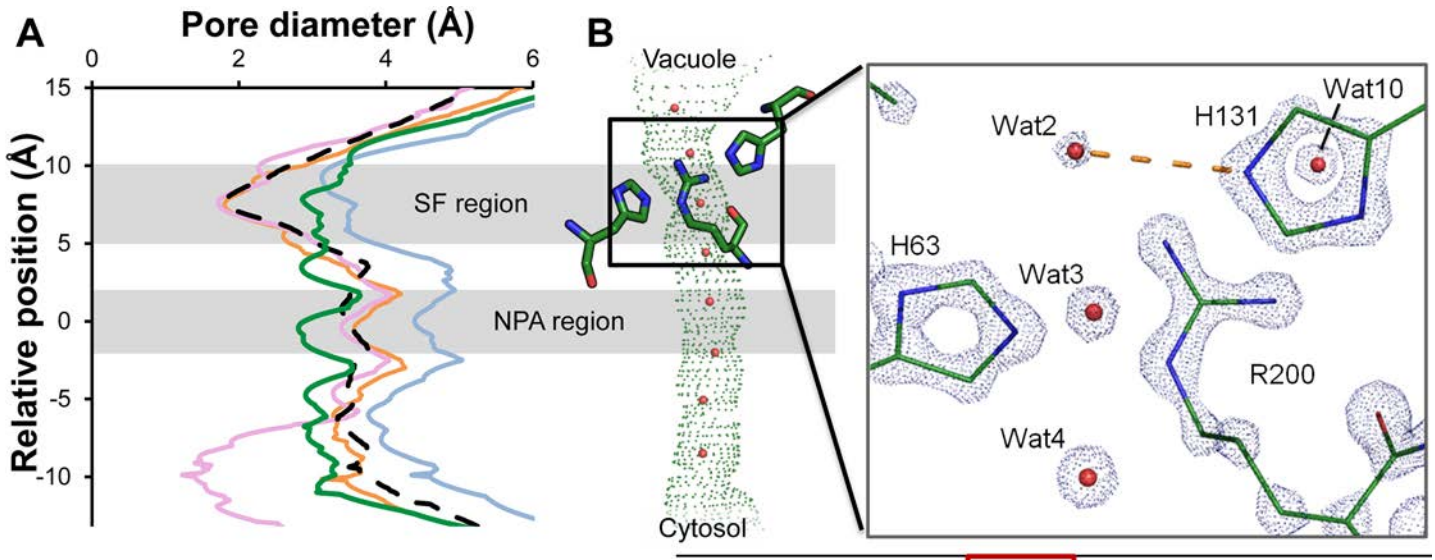

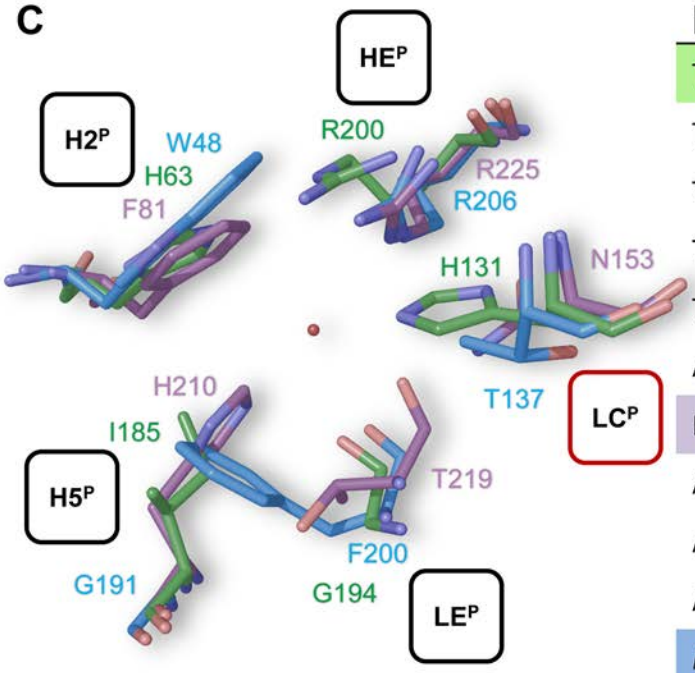

D	$H2^P$	LC^P	$H5^P$	LE^P	HE^P
TIP2s	H63	H131	I185	G194	R200
TIP4s	*	*	*	A	*
TIP6s	*	*	*	A	*
TIP3s	*	F	*	A	*
TIP1s	*	F	*	A	*/V
AQP8s	*	F	*	A	*
PIPs	F	N	H	T	*
AQP1,2,5,6s	F	N	H	C	*
AQP0s	F	N	H	A	*
AQP4s	F	T	H	A	*
*Ec*GlpF	W	T	G	F	*

Fig 3. Pore diameter and the extended selectivity filter. (A) Individual profiles of *At*TIP2;1 (green), glycerol-permeable *Ec*GlpF (blue), water-specific *So*PIP2;1 (closed conformation; purple), and *Hs*AQP4 (orange), as well as average diameter of five other open water-specific AQP structures (dashed line). Protein Data Bank IDs are provided in S1 Table. NPA region and selectivity filter (SF) indicated by shading. In contrast to previously reported structures of AQPs, where the SF region constitutes the most narrow part of the channel, the pore diameter of *At*TIP2;1 is more uniform throughout the channel. (B) Graphic representation of a side view of the *At*TIP2;1 pore aligned with (A). The selectivity filter is highlighted by stick representation of residues in positions $H2^P$, HE^P, and LC^P (left to right). Nondisplayed residues at positions $H5^P$ and LE^P are located in front of the visual plane. Close-up depicts electron density at 4σ. The high resolution of the structure makes it possible to pinpoint the nitrogen atoms in imidazole rings of histidines. The Nε of LC^P-His 131 forms a hydrogen bond (dashed yellow line) to a water molecule (Wat2) in the pore. (C) Vacuolar (top view of *At*TIP2;1) and corresponding extracellular view (*So*PIP2;1 and *Ec*GlpF) on the amino acid residues at the five positions ($H2^P$, LC^P, $H5^P$, LE^P, and HE^P) comprising the extended selectivity filter of the pore. *At*TIP2;1 (green) is compared to the water-specific *So*PIP2;1 (purple) and the glycerol-permeable *Ec*GlpF (blue). In *At*TIP2;1, histidines at $H2^P$ and LC^P stabilize the arginine (Arg 200) at HE^P in a novel orientation, which is clearly different from its positioning in structures of water-specific and glycerol-permeable AQPs. The spatial orientation of the backbone carbonyls at position LE^P is similar in *At*TIP2;1 and *Ec*GlpF, whereas it deviates in the water-specific *So*PIP2;1. The Ile 185 at $H5^P$ of *At*TIP2;1 results in a wider SF region compared to water-specific AQPs that have a histidine at this position. (D) The conservation of residues in the extended selectivity filter displayed in (C). The LC^P position that extends the selectivity filter is boxed in red. Plant TIPs and mammalian AQP8s are similar and distinctly different from water-specific AQPs in animals and plants (PIPs, plasma membrane intrinsic proteins), as well as the glycerol channel GlpF. Conservation patterns suggest a similar orientation of the conserved arginine at position HE^P of the selectivity filter of all TIPs and

AQP8s, and furthermore that individual subgroups of TIPs and water-specific AQPs might have evolved specialized substrate profiles (details in S2 Table). Asterisk denotes identity to TIP2s, and colors highlight selectivity filters shown in (C).

doi:10.1371/journal.pbio.1002411.g003

in loop C (Fig 3D), which can form a hydrogen bond to the backbone carbonyl of the amino acid residue at position LE^P. This group II-specific interaction directs the LE^P carbonyl to the center of the pore and quasiparallel to the membrane. In this conformation, the peptide bonds of this and the two preceding residues are contorted. In contrast, the AQPs lacking an asparagine at position LC^P place the backbone carbonyl of the amino acid residue at position LE^P (Gly 194 in *At*TIP2;1)—and preceding residues of loop E—in a more relaxed conformation, resembling that of a corresponding carbonyl (Gly 80) in the quasisymmetry-related loop B (Fig 1A). The variation of the carbonyls of the amino acid residues at position LE^P is spatially small and hence has little effect on the pore diameter per se, but it significantly affects hydrogen bonding to substrates. Thus, the identity of the amino acid residue at position LC^P in loop C appears to be relevant for substrate specificity, not only in ammonia permeable AQPs but also in water-specific isoforms.

Ammonia Specificity

To investigate the contribution of the amino acid residues in the extended selectivity filter to substrate specificity, we analyzed the permeability of the water-specific human AQP1 (*Hs*AQP1) and *At*TIP2;1 using in vivo and in vitro assays. Both these channels have the conserved arginine at position HE^P of the selectivity filter but, as established by our structure, the spatial location of its side chain relative to the pore differs. Expectedly, substituting all four deviating residues of the extended selectivity filter in a quadruple mutant of *At*TIP2;1 to the corresponding residues of *Hs*AQP1 abolished complementation in a yeast growth assay probing for ammonia permeability (Fig 4). Single point mutations at each of the four positions specify that all of the individual substitutions except the exchange of histidine for phenylalanine at $H2^P$ are compatible with ammonia permeability in *At*TIP2;1. The incompatibility of the phenylalanine may be explained by its different electrostatics and slightly larger size, which would be in conflict with the orientation of the arginine at position HE^P in the selectivity filter of *At*TIP2;1. The spatial orientation of the arginine at position HE^P in *At*TIP2;1 is constrained by loop C and the histidine at position LC^P, hence the introduced phenylalanine at $H2^P$ is likely to adopt an alternative position where it occludes the pore. The compatibility of the three other single mutations may at first appearance be explained by their polar nature, allowing formation of hydrogen bonds to ammonia. However, as mentioned above, at position LE^P, the hydrogen bond to the substrate is offered by the backbone carbonyl rather than the side chain. Interestingly, a double mutation in helix 5 (position $H5^P$) and loop E (position LE^P) of the selectivity filter failed to demonstrate ammonia permeability in the growth assay. This may indicate that a small and flexible residue at position LE^P of *At*TIP2;1 is required to allow its carbonyl to interact with the substrate in the presence of a histidine at position $H5^P$.

The identification of determinants for substrate specificity based on functional knockout mutants is complicated by possible trivial explanations for loss of function, such as misfolding of the protein or failure to reach the plasma membrane. Therefore, rather than just trying to eradicate the ammonia specificity of *At*TIP2;1 by mutations, we chose to focus on gain-of-function mutants of the water-specific *Hs*AQP1 in an attempt to mimic the ammonia and water permeability of *At*TIP2;1. Hence, the four deviating residues in the extended selectivity filter of *Hs*AQP1 were mutated in a stepwise fashion to probe if a histidine at LC^P, which may force the arginine at LE^P of *Hs*AQP1into an *At*TIP2;1-like position, was enough to achieve a matching substrate selectivity, or if additional substitutions were required. Unexpectedly, only the

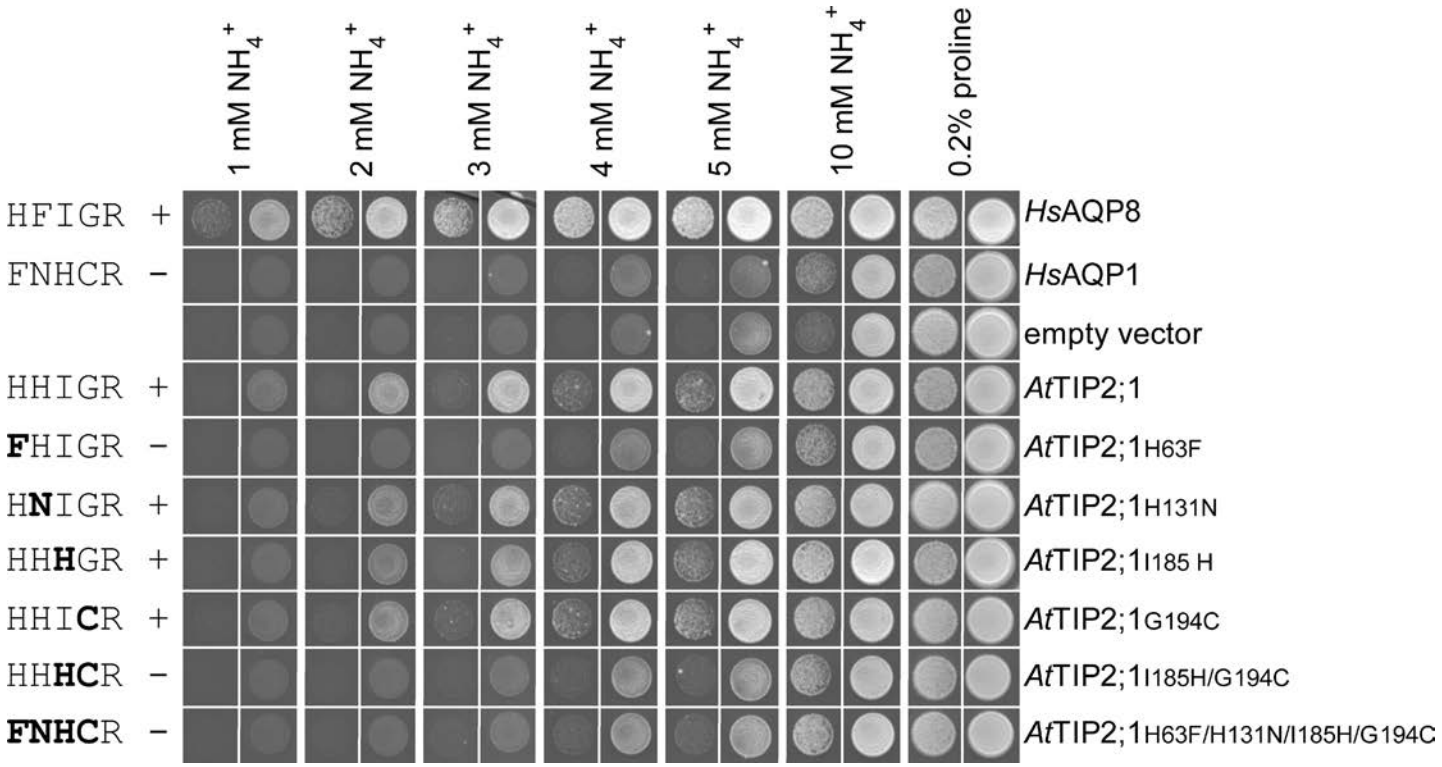

Fig 4. Growth complementation of ammonium uptake-defective yeast strain by mutants of *At*TIP2;1. The 31019b yeast strain (*Δmep1–3*) was transformed with the empty vector pYeDP60u or with pYeDP60u-carrying cDNA encoding the positive controls *Hs*AQP8 or *Hs*AQP1, or *At*TIP2;1 or its mutants. The five amino acid residues of the extended selectivity filter in each construct are indicated in one letter code to the left in the order $H2^P$, LC^P, $H5^P$, LE^P, and HE^P, showing substitutions in bold. Complementation and failure to complement are indicated by + and –, respectively. Transformants were spotted at an OD_{600} of 1 (right column) and 0.01 (left column) on plates containing 0.2% proline or the indicated concentrations of ammonium as a sole nitrogen source and growth was recorded after 13 d at 28°C. Each panel showing growth at a specific concentration is compiled by individual pictures of each spot taken from a distinct growth condition. All single pictures were treated in the same manner.

doi:10.1371/journal.pbio.1002411.g004

quadruple *Hs*AQP1 mutant ($H2^P$-F56H, LC^P-N127H, $H5^P$-H180I, LE^P-C189G) showed significant growth compared to the empty vector control in the yeast complementation assay for ammonia permeability (Fig 5). Stopped-flow experiments were conducted to quantitate ammonia and water permeability rates of the *Hs*AQP1 mutants and the controls. To compare relative specificities independently of differences in expression levels of the correctly folded protein in the yeast plasma membrane, the ratios of these rates were calculated (Table 2). Albeit the two rates represent alkalization and swelling rates in two different arbitrary units, their ratios offer an informative measure of the relative specificity in comparisons between mutated and wild type proteins. Whereas wild type *Hs*AQP1 only conducts water, *At*TIP2;1 showed a significant ammonia permeation rate, corresponding to approximately 3% of the water permeation rate in this strain. Interestingly, the same ratio was only obtained for the quadruple mutant of *Hs*AQP1, showing that these four substitutions are sufficient to reproduce an *At*TIP2;1-like specificity in *Hs*AQP1. Two other mutant forms of *Hs*AQP1, namely the $H5^P$-H180I single mutant and the triple mutant ($H2^P$-F56H, LC^P-N127H, $H5^P$-H180I), exhibited a higher specificity for ammonia than *At*TIP2;1 and similar absolute ammonia rates as the quadruple mutant, but surprisingly failed to complement the ammonia transport deletion strain in the growth assay. Insufficient water permeability of these mutants may explain these observations, implying that a dual permeability might be necessary for an efficient ammonia uptake in vivo. The impaired water permeability is likely to be a result of the higher hydrophobicity of

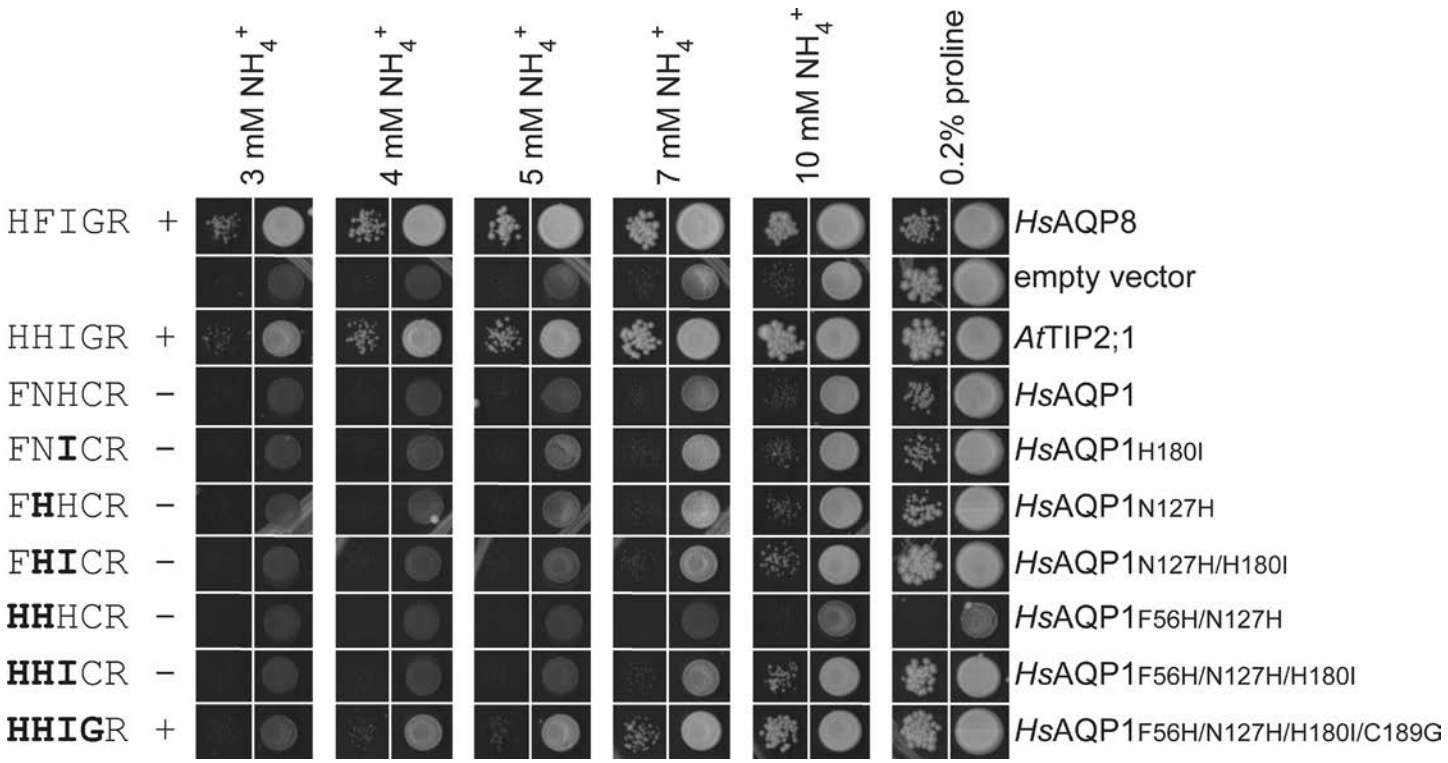

Fig 5. Growth complementation of ammonium uptake-defective yeast strain by mutants of *Hs*AQP1. The 31019b yeast strain (*Δmep1–3*) was transformed with the empty vector pYeDP60u or with pYeDP60u carrying cDNA encoding the positive controls *Hs*AQP8 or *At*TIP2;1, or *Hs*AQP1 or its mutants. The five amino acid residues of the extended selectivity filter in each construct are indicated in one letter code to the left in the order $H2^P$, LC^P, $H5^P$, LE^P, and HE^P, showing substitutions in bold. Complementation and failure to complement are indicated by + and –, respectively. Transformants were spotted at an OD_{600} of 1 (right column) and 0.0001 (left column) on plates containing 0.2% proline or the indicated concentrations of ammonium as a sole nitrogen source and growth was recorded after 13 d at 28°C. Each panel showing growth at a specific concentration is compiled by individual pictures of each spot taken from a distinct growth condition. All single pictures were treated in the same manner.

doi:10.1371/journal.pbio.1002411.g005

isoleucine replacing the histidine at position $H5^P$ of *Hs*AQP1. Apparently, water permeability is restored in the quadruple mutant by the LE^P-C189G mutation. This is consistent with conservation of a small amino acid residue (alanine or glycine) at LE^P of TIPs. A small residue may allow the carbonyl oxygen in LE^P—not hydrogen bonded to an amino acid at position LC^P—to adopt the relaxed position and interact with waters in the selectivity filter more efficiently. In contrast to earlier mutational studies [4], our new structural insight has allowed us to rationally design and implant a TIP2-like substrate profile to a water-specific AQP.

Although the high resolution structure of *At*TIP2;1 allowed us to discriminate between nitrogen and carbon atoms in side chains of histidines (Fig 3B), it would not be possible to distinguish nitrogen of ammonia from oxygen of water in the pore of *At*TIP2;1 due to their similar electron density and expected low ammonia occupancy. To get a more detailed view of the substrate specificity in *At*TIP2;1, we therefore employed MD simulations. Water permeation was seen at high frequency ($p_f \pm$ SD) corresponding to approximately $25 \pm 4 \times 10^{-14}$ cm^3 s^{-1} (S2 Fig), which is about four times as high as estimated for human AQP1. The high water permeation in *At*TIP2;1 is consistent with its low free energy for water (S3 Fig). Notably, spontaneous ammonia permeation events were observed in unbiased simulations with a length of 400 ns (S1 Movie) and verified by umbrella sampling simulations yielding a free energy barrier of approximately 15 kJ/mol (Fig 6A) in line with a high ammonia permeability. Further analysis shows that desolvation effects are compensated for by several hydrogen bonding residues at the

Table 2. Transport rates for ammonia and water in yeast cells expressing *At*TIP2;1, *Hs*AQP1, or mutants of *Hs*AQP1 mimicking the selectivity filter of *At*TIP2;1.

Construct (SF position)	Ammonia × 10^{-2} (s^{-1})*	Water (s^{-1})*	Background corrected rates† (s^{-1})		Ammonia/ water‡ × 10^{-2}	Specificity§
			Ammonia × 10^{-2}	Water		
Empty vector	6.7 ± 0.1	0.25 ± 0.01	0	0	NA	NA
*At*TIP2;1	39.1 ± 0.1	10.5 ± 0.1	32.4	10.2	3.2 ± 0.03	*At*TIP2;1-like
*Hs*AQP1 wt	6.3 ± 0.04	33.5 ± 0.2	0	33.2	0	Water
N127H (LC^P)	4.7 ± 0.03	1.4 ± 0.001	0	1.13	0	Water
F56H ($H2^P$) N127H (LC^P)	6.1 ± 0.04	1.9 ± 0.01	0	1.62	0	Water
H180I ($H5^P$)	11.5 ± 0.1	0.57 ± 0.0005	4.8	0.32	15 ± 1	Ammonia
N127H (LC^P) H180I ($H5^P$)	5.5 ± 0.03	0.31 ± 0.0004	0	0.05	NA	NA
F56H ($H2^P$) N127H (LC^P) H180I ($H5^P$)	9.9 ± 0.1	0.33 ± 0.0005	3.2	0.07	44 ± 3	Ammonia
F56H ($H2^P$) N127H (LC^P) H180I ($H5^P$) C189G (LE^P)	12.4 ± 0.1	2.2 ± 0.02	5.7	1.91	3.0 ± 0.1	*At*TIP2;1-like

*Rates ± standard error of the fit calculated in GraphPad Prism.

†Rates for the strain with empty vector were subtracted for background correction. Negative rates were set to 0.

‡Background corrected rates were used to calculate the ratio as a measure of the substrate specificity. Ratios are presented ± propagated errors derived from given rates and their standard errors of the fit (see *).

§A lower ratio than *At*TIP2;1 is classified as water specificity, a higher as ammonia specificity, and a similar ratio as *At*TIP2;1-like.

NA, not applicable due to insignificant water and ammonia transport rates; wt, wild type.

doi:10.1371/journal.pbio.1002411.t002

selectivity filter (Fig 6A–6C), substantially lowering the energetic barrier in this region, where it peaks for the water-specific *Hs*AQP1 [25]. In contrast to a simple model membrane (S3 Fig), the tonoplast contains sterols [26], which increase the impermeability to polar molecules. Therefore, the ammonia permeability of *At*TIP2;1 is compared to a cholesterol containing model membrane with a free energy barrier for ammonia of 20 kJ/mol (Fig 6A). Due to these differences in energy barriers, the permeability of *At*TIP2;1 is an order of magnitude higher.

Accumulation of Ammonium at the Surface

It is debated whether aquaammoniaporins are permeated by ammonium ions or not [27]. This has physiological relevance, since an effective exclusion of ammonium ions is necessary to acid-trap it in the vacuole. MD simulations containing ammonium ions showed no spontaneous permeation events, as expected due to electrostatic repulsion and desolvation effects in the pore. This brings to mind the ammonia transporter AmtB, which is generally considered to have a similar ammonium/ammonia selectivity, but where ammonia permeation has been proposed to be stimulated by ammonium recruitment to the noncytosolic vestibule [28]. We therefore investigated if ammonium ions accumulate on the vacuolar surface of *At*TIP2;1. A comparison of the electrostatics reveals that the vacuolar surface of *At*TIP2;1 is distinctly more negative than the corresponding surface of another plant AQP, the extracellular surface of the plasma membrane located water-specific *So*PIP2;1 that we established the structure of at 2.1 Å resolution [14] (S4 Fig). The negative vacuolar surface of *At*TIP2;1 is predominant at exposed acidic residues (Asp 48, Asp 52, Asp 210). Indeed, our MD simulations show a local enrichment of ammonium ions at these acidic residues (Fig 7A). Although the exact positions of acidic residues vary, a negative vacuolar surface constitutes a conserved feature among TIPs, which implies a generality of this finding.

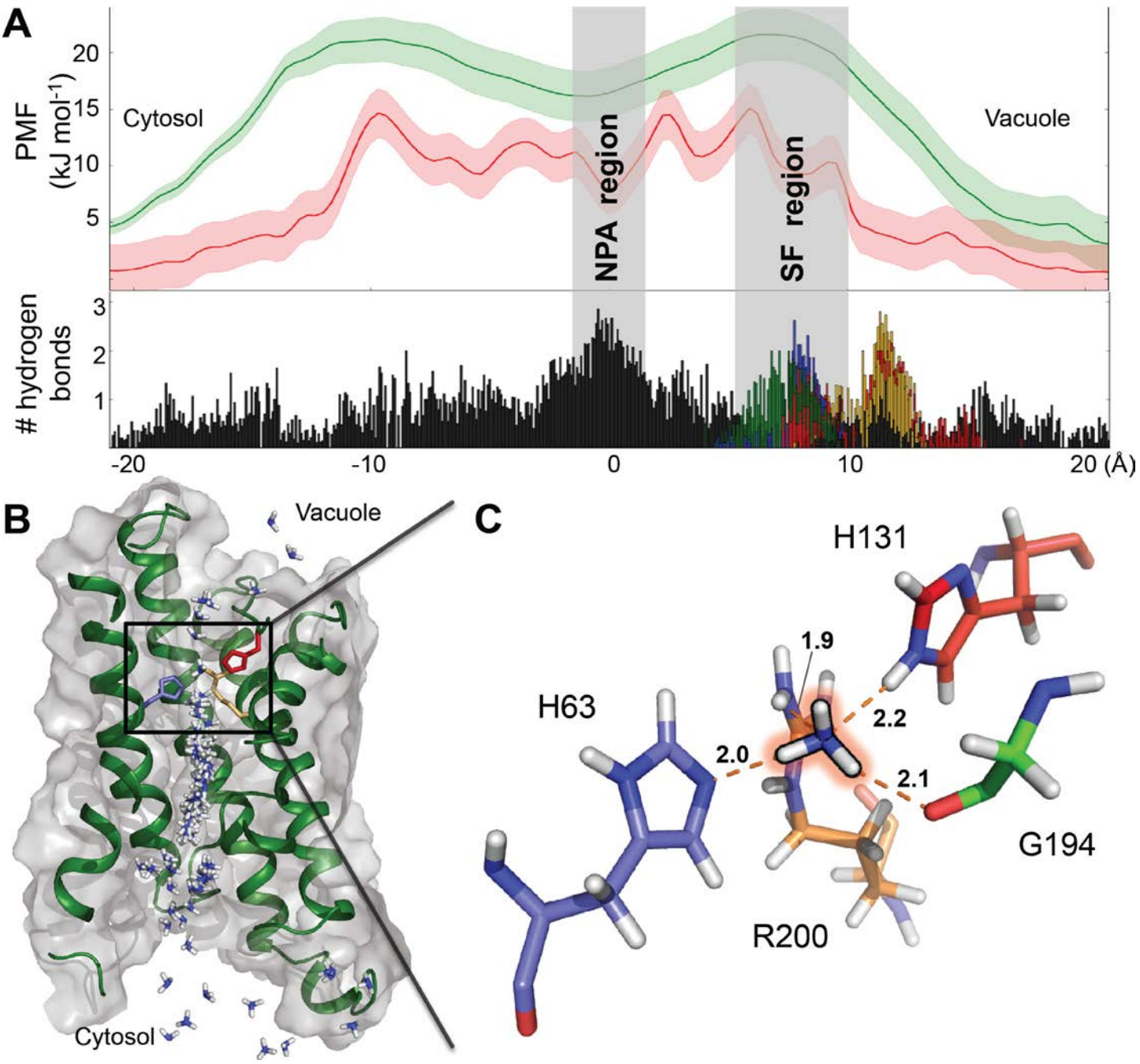

Fig 6. MD simulations of *At*TIP2;1. (A) The potential mean force (PMF) profiles for ammonia through *At*TIP2;1 (red) and through a model membrane containing 20% cholesterol (green). In the lower part of the panel, the number of hydrogen bonds between ammonia and *At*TIP2;1 are shown as function of position along the pore axis. Interactions with residues in the extended selectivity filter depicted in (C) are color-coded to resolve their contribution ($H2^P$-His 63 (blue), LC^P-His 131 (red), LE^P-Gly 194 (green) and HE^P-Arg 200 (brown)), and demonstrate hydrogen bonding to each of the four polar residues of the extended selectivity filter. (B) Snapshots of ammonia permeation. Cross section of *At*TIP2;1 shown as grey surface and green cartoon of the backbone. Side chains of selected amino acid residues in the selectivity filter are displayed as sticks and color coded as in (C). (C) Close-up of an ammonia molecule at the center, forming hydrogen bonds to four residues ($H2^P$-His 63, LC^P-His 131, LE^P-Gly 194, and HE^P-Arg 200) of the selectivity filter. The hydrogen bonds are indicated by orange dashes and distances are given in Å. Ile 185 at position $H5^P$ of the selectivity filter, located in front of the visual plane, is not shown. The underlying data of panel A can be found in S1 Data.

doi:10.1371/journal.pbio.1002411.g006

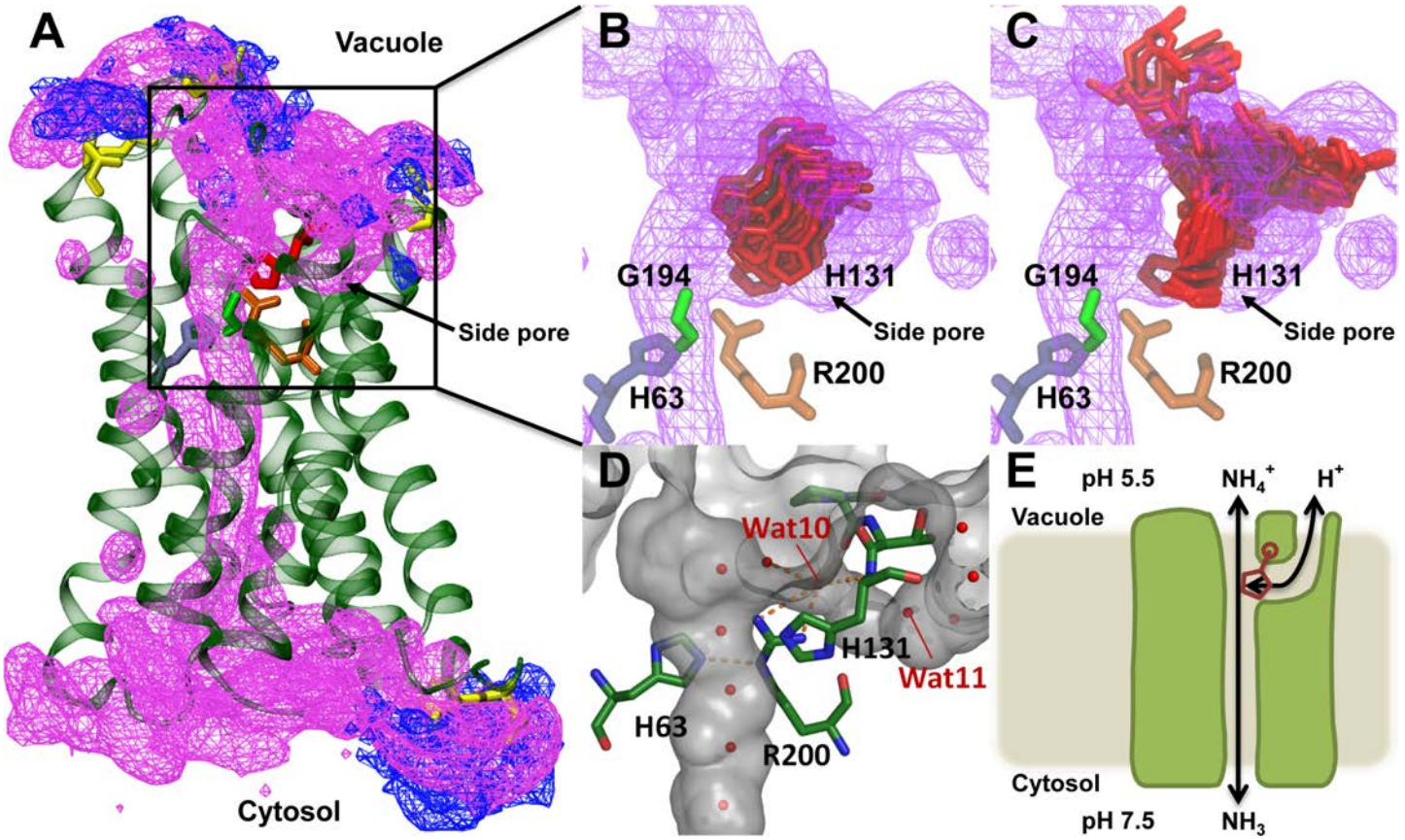

Fig 7. Ammonium accumulation and possible proton pathway. (A) MD simulations showing ammonium accumulation (blue mesh) at aspartate residues (yellow sticks) at vacuolar (top) and cytosolic (bottom) side of *At*TIP2;1. Water density (purple mesh) outlines the vertical main pore of the monomer and confirms existence of a water-filled side pore beneath loop C. Residues of the extended selectivity filter are depicted as sticks ($H2^P$-His 63 (blue), LC^P-His 131 (red), LE^P-Gly 194 (green), and HE^P-Arg 200 (brown)). (B) and (C) MD simulations demonstrating flexibility of His 131 at position LC^P being neutral (B) and positively charged (C). Color code as in (A). (D) Surface representation of the crystal structure depicting the water-filled side pore beneath loop C. Hydrogen bonds of water 10 (Wat10) as well as between Arg 200 at position HE^P in helix E and His 63 at position $H2^P$ in helix 2 are indicated by dashed orange lines. (E) Tentative working model of ammonia-permeating *At*TIP2;1. Ammonium may contribute to ammonia permeation by accumulating on the vacuolar protein surface and by possibly having its protons shuttled back into the acidic vacuole by His 131 (red) at position LC^P in loop C via a water-filled side pore.

doi:10.1371/journal.pbio.1002411.g007

Conceivable Function of the Side Pore

Considering the low pH in some vacuoles and accumulation of ammonium on the vacuolar surface of *At*TIP2;1, the permeation efficiency would clearly benefit if ammonium contributes to channeling of ammonia. How then is ammonium deprotonated? The distal position of the second vacuolar loop (loop C) relative to Arg 200 at position HE^P in helix E hints at an explanation. In fact, structure and MD simulations concur that loop C leaves enough space for a continuous side pore reaching from the selectivity filter all the way to the vacuolar surface (Fig 7A–7D). In all previously reported AQP structures, the HE^P-arginine is directly hydrogen bonded to the backbone carbonyl oxygen of the residue corresponding to Pro 129 of loop C. In *At*TIP2;1, this contact is instead mediated via a water molecule (Wat 10; Fig 7D) occupying a similar position as the arginine-binding carbonyl oxygen in other AQP structures. Interestingly, the peptide bond preceding the TIP2-specific histidine (His 131) at position LC^P in loop C retains an unusually large dihedral angle (19°) [29], and this contortion would be even larger with a deeper position of loop C. To explore if His 131 at position LC^P and the side pore could

play a role in facilitating deprotonation of ammonium, we conducted further MD simulations. Ammonium deprotonation via LC^P-His 131 through the side pore most likely requires a positional shift of this residue away from ammonia and towards a water molecule in the side pore (Wat 11) to get in hydrogen bond distance. The simulations indicate that the angle of the His 131 side chain (chi 1) remains as in the crystal structure when neutral (Fig 7B and S5 Fig), whereas in a protonated, i.e. positively charged state, an alternative orientation towards Wat 11 is indeed observed (Fig 7C, S5 Fig and S6 Fig). Furthermore, as simulations support the side pore as being continuously solvated, from His 131 to the vacuolar exit, it offers a proton wire for return of protons to the vacuolar environment, as ammonium is transferred to the pore as ammonia. These findings lead us to speculate about a possible TIP2-specific mechanism (Fig 7E) where histidine (His 131) at position LC^P in loop C shuttles protons from the main pore to the vacuolar surface via the side pore, using a Grotthuss mechanism, putatively enhancing the permeation rate of ammonia from the vacuole under nonequilibrium flux conditions.

Discussion

The atomic structure of the water and ammonia permeable *At*TIP2;1 provides new insights into the substrate selectivity of AQPs. The structure reveals an extended selectivity filter, including a fifth amino acid residue at position LC^P in loop C that also may play a role in defining substrate profiles of the entire AQP superfamily. The importance of the extended selectivity filter is demonstrated by mutational studies in vivo and in vitro, showing gain-of-function of *At*TIP2;1 substrate selectivity in the water-specific human AQP1. MD simulations support ammonia conductance and a lack of ammonium permeability. As expected from the structure, ammonia interacts with LC^P-His 131 and behaves similar to water in the pores of AQPs [18], reorienting in the NPA region at the N-termini of helix B and helix E due to their macro dipoles (S1 Movie). Based on structural analyses and simulations, we describe a selectivity filter that is highly permeable to ammonia due to its width and many potential polar contacts with the substrate and speculate on a mechanism in which ammonia permeation may be further increased by ammonium accumulation at the vacuolar protein surface, deprotonation through the TIP2-specific LC^P-His 131, and proton transfer via a previously unidentified water-filled side pore. It should be stressed that there is only limited support from simulations for this speculation, and without confirmatory structures it is difficult to specifically target the side pore by mutations or to predict if it is a conserved feature of other TIPs and AQP8s. However, we find it most likely that the conserved arginine at position HE^P in helix E of other TIPs and AQP8s adopt the same conformation, as shown here for *At*TIP2;1, due to aromatic residues at position LC^P in loop C and hydrogen bonding residues at position $H2^P$ in helix 2. The conservation patterns in the selectivity filter of AQP8s and separate subgroups of TIPs indicate that a functional differentiation has evolved among aquaammoniaporins. TIP2s and TIP4s of higher plants are similar to TIP6s found in primitive plants like mosses and are therefore likely to represent original functions and mechanistic features of TIPs. In contrast, TIP1s and TIP3s, which appear with the emergence of seed plants, as well as AQP8s in animals, lack the histidine at position LC^P, which is proposed here to enhance deprotonation of ammonium. Such variations among aquaammoniaporins may relate to pH-dependent properties, which however remains to be investigated. In this context, it should be mentioned that both AQP8 and an AtTIP2;1 mutant lacking the histidine at position LC^P complemented ammonia permeability in the growth assay equally well or better than the wild type AtTIP2;1, demonstrating that a histidine at this position is not essential for efficient ammonia uptake under these conditions. The *At*TIP2;1 structure will facilitate modeling of other AQPs including human AQP8 and may therefore also help to elucidate the molecular basis of ammonia permeation in man.

From our results, it is clear that *At*TIP2;1 can enhance the ammonia permeability of membranes, but conditions linking an ammonia-related phenotype to TIPs have so far not been reported in plants [30]. Plants emit significant amounts of ammonia from their leaves, and ammonia generated by photorespiration further accentuate losses, implying a limited capacity of ammonia reassimiliation enzymes [31]. We expect that high ammonia permeability of the tonoplast and rapid acid-entrapment of ammonium in the vacuole is especially important under transient periods of photorespiration when it counteracts high levels of ammonia in the cytosol and thereby reduces losses over the plasma membrane, giving reassimilation pathways time to incorporate more of the generated ammonia. Hence, we propose that expression of ammonia-permeable mutant AQP isoforms in the plasma membrane, such as PIP2 mutants having a TIP2-like extended selectivity filter, combined with regulation of TIP expression can be used to vary the relative ammonia permeability of the plasma membrane and the tonoplast to explore effects on ammonia emission under these conditions. Control of ammonia emission by regulation of ammonia permeability in membranes could potentially open up a new way to improve the nitrogen use efficiency in plants.

Materials and Methods

For details, see Supporting Information S1 Text.

*At*TIP2;1 with an N-terminal deca-His-tag was expressed in *Pichia pastoris* and purified as previously described [32]. Briefly, membranes were urea washed and solubilized with 10% n-octyl-β-D-glucoside (OG). The protein was purified by nickel affinity chromatography, employing a 100 mM imidazole wash, followed by size exclusion chromatography using an S200 column. Functionality was verified by stopped-flow analyses of proteoliposomes.

Hanging drop vapor-diffusion crystallization was performed at room temperature using a reservoir solution consisting of 50 mM magnesium/sodium acetate pH 5.0 and 28% (v/v) PEG 400 and crystals were flash-cooled in liquid nitrogen. Data were collected at 1 Å wavelength on the X06SA (PXI) beamline at the Swiss Light Source, Villigen, Switzerland. The structure was solved by molecular replacement and the model built manually. Refinement excluded 3% reflections, including twin-mates, and resulted in a twin fraction of 40.7%, reaching R_{work} and R_{free}-values of 10.2% and 11.2%, respectively. Ramachandran outliers and residues in unfavored regions were manually inspected.

Mutant studies of *At*TIP2;1 and *Hs*AQP1 were executed using protoplasts and intact cells from *Saccharomyces cerevisiae*, as previously described [33].

The simulations were conducted with the GROMACS 4.5 software [34] using the CHARMM36 forcefield [35]. To study the properties of *At*TIP2;1, the protein was embedded in a 1-Palmitoyl-2-oleoylphosphatidylcholine (POPC) bilayer. Three unbiased 500 ns simulations were conducted to study the equilibrium behaviour of *At*TIP2;1, in the presence of water, ammonia or ammonium ions. Umbrella sampling was employed to calculate the PMF for permeation of water and ammonia [36,37].

Supporting Information

S1 Data. Numerical data used in preparation of Figs 2A–2D and 6A, S2, S3, S5 and S6 Figs. (XLSX)

S1 Fig. Selectivity filter carbonyls in loop E cluster in two distinct spatial groups. (A) HE^P-arginine (R200) of *At*TIP2;1 is shown for orientation. Carbonyls at LE^P of water-specific AQPs form group II (violet shading), and most of them are within hydrogen-bonding distance to two water molecules in their structures as illustrated by *So*PIP2;1 (PDB ID 1Z98; violet). Carbonyls

of non-water-specific channels gather in a different location (group I; green shading). Among those are *At*TIP2;1 (green), glycerol transport facilitating, and uncharacterized proteins (*Af*AqpM, *Pf*AQP, *Ec*GlpF, *Mm*AqpM), but the water-specific *Hs*AQP4 also belongs to this group. Like all other members of this group, *Hs*AQP4 is lacking the LC^P-asparagine (N153 in *So*PIP2;1, Fig 3D) that is conserved among the other water-specific proteins (blue shading, only asparagines residues are shown). Each carbonyl in group II can form a hydrogen bond to the carboxamide of this asparagine, if the carboxamide is oriented the right way. A certain flexibility is suggested by the special case of *Hs*AQP0, where different structures are available (1YMG and 2B6O shown) and the carbonyl is seen with both orientations. Apart from the glycerol facilitators, it appears that small residues like glycine and alanine in LE^P (Fig 3D) are required in group I, whereas slightly larger residues like cysteine or threonine can be accommodated in group II. Only backbone is shown in LE^P. (B) Close up of *At*TIP2;1 (green) and *So*PIP2;1 (violet), showing hydrogen bonding of carbonyls at LE^P and water interacting with LC^P-His 131. Side chain of LE^P-Thr 219 is not shown. Main pore of *At*TIP2;1 analyzed by HOLE [38].
(TIF)

S2 Fig. Osmotic permeability (p_f) values calculated from MD simulations. p_f values were calculated separately for each monomer in seven 50-ns time windows. The contribution of the individual monomers to the p_f values of the tetramer are indicated by different colors and average values per monomer and standard deviation in each time window are indicated by the black line and error bars. The underlying data can be found in S1 Data.
(TIF)

S3 Fig. PMF for water across the *At*TIP2;1 channel calculated from the equilibrium trajectory (black). The error bars are the standard deviation of the PMF over the four monomers of the protein. PMF profile for ammonia across a model membrane without cholesterol is shown in blue. The underlying data can be found in S1 Data.
(TIF)

S4 Fig. Corresponding vacuum electrostatic maps of two plant AQPs. The noncytosolic surface of the tetramer of *So*PIP2;1 (left, facing the apoplast) and *At*TIP2;1 (right, facing the interior of the vacuole). Positive and negative electrostatic potentials calculated by PyMol [39] are marked by gradients of blue and red, respectively.
(TIF)

S5 Fig. Dihedral populations of LC^P-His 131 at three different protonated states. Chi1 angles in MD simulations with doubly protonated (positively charged; blue), Nδ protonated (neutral; yellow), and Nε protonated (neutral; red) His 131. The underlying data can be found in S1 Data.
(TIF)

S6 Fig. Dihedral chi1 angle of the LC^P-His 131 residue in the doubly protonated His 131 simulation summarized in S5 Fig. The data is shown for final ~350 ns of the 500 ns trajectory after the first observed transition. The His 131 residue spontaneously exchanges between its possible configurations in all the four monomers of the protein. The underlying data can be found in S1 Data.
(TIF)

S1 Movie. MD simulation demonstrates spontaneous ammonia permeation. *At*TIP2;1 monomer is displayed in side view with LC^P-His 131 of the selectivity filter as well as Asn 83 and Asn 197 in the NPA region shown as sticks. An ammonia molecule (sphere representation)

enters the main pore from the cytosolic side of the protein. During permeation of the pore, ammonia reorients such that its free electron pair points towards the asparagines at the protein center. In the course of the video, which corresponds to 2.94 ns, the imidazole group of LC^P-His 131 can be observed rotating by 180° and back again.
(MP4)

S1 Table. Protein structures used in Fig 3A.
(PDF)

S2 Table. Logos and list of accession numbers for protein sequences used to generate Fig 3D.
(PDF)

S3 Table. List of primers used to generate wild type and mutated AQP constructs.
(PDF)

S1 Text. Supporting Materials and Methods.
(DOCX)

Acknowledgments

We thank Adine Karlsson for technical assistance and the protein crystallization facility at Max IV laboratory for initial help. We are grateful for assistance with crystal screening at Maxlab, Lund, Sweden, beam lines 911-2/3, and data collection at the Swiss Light Source, the Paul Scherrer Institute, Villigen, Switzerland beam line X06SA.

Author Contributions

Conceived and designed the experiments: AK PK UJ PG SSK BLdG GPB FC. Performed the experiments: AK GPB SSK. Analyzed the data: AK PG UJ PN GPB FC SSK BLdG. Wrote the paper: AK PG UJ PK PN GPB FC SSK BLdG. Drafting of manuscript: AK PG UJ.

References

1. Maurel C, Reizer J, Schroeder JI, Chrispeels MJ. The vacuolar membrane protein gamma-TIP creates water specific channels in Xenopus oocytes. Embo J 1993; 12: 2241–2247. PMID: 8508761
2. Jahn TP, Moller AL, Zeuthen T, Holm LM, Klaerke DA, Mohsin B, et al. Aquaporin homologues in plants and mammals transport ammonia. FEBS Letters 2004; 574: 31–36. PMID: 15358535
3. Loque D, Ludewig U, Yuan L, von Wiren N. Tonoplast intrinsic proteins AtTIP2;1 and AtTIP2;3 facilitate NH3 transport into the vacuole. Plant Physiol 2005; 137: 671–680. PMID: 15665250
4. Dynowski M, Mayer M, Moran O, Ludewig U. Molecular determinants of ammonia and urea conductance in plant aquaporin homologs. FEBS Letters 2008; 582: 2458–2462. doi: 10.1016/j.febslet.2008.06.012 PMID: 18565332
5. Anderberg HI, Kjellbom P, Johanson U. Annotation of Selaginella moellendorffii Major Intrinsic Proteins and the Evolution of the Protein Family in Terrestrial Plants. Frontiers in plant science 2012; 3: 33. doi: 10.3389/fpls.2012.00033 PMID: 22639644
6. Maeshima M. TONOPLAST TRANSPORTERS: Organization and Function. Annual review of plant physiology and plant molecular biology 2001; 52: 469–497. PMID: 11337406
7. Wudick MM, Luu DT, Maurel C. A look inside: localization patterns and functions of intracellular plant aquaporins. The New phytologist 2009; 184: 289–302. doi: 10.1111/j.1469-8137.2009.02985.x PMID: 19674338
8. Coskun D, Britto DT, Li M, Becker A, Kronzucker HJ. Rapid Ammonia Gas Transport Accounts for Futile Transmembrane Cycling under NH3/NH4+ Toxicity in Plant Roots. Plant physiology 2013; 163: 1859–1867. doi: 10.1104/pp.113.225961 PMID: 24134887

9. Agemark M, Kowal J, Kukulski W, Norden K, Gustavsson N, Johanson U, et al. Reconstitution of water channel function and 2D-crystallization of human aquaporin 8. Biochimica et biophysica acta 2012; 1818: 839–850. doi: 10.1016/j.bbamem.2011.12.006 PMID: 22192778
10. Saparov SM, Liu K, Agre P, Pohl P. Fast and selective ammonia transport by aquaporin-8. The Journal of biological chemistry 2007; 282: 5296–5301. PMID: 17189259
11. Soria LR, Marrone J, Calamita G, Marinelli RA. Ammonia detoxification via ureagenesis in rat hepatocytes involves mitochondrial aquaporin-8 channels. Hepatology 2013; 57: 2061–2071. doi: 10.1002/hep.26236 PMID: 23299935
12. Fu D, Libson A, Miercke LJ, Weitzman C, Nollert P, Krucinski J, et al. Structure of a glycerol-conducting channel and the basis for its selectivity. Science 2000; 290: 481–486. PMID: 11039922
13. Sui H, Han BG, Lee JK, Walian P, Jap BK. Structural basis of water-specific transport through the AQP1 water channel. Nature 2001; 414: 872–878. PMID: 11780053
14. Tornroth-Horsefield S, Wang Y, Hedfalk K, Johanson U, Karlsson M, Tajkhorshid E, et al. Structural mechanism of plant aquaporin gating. Nature 2006; 439: 688–694. PMID: 16340961
15. Horsefield R, Norden K, Fellert M, Backmark A, Tornroth-Horsefield S, Terwisscha van Scheltinga AC, et al. High-resolution x-ray structure of human aquaporin 5. Proceedings of the National Academy of Sciences of the United States of America 2008; 105: 13327–13332. doi: 10.1073/pnas.0801466105 PMID: 18768791
16. Kosinska Eriksson U, Fischer G, Friemann R, Enkavi G, Tajkhorshid E, Neutze R. Subangstrom resolution X-ray structure details aquaporin-water interactions. Science 2013; 340: 1346–1349. doi: 10.1126/science.1234306 PMID: 23766328
17. Murata K, Mitsuoka K, Hirai T, Walz T, Agre P, Heymann JB, et al. Structural determinants of water permeation through aquaporin-1. Nature 2000; 407: 599–605. PMID: 11034202
18. de Groot BL, Grubmuller H. Water permeation across biological membranes: mechanism and dynamics of aquaporin-1 and GlpF. Science 2001; 294: 2353–2357. PMID: 11743202
19. Zhu FQ, Tajkhorshid E, Schulten K. Collective diffusion model for water permeation through microscopic channels. Physical Review Letters 2004; 93: Artn 224501.
20. Wu B, Steinbronn C, Alsterfjord M, Zeuthen T, Beitz E. Concerted action of two cation filters in the aquaporin water channel. The EMBO journal 2009; 28: 2188–2194. doi: 10.1038/emboj.2009.182 PMID: 19574955
21. Daniels MJ, Chaumont F, Mirkov TE, Chrispeels MJ. Characterization of a new vacuolar membrane aquaporin sensitive to mercury at a unique site. The Plant cell 1996; 8: 587–599. PMID: 8624437
22. Beitz E, Wu B, Holm LM, Schultz JE, Zeuthen T. Point mutations in the aromatic/arginine region in aquaporin 1 allow passage of urea, glycerol, ammonia, and protons. Proceedings of the National Academy of Sciences of the United States of America 2006; 103: 269–274. PMID: 16407156
23. Yang B, Verkman AS. Water and glycerol permeabilities of aquaporins 1–5 and MIP determined quantitatively by expression of epitope-tagged constructs in Xenopus oocytes. The Journal of biological chemistry 1997; 272: 16140–16146. PMID: 9195910
24. Geyer RR, Musa-Aziz R, Qin X, Boron WF. Relative CO2/NH3 selectivities of mammalian aquaporins 0–9. American journal of physiology Cell physiology 2013; 304: C985–994. doi: 10.1152/ajpcell.00033.2013 PMID: 23485707
25. Hub JS, de Groot BL. Mechanism of selectivity in aquaporins and aquaglyceroporins. Proceedings of the National Academy of Sciences of the United States of America 2008; 105: 1198–1203. doi: 10.1073/pnas.0707662104 PMID: 18202181
26. Yoshida S, Uemura M. Lipid Composition of Plasma Membranes and Tonoplasts Isolated from Etiolated Seedlings of Mung Bean (Vigna radiata L.). Plant physiology 1986; 82: 807–812. PMID: 16665114
27. Litman T, Sogaard R, Zeuthen T. Ammonia and urea permeability of mammalian aquaporins. Handbook of experimental pharmacology 2009: 327–358. doi: 10.1007/978-3-540-79885-9_17 PMID: 19096786
28. Akgun U, Khademi S. Periplasmic vestibule plays an important role for solute recruitment, selectivity, and gating in the Rh/Amt/MEP superfamily. Proceedings of the National Academy of Sciences of the United States of America 2011; 108: 3970–3975. doi: 10.1073/pnas.1007240108 PMID: 21368153
29. Berkholz DS, Driggers CM, Shapovalov MV, Dunbrack RL, Karplus PA. Nonplanar peptide bonds in proteins are common and conserved but not biased toward active sites. Proceedings of the National Academy of Sciences 2012; 109: 449–453.
30. Li G, Santoni V, Maurel C. Plant aquaporins: roles in plant physiology. Biochimica et biophysica acta 2014; 1840: 1574–1582. doi: 10.1016/j.bbagen.2013.11.004 PMID: 24246957

31. Kumagai E, Araki T, Hamaoka N, Ueno O. Ammonia emission from rice leaves in relation to photorespiration and genotypic differences in glutamine synthetase activity. Annals of botany 2011; 108: 1381–1386. doi: 10.1093/aob/mcr245 PMID: 21937483

32. Karlsson M, Fotiadis D, Sjovall S, Johansson I, Hedfalk K, Engel A, et al. Reconstitution of water channel function of an aquaporin overexpressed and purified from Pichia pastoris. FEBS letters 2003; 537: 68–72. PMID: 12606033

33. Bertl A, Kaldenhoff R. Function of a separate NH3-pore in Aquaporin TIP2;2 from wheat. FEBS Letters 2007; 581: 5413–5417. PMID: 17967420

34. Pronk S, Pall S, Schulz R, Larsson P, Bjelkmar P, Apostolov R, et al. GROMACS 4.5: a high-throughput and highly parallel open source molecular simulation toolkit. Bioinformatics 2013; 29: 845–854. doi: 10.1093/bioinformatics/btt055 PMID: 23407358

35. Klauda JB, Venable RM, Freites JA, O'Connor JW, Tobias DJ, Mondragon-Ramirez C, et al. Update of the CHARMM All-Atom Additive Force Field for Lipids: Validation on Six Lipid Types. Journal of Physical Chemistry B 2010; 114: 7830–7843.

36. Hub JS, de Groot BL, van der Spoel D. g_wham-A Free Weighted Histogram Analysis Implementation Including Robust Error and Autocorrelation Estimates. Journal of Chemical Theory and Computation 2010; 6: 3713–3720.

37. Hub JS, Winkler FK, Merrick M, de Groot BL. Potentials of mean force and permeabilities for carbon dioxide, ammonia, and water flux across a Rhesus protein channel and lipid membranes. Journal of the American Chemical Society 2010; 132: 13251–13263. doi: 10.1021/ja102133x PMID: 20815391

38. Smart OS, Goodfellow JM, Wallace BA. The pore dimensions of gramicidin A. Biophysical journal 1993; 65: 2455–2460. PMID: 7508762

39. Schrodinger, LLC, The PyMOL Molecular Graphics System, Version 1.5.0.4 (2010).

Crystal Structure of an Ammonia-Permeable Aquaporin
Supporting information

S1 Text. Supporting Materials and Methods

Protein expression and purification

A generic vector was constructed by modification of pPICZB (Invitrogen), introducing a deca-His-tag followed by a spacer 3' of the MCS (FOR_TEV). The *At*TIP2;1 sequence with an N-terminal TEV-site was cloned into FOR_TEV and transformed into *Pichia pastoris*. A culture of a high-expressing clone was grown in a 3 L bioreactor (HANNA, Belach Bioteknik) and induced by continuous feed of methanol. Cells were harvested after 2 days induction at an OD_{600} of 328 and the overexpressed protein was purified as previously described (1). Briefly, bead-beater-extracted membranes were washed with 4 M urea (2) and solubilized at room temperature in Buffer A (20 mM Hepes pH 7.8, 50 mM NaCl) supplied with 10% n-octyl-β-D-glucoside (OG), 2 mM β-mercapto-ethanol and 1 mM PMSF. *At*TIP2;1 was purified in Buffer A supported by either 0.6% n-nonyl-β-D-glucoside (NG) for mercury inhibition assays or 0.8% OG for other liposome assays and crystallization. Solubilized membranes were bound to Ni-NTA beads (Qiagen) for at least two hours at 4°C. Ni-affinity chromatography was done on column maintaining reducing conditions of 4 mM β-mercapto-ethanol. Bound proteins were washed with 100 mM imidazole prior to elution. Eluted proteins were immediately separated further in Buffer A containing 2 mM dithiothreitol (DTT) by size exclusion chromatography on a S200 (GE Healthcare) at 4°C. The tetrameric fraction was concentrated to 13 – 17 mg protein/mL and stored at 4°C.

Crystallization and structure determination

Vapor-diffusion crystallization was performed at room temperature with 1 + 1 µL hanging drops. Several initial crystal hits were found within 3 – 7 days in MemGold (Molecular Dimensions) and PEGRx2 screen (Hampton Research). Initial diffraction was seen at

beamlines I911-2 and -3 at Max-Lab, Lund, Sweden. Data for the presented structure was collected at 1 Å wavelength on the X06SA (PXI) beamline at the Swiss Light Source, Villigen, Switzerland on a crystal grown over a reservoir solution of 50 mM magnesium/sodium acetate pH 5.0 and 28% (v/v) PEG 400. Data was integrated with XDS (3) and molecular replacement was based on the structure of *Hs*AQP4 PDB ID code 3GD8). Refinement was done with Refmac5 initially using detwinned data (detwin) and manually build with Coot(4) included in CCP4 package (5, 6). For further refinement 3% reflections (including twin-mates) were excluded from original twinned data for R_{free}. Final refinement included hydrogens and resulted in a twin fraction of 40.7%. Structures were analyzed and pictures created in PyMOL (7). Rampage (8) locates 233 amino acid residues (98.7%) in the favored and 3 (1.3%) in the allowed region and crystallographic statistics calculated by MolProbity (9) are found in Table 1. Pore diameters of selected AQPs (Table S1) were analyzed with the program HOLE (10) excluding waters and non-proteogenic molecules.

Functional assays of purified protein

For kinetic assays, liposomes with and without protein were made by dialysis. For water transport assays at different pH, 66 µg protein and 2 mg *E. coli* POLAR lipids (Avanti), lipid-to-protein-ratio 30 (LPR 30), were dialyzed per mL Tris-buffer (20 mM pH 8.0, 100 mM NaCl, 2 mM DTT). Likewise for mercury inhibition, His-trap purified and desalted (PD-10, GE Healthcare) protein was reconstituted in liposomes at LPR 50. Vesicles for ammonia transport (LPR 16) were reconstituted in MOPS buffer (5 mM pH 5.6, 100 mM NaCl, 2 mM DTT) containing 0.5 mM carboxy-fluorescein. To determine water permeability, extruded vesicles (9 times by 200 nm filter) were diluted 10 times in either Tris-buffer (20 mM pH 8.0, 100 mM NaCl) or MOPS buffer (50 mM pH 5.0, 100 mM NaCl) resulting in pH 5.4. The diluted proteoliposomes were subjected to a 100 mM sorbitol gradient in a stopped-flow device (SF-61DX2, TgK Scientific Limited), and out-flow of water was followed by

observing 90°-scattering at 500 nm. To inhibit protein-facilitated transport, proteoliposomes at pH 8.0 (LPR 50) were preincubated 30 min with 1 mM $HgCl_2$. A single exponential decay function was fitted to an average of 7–15 curves by Kinetic studio (TgK Scientific Limited). Vesicles to measure ammonia transport were pelleted by centrifuging 1 h at 145,000×g and 4°C, washed with 10 mL buffer without carboxy-fluorescein and centrifuged again immediately before use. The pellet was resuspended with MOPS buffer to a final lipid concentration of 0.2 mg/mL and filtered with a 200 nm syringe filter (Sarstedt). In stopped-flow experiments, NaCl was partially exchanged for NH_4Cl, and a change in fluorescence was recorded at an excitation of 490 nm using a cut-off filter of <495 nm. When NH_3, which constitutes approximately 0.022% of the total NH_4^+/NH_3 pool at pH 5.6, permeates the membrane the weakly buffered solution in the liposomes is alkalized and the quantum yield of carboxy-fluorescein increases. The single exponential rate constant of a decay function was fitted to ca. 10 curves between 3.8 ms (delay time) and 50 ms using GraphpadPrism (11).

Generation of constructs for mutational studies

The PCR products for mutated and non-mutated aquaporin constructs were directionally sub-cloned, using a uracil excision-based improved high-throughput USER cloning technique (12), into the USER-compatible yeast expression vector pYeDP60u (13). Point mutations were introduced into *Hs*AQP1 by PCR using the corresponding mutation primers (Table S3). The different PCR products were assembled into pYeDP60u using the efficient method for simultaneous fusion and cloning of multiple PCR products (14). All constructs were verified by DNA sequencing.

Yeast strain and growth assay

The *Saccharomyces cerevisiae* yeast strain 31019b (15) was transformed with pYeDP60u or pYeDP60u containing cDNA encoding the respective aquaporin isoforms or their mutants. Transformants were spotted on synthetic medium containing 2% galactose, 50 mM succinic

acid / Tris base, pH 5.5, 0.7% yeast nitrogen base without amino acids and ammonium (Difco) supplemented with 0.2% proline or different concentrations of $(NH_4)_2SO_4$ as a sole nitrogen source. After 9 to 13 days of incubation at 28°C, differences in growth and survival in the complementation assays were recorded. The yeast growth assay was repeated in four independent experiments with consistent results.

Permeability of yeast cells and protoplasts

Overexpression in yeast and preparation of intact cells and protoplast for stopped-flow experiments was performed as previously described (16). Briefly, *S. cerevisiae* strains containing vectors to express the different constructs were grown in 5 mL liquid SD-ura medium overnight at 30°C. 200 µL of each of these precultures were used to inoculate 25 mL SGal-ura medium and incubated for 48 h at 30°C. For preparation of protoplasts, 10 mL of each culture was pelleted gently (500×g, 5 min) and cells were washed with 4 mL equilibration buffer (50 mM potassium phosphate pH 7.2, 40 mM β-mercapto-ethanol). Cell walls were degraded for 30 min at 30°C in digestion buffer (equilibration buffer complemented with 2.4 M sorbitol, 50 mg/mL bovine serum albumin, and 0.5 mg/mL Zymolyase 20T). Protoplast were washed with 4 mL buffer 1A (10 mM Tris pH 8.0, 50 mM NaCl, 5 mM $CaCl_2$, 1.8 M sorbitol), resuspended in 1 mL buffer 1A and stored on ice until used. To determine water permeability, protoplasts were subjected to a 300 mM hypo-osmolar sorbitol gradient and water influx was followed by recording scattering (see above). A single exponential decay function was fitted to 12 – 16 normalized curves by GraphPad Prism (11).

To prepare samples for ammonia measurements, 10 mL intact cells per construct were washed in loading buffer (50 mM Hepes pH 7.0, 5 mM 2-deoxy-glucose) and incubated in 50 µM fluorescein diacetate for 20 to 30 min at 30°C. Fluorescein loaded cells were washed with buffer 2A (5 mM Tris pH 8.0, 50 mM NaCl) and stored at 4°C in the dark until use.

Cells were washed again prior to the stopped-flow experiment, if not used immediately after dye load. Fluorescein loaded intact yeast cells were rapidly mixed with equal volumes of buffer 2B (as buffer 2A, but NaCl exchanged for 50 mM NH_4Cl) creating a 1.3 mM inward ammonia gradient. Increased fluorescence (excitation wavelength 490 nm) upon alkalization was detected at 90° angle behind a long-pass filter with a cut-on wavelength of 530 nm. Between 2 and 14 curves were normalized per sample to fit an exponential function in GraphPad Prism.

MD simulations

The simulations were conducted with GROMACS 4.5 (17). The protein was embedded in a 1-Palmitoyl-2-oleoylphosphatidylcholine (POPC) bilayer of 304 molecules using g_membed (18). The system was simulated in the presence of 28,566 explicit molecules of TIP3P water (19) and an ion concentration of 0.15 M KCl. The temperature was kept at 300 K using a Velocity rescale thermostat (20) and the pressure was similarly maintained at 1 atmosphere using a Berendsen barostat (21). The CHARMM36 forcefield was used for all simulations (22). The electrostatic interactions in the system were treated explicitly with a PME method using a real space cut-off of 1.2 nm (23). The Lennard-Jones interactions were treated with a switch function with the switch at a distance of 0.8 nm and a cut-off at 1 nm. The parameters used for simulating the ammonia were obtained from the charmm small molecules library (24). The ammonium parameters were obtained by modifying the methylammonium ion parameters (24). The lipid bilayers were created with the CHARMM-GUI web application (25).

Three unbiased 500 ns simulations were run, studying the equilibrium behavior of the channel. The first of these was performed in the presence of water only to calculate the osmotic permeability (p_f). This was done using the collective diffusion method (26, 27). To calculate the averages for the p_f, the last 350 ns of the simulation were taken and divided into

seven sections of 50 ns each. The p_f was separately computed for each monomer and the average over the four monomers per section was used as the measure of the p_f and the standard deviation was used to estimate the statistical error. In conjunction with this first unbiased simulation, two additional simulations were conducted for 300 ns to study the effect of different protonation states on the chi1 angle populations of His 131. From these simulations the first 100 ns were discarded to account for the equilibration and the last 200 ns were used for analysis.

The second and the third unbiased simulations were carried out in the presence of 100 molecules of ammonia and ammonium ions, respectively. The molecules were equally distributed into the two compartments formed by the bilayer. In these simulations the first 100 ns were discarded to allow for equilibration. The densities for the ammonium ions and water were plotted with the volmap tool from VMD (28).

To calculate the Potential of Mean Force (PMF) for the permeation of ammonia, the g_wham tool from GROMACS 4.5 was used (29) in the same manner as used by Hub *et al.* (30). In order to ensure that the comparison between the PMFs presented is meaningful we use the cylindrical restraints as used by Hub *et al*. (31). In this framework we introduce a flat bottom potential around the ammonia molecule, which restricts the target of umbrella sampling within a radial boundary of radius 2 nm. Within its boundary it experiences zero potential. Outside this boundary it experiences a harmonic potential with a force constant of 1,000 kJ mol^{-1} nm^{-2}. This precaution ensures that the entropic effects of entering the channel pore are meaningfully accounted for when comparing different PMF profiles for *At*TIP2;1. We do not symmetrize the potentials. The model membrane consisted of equal amounts of POPC and 1,2-dipalmitoyl-glycero-3-phosphocholine (DPPC) lipids, with or without 20% cholesterol. The channel axis along the z coordinate was used for sampling. It was divided into 280 windows of 0.25 Å each to yield a length of 7 nm centered at the NPA motifs. Each window

was simulated for 1.5 ns, 500 ps of which were discarded to allow for equilibration. A force constant of 1,000 kJ $mol^{-1}nm^{-2}$ was used to restrain the ammonia molecule in the window. The errors were calculated with the 50 iterations of the bootstrap algorithm as implemented in the g_wham tool (29).

Images in Fig. 4A–C and Movie S1 were created with the VMD program (28). Movie S1 shows 147 consecutive frames, which are 20 ps apart from each other. For clarity, the trajectory of cartoon representation is smoothened with a window size of 5. The trajectories of amino acid residues highlighted as sticks are averaged over 2 frames (window size 1), while the ammonia molecule is depicted frame wise.

References

1. Karlsson M*, et al.* (2003) Reconstitution of water channel function of an aquaporin overexpressed and purified from Pichia pastoris. *FEBS Letters* 537(1-3):68-72.
2. Hasler L*, et al.* (1998) Purified lens major intrinsic protein (MIP) forms highly ordered tetragonal two-dimensional arrays by reconstitution. *Journal of Molecular Biology* 279(4):855-864.
3. Kabsch W (2010) Xds. *Acta Crystallogr D Biol Crystallogr* 66(Pt 2):125-132.
4. Emsley P, Lohkamp B, Scott WG, & Cowtan K (2010) Features and development of Coot. *Acta Crystallographica Section D* 66(4):486-501.
5. Corporate A (1994) The CCP4 suite: programs for protein crystallography. *Acta Crystallogr D Biol Crystallogr* 50(Pt-5):760-763.
6. Potterton E, Briggs P, Turkenburg M, & Dodson E (2003) A graphical user interface to the CCP4 program suite. *Acta Crystallographica Section D* 59(7):1131-1137.
7. Schrodinger, LLC, The PyMOL Molecular Graphics System, Version 1.5.0.4 (2010)).
8. Lovell SC*, et al.* (2003) Structure validation by Cα geometry: φ,ψ and Cβ deviation. *Proteins: Structure, Function, and Bioinformatics* 50(3):437-450.
9. Chen VB*, et al.* (2010) MolProbity: all-atom structure validation for macromolecular crystallography. *Acta Crystallogr D Biol Crystallogr* 66(Pt 1):12-21.
10. Smart OS, Goodfellow JM, & Wallace BA (1993) The pore dimensions of gramicidin A. *Biophys J* 65(6):2455-2460.
11. GraphPad Software SDCU, www.graphpad.com (2007) GraphPad Prism version 5.01 for Windows.
12. Nour-Eldin HH, Hansen BG, Norholm MH, Jensen JK, & Halkier BA (2006) Advancing uracil-excision based cloning towards an ideal technique for cloning PCR fragments. *Nucleic Acids Res* 34(18):e122.
13. Hamann T & Moller BL (2007) Improved cloning and expression of cytochrome P450s and cytochrome P450 reductase in yeast. *Protein Expr Purif* 56(1):121-127.
14. Geu-Flores F, Nour-Eldin HH, Nielsen MT, & Halkier BA (2007) USER fusion: a rapid and efficient method for simultaneous fusion and cloning of multiple PCR products. *Nucleic Acids Res* 35(7):e55.

15. Marini AM, Soussi-Boudekou S, Vissers S, & Andre B (1997) A family of ammonium transporters in Saccharomyces cerevisiae. *Mol Cell Biol* 17(8):4282-4293.
16. Bertl A & Kaldenhoff R (2007) Function of a separate NH3-pore in Aquaporin TIP2;2 from wheat. *FEBS Letters* 581(28):5413-5417.
17. Pronk S*, et al.* (2013) GROMACS 4.5: a high-throughput and highly parallel open source molecular simulation toolkit. *Bioinformatics* 29(7):845-854.
18. Wolf MG, Hoefling M, Aponte-Santamaria C, Grubmuller H, & Groenhof G (2010) g_membed: Efficient insertion of a membrane protein into an equilibrated lipid bilayer with minimal perturbation. *J Comput Chem* 31(11):2169-2174.
19. Jorgensen WL, Chandrasekhar J, Madura JD, Impey RW, & Klein ML (1983) Comparison of Simple Potential Functions for Simulating Liquid Water. *J Chem Phys* 79(2):926-935.
20. Bussi G, Donadio D, & Parrinello M (2007) Canonical sampling through velocity rescaling. *J Chem Phys* 126(1):Artn 014101.
21. Berendsen HJC, Postma JPM, Vangunsteren WF, Dinola A, & Haak JR (1984) Molecular-Dynamics with Coupling to an External Bath. *J Chem Phys* 81(8):3684-3690.
22. Klauda JB*, et al.* (2010) Update of the CHARMM All-Atom Additive Force Field for Lipids: Validation on Six Lipid Types. *J Phys Chem B* 114(23):7830-7843.
23. Darden T, York D, & Pedersen L (1993) Particle Mesh Ewald - an N.Log(N) Method for Ewald Sums in Large Systems. *J Chem Phys* 98(12):10089-10092.
24. Foloppe N & MacKerell AD (2000) All-atom empirical force field for nucleic acids: I. Parameter optimization based on small molecule and condensed phase macromolecular target data. *J Comput Chem* 21(2):86-104.
25. Jo S, Kim T, Iyer VG, & Im W (2008) CHARMM-GUI: a web-based graphical user interface for CHARMM. *J Comput Chem* 29(11):1859-1865.
26. Zhu FQ, Tajkhorshid E, & Schulten K (2004) Collective diffusion model for water permeation through microscopic channels. *Phys Rev Lett* 93(22):Artn 224501.
27. Aponte-Santamaria C, Hub JS, & de Groot BL (2010) Dynamics and energetics of solute permeation through the Plasmodium falciparum aquaglyceroporin. *Phys Chem Chem Phys* 12(35):10246-10254.
28. Humphrey W, Dalke, A. and Schulten, K. (1996) VMD - Visual Molecular Dynamics. pp 33-38.
29. Hub JS, Winkler FK, Merrick M, & de Groot BL (2010) Potentials of mean force and permeabilities for carbon dioxide, ammonia, and water flux across a Rhesus protein channel and lipid membranes. *J Am Chem Soc* 132(38):13251-13263.
30. Hub JS, de Groot BL, & van der Spoel D (2010) g_wham-A Free Weighted Histogram Analysis Implementation Including Robust Error and Autocorrelation Estimates. *J Chem Theory Comput* 6(12):3713-3720.
31. Hub JS & de Groot BL (2008) Mechanism of selectivity in aquaporins and aquaglyceroporins. *Proc Natl Acad Sci U S A* 105(4):1198-1203.

Supporting Figures

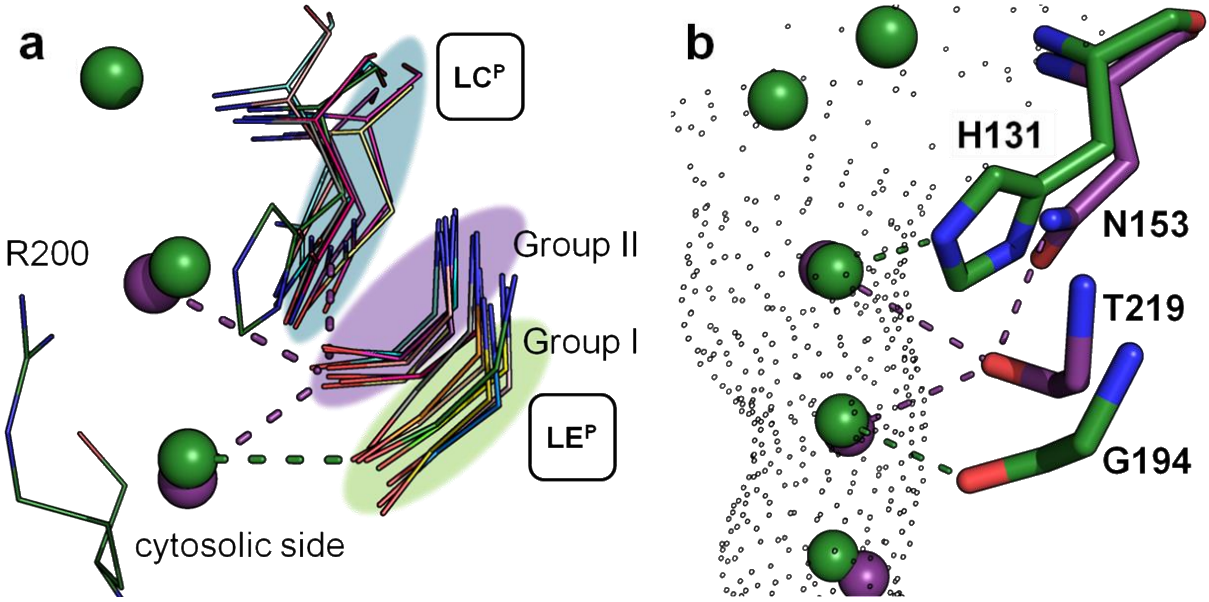

S1 Fig. Selectivity filter carbonyls in loop E cluster in two distinct spatial groups.
(A) HE^P-arginine (R200) of *At*TIP2;1 is shown for orientation. Carbonyls at LE^P of water-specific AQPs form group II (violet shading), and most of them are within hydrogen-bonding distance to two water molecules in their structures as illustrated by *So*PIP2;1 (PDB ID 1Z98; violet). Carbonyls of non-water-specific channels gather in a different location (group I; green shading). Among those are *At*TIP2;1 (green), glycerol transport facilitating, and uncharacterized proteins (*Af*AqpM, *Pf*AQP, *Ec*GlpF, *Mm*AqpM), but the water-specific *Hs*AQP4 also belongs to this group. Like all other members of this group, *Hs*AQP4 is lacking the LC^P-asparagine (N153 in *So*PIP2;1, Fig 3D) that is conserved among the other water-specific proteins (blue shading, only asparagines residues are shown). Each carbonyl in group II can form a hydrogen bond to the carboxamide of this asparagine, if the carboxamide is oriented the right way. A certain flexibility is suggested by the special case of *Hs*AQP0, where different structures are available (1YMG and 2B6O shown) and the carbonyl is seen with both orientations. Apart from the glycerol facilitators, it appears that small residues like glycine and alanine in LE^P (Fig 3D) are required in group I, whereas slightly larger residues like cysteine or threonine can be accommodated in group II. Only backbone is shown in LE^P.
(B) Close up of *At*TIP2;1 (green) and *So*PIP2;1 (violet), showing hydrogen bonding of carbonyls at LE^P and water interacting with LC^P-His 131. Side chain of LE^P-Thr 219 is not shown. Main pore of *At*TIP2;1 analyzed by HOLE [38].

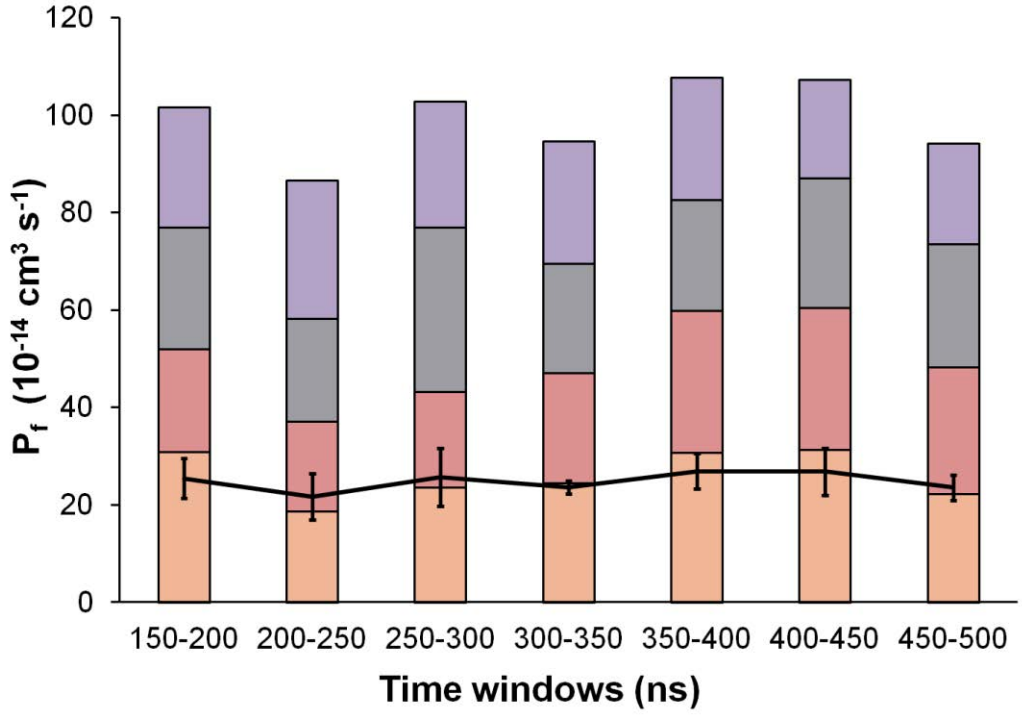

S2 Fig. Osmotic permeability (p_f) values calculated from MD simulations.
p_f values were calculated separately for each monomer in seven 50-ns time windows. The contribution of the individual monomers to the p_f values of the tetramer are indicated by different colors and average values per monomer and standard deviation in each time window are indicated by the black line and error bars. The underlying data can be found in S1 Data. doi:10.1371/journal.pbio.1002411.s003

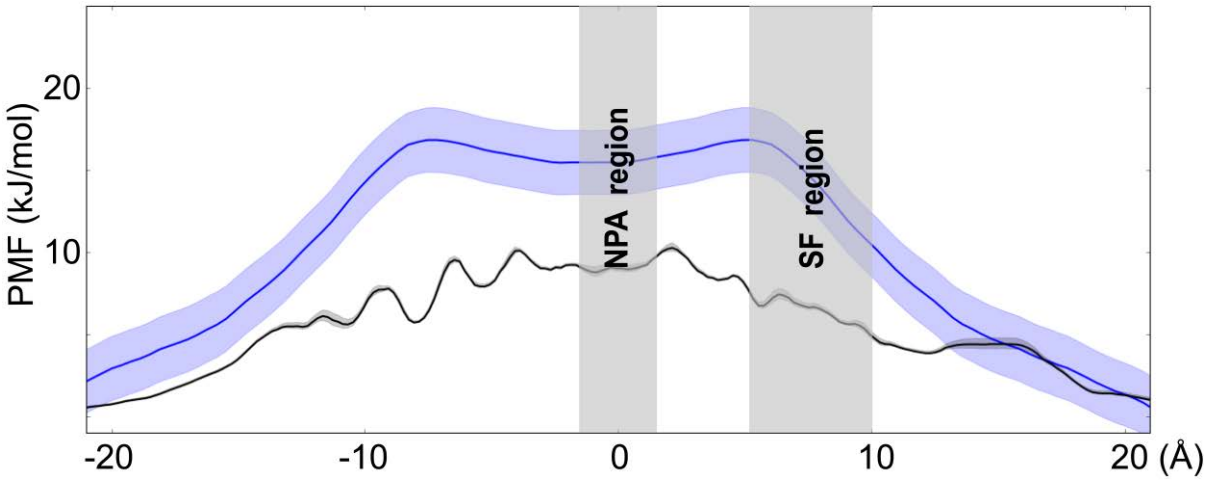

S3 Fig. PMF for water across the *At*TIP2;1 channel calculated from the equilibrium trajectory (black).
The error bars are the standard deviation of the PMF over the four monomers of the protein. PMF profile for ammonia across a model membrane without cholesterol is shown in blue. The underlying data can be found in S1 Data. doi:10.1371/journal.pbio.1002411.s004

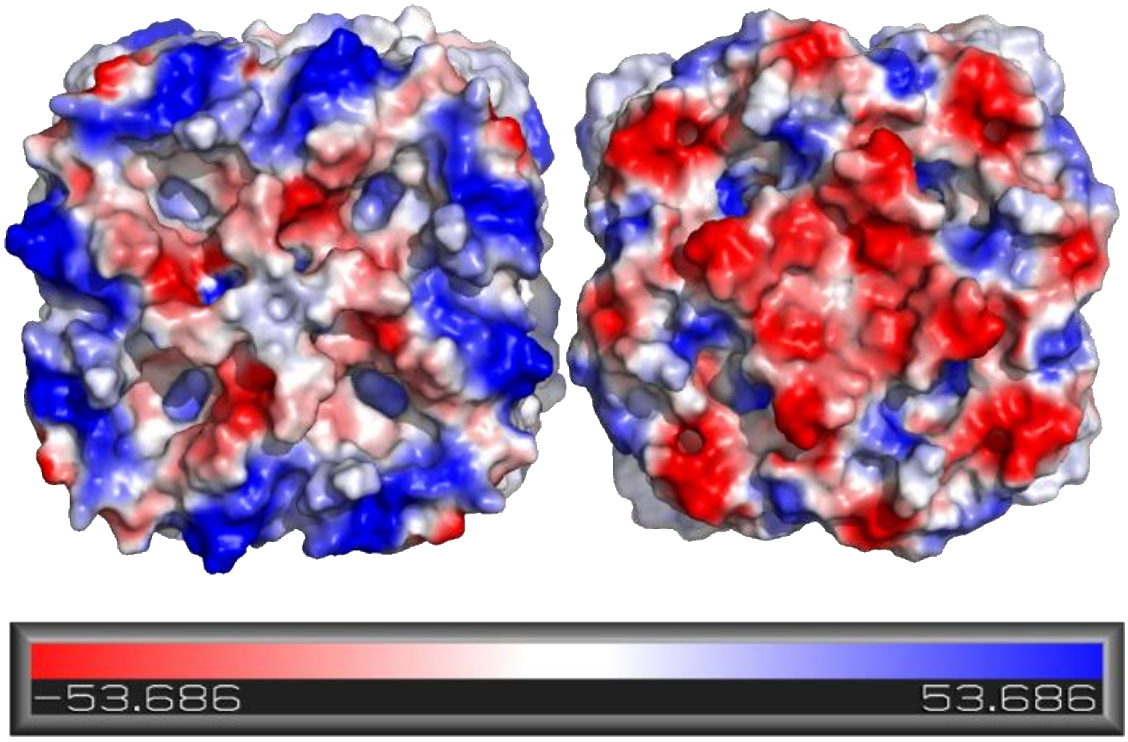

S4 Fig. Corresponding vacuum electrostatic maps of two plant AQPs.
The noncytosolic surface of the tetramer of *So*PIP2;1 (left, facing the apoplast) and *At*TIP2;1 (right, facing the interior of the vacuole). Positive and negative electrostatic potentials calculated by PyMol [39] are marked by gradients of blue and red, respectively.
doi:10.1371/journal.pbio.1002411.s005

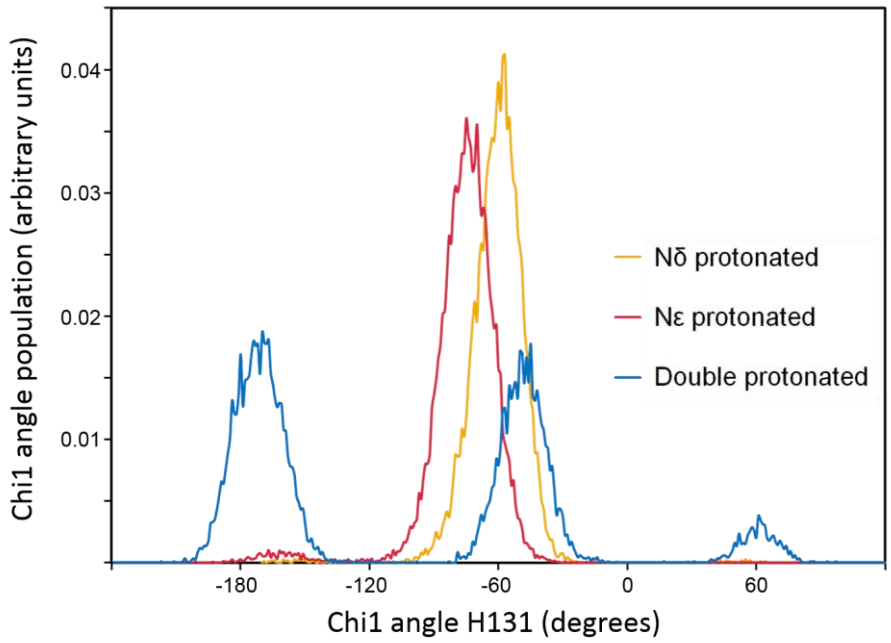

S5 Fig. Dihedral populations of LC^{P}-His 131 at three different protonated states.
Chi1 angles in MD simulations with doubly protonated (positively charged; blue), Nδ protonated (neutral; yellow), and Nε protonated (neutral; red) His 131. The underlying data can be found in S1 Data. doi:10.1371/journal.pbio.1002411.s006

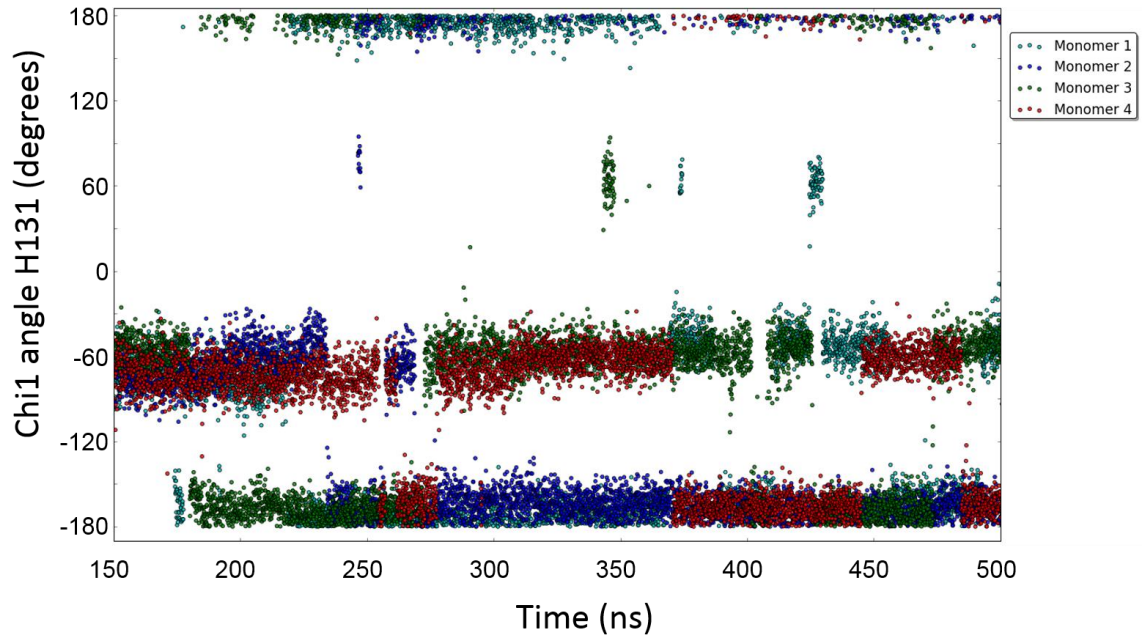

S6 Fig. Dihedral chi1 angle of the LC^{P}-His 131 residue in the doubly protonated His 131 simulation summarized in S5 Fig.
The data is shown for final ~350 ns of the 500 ns trajectory after the first observed transition. The His 131 residue spontaneously exchanges between its possible configurations in all the four monomers of the protein. The underlying data can be found in S1 Data. doi:10.1371/journal.pbio.1002411.s007

frontiers in Plant Science

ORIGINAL RESEARCH
published: 30 August 2016
doi: 10.3389/fpls.2016.01249

Increased Permeability of the Aquaporin *So*PIP2;1 by Mercury and Mutations in Loop A

*Andreas Kirscht†, Sabeen Survery†, Per Kjellbom and Urban Johanson**

Department of Biochemistry and Structural Biology, Center for Molecular Protein Science, Lund University, Lund, Sweden

Aquaporins (AQPs) also referred to as Major intrinsic proteins, regulate permeability of biological membranes for water and other uncharged small polar molecules. Plants encode more AQPs than other organisms and just one of the four AQP subfamilies in *Arabidopsis thaliana*, the water specific plasma membrane intrinsic proteins (PIPs), has 13 isoforms, the same number as the total AQPs encoded by the entire human genome. The PIPs are more conserved than other plant AQPs and here we demonstrate that a cysteine residue, in loop A of *So*PIP2;1 from *Spinacia oleracea*, is forming disulfide bridges. This is in agreement with studies on maize PIPs, but in contrast we also show an increased permeability of mutants with a substitution at this position. In accordance with earlier findings, we confirm that mercury increases water permeability of both wild type and mutant proteins. We report on the slow kinetics and reversibility of the activation, and on quenching of intrinsic tryptophan fluorescence as a potential reporter of conformational changes associated with activation. Hence, previous studies in plants based on the assumption of mercury as a general AQP blocker have to be reevaluated, whereas mercury and fluorescence studies of isolated PIPs provide new means to follow structural changes dynamically.

Keywords: aquaporin, water channel, major intrinsic protein, *Spinacia oleracea*, tryptophan fluorescence

OPEN ACCESS

Edited by:
Rupesh Kailasrao Deshmukh, Laval University, Canada

Reviewed by:
Gunvant Baliram Patil, University of Missouri, USA
Dirk Schneider, University of Mainz, Germany
Micaela Carvajal, Spanish National Research Council, Spain

****Correspondence:***
Urban Johanson
urban.johanson@biochemistry.lu.se

† These authors shared first authorship, names in alphabetical order.

Specialty section:
This article was submitted to Plant Physiology, a section of the journal Frontiers in Plant Science

Received: *29 May 2016*
Accepted: *08 August 2016*
Published: *30 August 2016*

Citation:
Kirscht A, Survery S, Kjellbom P and Johanson U (2016) Increased Permeability of the Aquaporin SoPIP2;1 by Mercury and Mutations in Loop A. Front. Plant Sci. 7:1249. doi: 10.3389/fpls.2016.01249

INTRODUCTION

Aquaporins (AQPs) are common in all domains of life and facilitate permeation of a wide range of small polar molecules through biological membranes (Abascal et al., 2014). AQPs are generally found as homotetramers, where each monomer constitutes a separate pore formed by six transmembrane helices and two short helices that are connected in the middle of the lipid bilayer at their N-termini (Fu et al., 2000; Sui et al., 2001; Törnroth-Horsefield et al., 2006; Horsefield et al., 2008; Kirscht et al., 2016). Members belonging to the plant subfamily of plasma membrane intrinsic proteins (PIPs) are specifically permeable to water and show a more strict amino acid sequence conservation than AQPs in other subfamilies (Danielson and Johanson, 2010). Function and abundance of these proteins is tightly regulated and the high number of isoforms suggests a highly redundant system for water homeostasis (Johanson et al., 2001; Alexandersson et al., 2005, 2010). Structure and regulation of one particular member of the PIP subfamily from spinach (*Spinacia oleracea*), *So*PIP2;1, which constitutes a dominating integral protein of the plasma membrane has been thoroughly studied (Johansson et al., 1996, 1998; Kukulski et al., 2005; Törnroth-Horsefield et al., 2006; Nyblom et al., 2009; Frick et al., 2013).

The structure of *So*PIP2;1 was solved in different conformations, which elucidated a general molecular gating mechanism for the regulation of PIPs, including some specific elements only relevant for members of the PIP2 subgroup (Törnroth-Horsefield et al., 2006). The gating of the pore is the result of conformational changes on the cytoplasmic side of the membrane and is controlled in several different ways, including, pH changes, binding of calcium and a PIP2 specific phosphorylation. The second cytosolic loop, Loop D, undergoes a major conformational change and its stabilization in certain positions is increasing the probability of an either open or closed conformation. In the closed conformation, unphosphorylated serine 274, situated close to the C-terminus, occupies a place near the tetrameric center of the protein while the preceding region resides in a grove between the monomers. When this positioning is impossible, e.g., by phosphorylation of serine 274, the C-terminus becomes unordered and the place earlier occupied by this residue is instead taken by the carbonyl oxygen of leucine 197 from the neighboring monomer, resulting in the unblocking of the pore in this monomer.

Already in early protein preparations, it became clear that interactions between monomers are strong in *So*PIP2;1 tetramers (Johansson et al., 1996). Even during separation by a standard SDS-PAGE, which denatures most proteins, a large fraction of the protein is found to stay as dimers and tetramers (Karlsson et al., 2003). PIPs differ from all other plant AQPs by a highly conserved cysteine in the first extracellular loop (loop A). The conserved cysteines (C69 in *So*PIP2;1) from all four monomers are located at the tetrameric center (Törnroth-Horsefield et al., 2006). Based on low resolution structures, it had been suggested that the reason for the conservation stems from the necessity to stabilize the PIP tetramers by fostering hydrogen bonds or complexing a metal ion (Kukulski et al., 2005).

To analyze the nature of possible interactions of the conserved cysteine (C69) in the tetramer, we probed possible disulfide bridges by addition of reducing agents. For further analysis, we created mutants and purified the heterologously expressed proteins. In this study, we measured stability changes for cysteine 69 mutants and compared these to their kinetic properties to elucidate the structural and functional basis for the strong evolutionary conservation of this amino acid residue. In addition we show that mercury – generally regarded as a blocker of AQPs – is activating *So*PIP2;1 and concentration-response experiments suggest that quenching of tryptophan fluorescence reports on conformational changes associated with the activation. Our findings of disulfide bridges and mercury activation are largely consistent with results recently published by other groups (Bienert et al., 2012; Frick et al., 2013).

RESULTS

A Conserved Cysteine Forms Disulfide Bridges between Monomers

To discern inter-monomeric interactions of *So*PIP2;1 further, we decided to study structural and functional properties of isolated wild type (WT) and mutant protein. Therefore, we overexpressed *So*PIP2;1 in *Pichia pastoris* and performed different stability tests of solubilized and purified protein. The isolated WT protein was incubated for various length of time with different reducing agents prior to analysis by SDS-PAGE, in order to monitor any effect of potentially disrupted disulfide bridges on the migration pattern in acrylamide gels (**Figure 1**). The relative amount of SDS resistant dimer in the gel could be decreased by DTT and β-mercaptoethanol. The latter was more effective, but none of the reducing agents could increase the monomer-to-dimer ratio further after the first hour of incubation. Surprisingly, the split of the dimer was not increased above 100 mM DTT and the final ratio of monomer to dimer was less than 1/10, while β-mercaptoethanol decreased the dimers by 50% at most (not

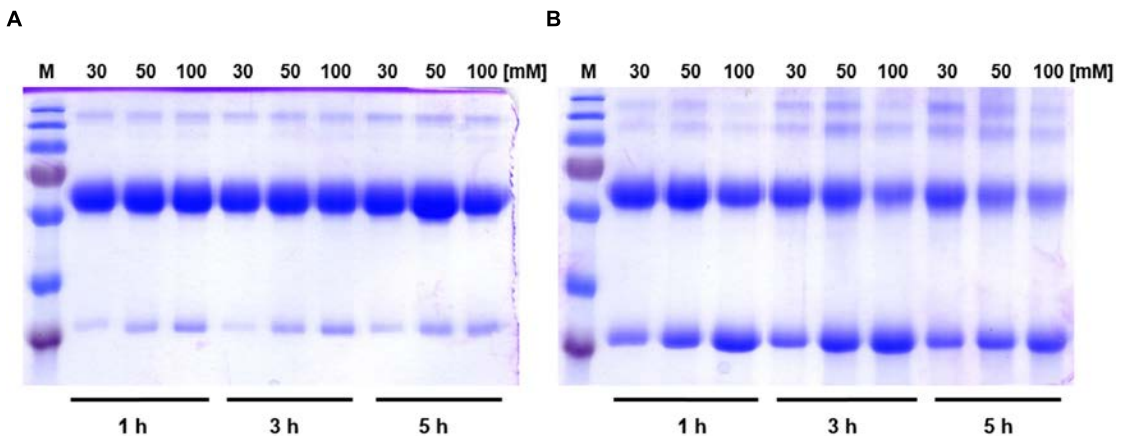

FIGURE 1 | The effect of reducing agents on relative amounts of dimers and monomers of *So*PIP2;1. (A) Incubation of *So*PIP2;1 with DTT. The concentration of DTT and the incubation time are shown at the top and at the bottom of the gel, respectively. It is evident from the gel that DTT is unable to completely reduce dimers into monomers, even after 5 h incubation with 100 mM DTT. **(B)** Effect of incubation of *So*PIP2;1 with β-mercaptoethanol. The concentration of β-mercaptoethanol and the incubation time are shown on top and bottom of the gel, respectively. The results show that β-mercaptoethanol is more effective than DTT, but it still fails to reduce the dimers into monomers completely. M = molecular weight marker (from top 250, 130, 100, 70, 55, 35, and 25 kDa).

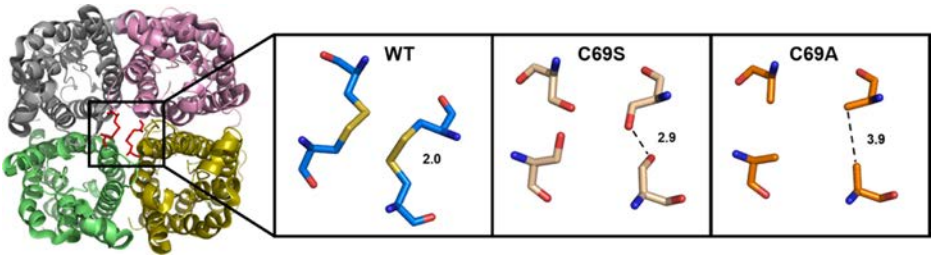

FIGURE 2 | Extracellular view of the *So*PIP2;1 wild type (WT) tetramer with the expected disulfide bridges at the center (Left). Close up on C69 with distances between cysteines (PDB ID: 2B5F) or modeled residues in mutant proteins with this cysteine replaced by serine **(Middle)** or alanine **(Right)**.

shown). Either this reflects the equilibrium between monomeric and dimeric fraction when all disulfide bonds are reduced, mainly stabilized by hydrophobic interactions (Törnroth-Horsefield et al., 2006), or some of the SDS solubilized dimers have disulfide bonds that are inaccessible so that they cannot be reduced under these conditions. The latter is supported by the apparent higher efficiency of β-mercaptoethanol which has about half the molecular weight compared to DTT. Adding urea to the reduction step increased the monomeric fraction (not shown). However, not even incubation for 1 h with 8 M urea and 300 mM DTT and resolving the samples on an 8 M denaturing urea gel was sufficient to completely remove the multimeric bands (Supplementary Figure 1). From a physical and evolutionary point of view it is of interest if the stability of the protein is changed upon removal of the cysteine. Two mutants, substituted at cysteine 69 with serine (C69S) or alanine (C69A) (**Figure 2**), were expressed and purified and their oligomeric patterns (as shown by standard SDS-PAGE) were compared to the WT protein (**Figure 3A**). Although dimeric bands were still visible in both mutants, they were significantly weaker as compared to the WT protein, which was expected from the destabilizing effect of reducing agents on dimers of the WT protein. In order to compare the thermodynamic stability of WT *So*PIP2;1 and the two cysteine 69 mutants, we performed thermal denaturation circular dichroism (CD) spectroscopic measurements. A thermal denaturation curve was constructed based on the normalized mean residual ellipticity (MRE) at 222 nm (**Figure 3B**). The midpoint of transition in WT (56.9°C) was slightly higher in comparison with the mutants (54.6°C for C69S and 53.4°C for C69A), suggesting that the interactions at this position do not contribute much toward the thermodynamic stability, which is expected since the contribution of disulfide bonds to protein stability is kinetic rather than thermodynamic (Clarke and Fersht, 1993). Considering the high stability of *So*PIP2;1 in lipid bilayers (Plasencia et al., 2011), it is not clear if the relatively small additional thermal stabilization due to the disulfide bonds is sufficient to explain the strict conservation of this cysteine.

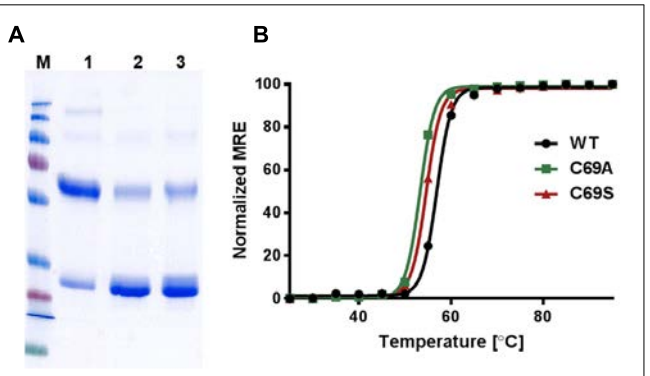

FIGURE 3 | Stability of WT *So*PIP2;1 and the mutants C69A and C69S. **(A)** The integrity and purity of WT and mutant protein after Ni-NTA affinity chromatography were assessed by SDS-PAGE. 1 = WT *So*PIP2;1, 2 = C69A, 3 = C69S. The purified WT *So*PIP2;1 exists as tetramers under native conditions. Under standard denaturing conditions (SDS-PAGE), the WT *So*PIP2;1 mainly runs as a dimer. In case of cysteine mutants, the monomeric form is predominant. This indicates that the cysteine residue in loop A is involved in disulfide bond formation between two PIP monomers. M = molecular weight marker (from top 250, 130, 100, 70, 55, 35, 25, 15, and 10 kDa). **(B)** Thermal denaturation of *So*PIP2;1 recorded by CD spectrometry. The midpoint of the two-state unfolding transition is slightly higher for the WT (56.9°C) compared to the mutants (C69S 54.6°C; C69A 53.4°C). The midpoints are based on one experiment. The normalized mean residual ellipticity (MRE) at 222 nm is plotted as a function of temperature.

Water Permeability Is Increased by Mutations in Loop A

To investigate if the disulfide bonds have an effect on function all three proteins were reconstituted in proteoliposomes to examine their kinetic properties. Since the activity assays confirmed functional proteins (**Figure 4A**), we assessed their permeabilities. The protein content in the liposomes was estimated by quantitative western blots and the monomeric permeabilities, the p_f-values, were calculated. Surprisingly, the mutant C69S shows increased water permeability ($P < 0.001$) and this is even more pronounced in the C69A mutant ($P < 0.0001$; **Figure 4B**). The location of this residue immediately raises the question about water transport through the central pore. This scenario would be consistent with the observed larger enhancement of water permeability when cysteine is exchanged with an amino acid residue smaller than serine. Alternatively the increase is purely caused by destabilization of the dimer, where the alanine mutant would not be able to form hydrogen bonds like the serine mutant, which may partially compensate for the missing disulfide bridges.

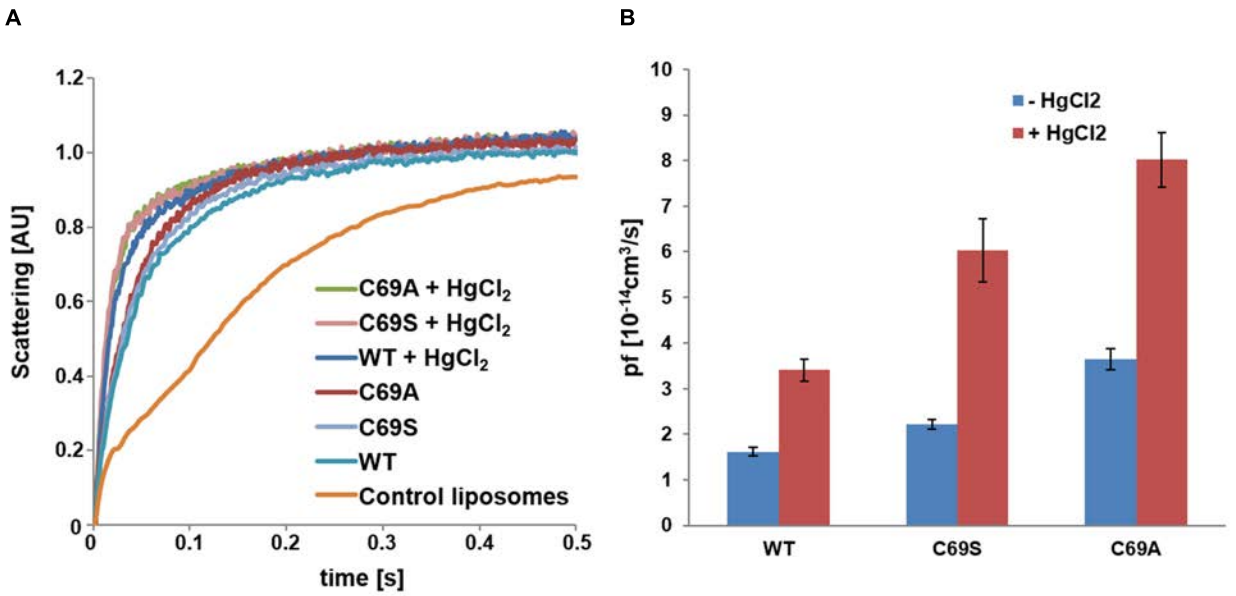

FIGURE 4 | Water conductivity of liposomes measured by stopped-flow spectrometry. (A) Change in scattering at 500 nm over time plotted for *So*PIP2;1 WT and C69 mutant proteoliposomes as compared to empty liposomes. Each plot represents an average of 10–17 curves. **(B)** Monomeric permeabilities without mercury (blue) and with 1 mM mercury (red). The rates were obtained from single exponential fits of 10 or more curves; error bars present their standard deviations. The water conductivities were higher for the mutants as compared to the WT protein and mercury increased the p_f-values of all proteins by a similar factor (2.1–2.7). The rate constants and the p_f-values are provided in Supplementary Table 1, while the statistics for comparisons of the p_f-values are reported in Supplementary Table 2.

Mercury Increases Water Permeability and Quench Intrinsic Tryptophan Fluorescence

If some water permeation is independent of the pore in the monomer, it could be measured by eliminating the conductivity of the monomeric pore. Beside reported pH and Ca^{2+} dependent gating, mercury is a well-known inhibitor of AQPs (Preston et al., 1993; Hukin et al., 2002). To our surprise, mercury instead increased the permeability of *So*PIP2;1 proteoliposomes ($P < 0.0001$; **Figure 4**). If this effect is a result of conformational changes, there is a chance to observe mercury binding by CD measurements or by monitoring the intrinsic tryptophan fluorescence of *So*PIP2;1. The CD spectrum of *So*PIP2;1 in detergent micelles did not change significantly upon the addition of mercury (data not shown). However, the tryptophan fluorescence was altered and quenched by a factor of three after an incubation with 200 μM mercury chloride (**Figure 5**). Moreover, the quenching could be reversed by chelating mercury with β-mercaptoethanol, supporting that it is caused by reversible conformational changes rather than denaturation of *So*PIP2;1. This is in accordance with the kinetic experiments, where mercury activation can be reversed by addition of β-mercaptoethanol (**Figure 6A**). It should be noted that the concentrations of reducing agent used for the reversal of quenching and activation, 1 and 2 mM, respectively, are much lower than the levels required to partially reduce the disulfide bridge of the dimers. Thus given the modest increase in activity of the C69S mutant completely lacking the disulfide bridge, any increase due to reduction of cysteine 69 is expected to be small. This is consistent with the more or less identical rates of untreated proteoliposomes and the activated and reversed ditto. To investigate the concentration dependency of the activation stopped-flow experiments were done and the EC_{50} for mercury was calculated to be around 4 μM (**Figure 6B**). Interestingly, a concentration-response curve of the quenching of tryptophan fluorescence gives an EC_{50} value of 1.6 μM (**Figure 7**). Thus the quenching in micelles may be caused by conformational changes associated with activation in proteoliposomes.

Activation by Mercury and by Loop A Mutations Are Additive

Cysteine 69 mutants present an increased water transport compared to the WT, which might be explained by opening of a tetrameric central pore or by indirect effects on the structure of the monomeric pore. WT *So*PIP2;1 can be activated by mercury, but are the cysteine mutants also affected by mercury? Analysis of stopped-flow data, showed that the activation by mercury and the increase of permeability by mutations were not overlapping, but additive (**Figure 4B**). While the p_f of the WT permeability changes from 1.6 ± 0.1 to 3.4 ± 0.2 [10^{-14} cm^3/s], the p_f of alanine and serine mutants are amplified by about the same factor, rising from 3.6 ± 0.2 to 8.0 ± 0.6 and 2.2 ± 0.1 to 6.0 ± 0.7 [10^{-14} cm^3/s], respectively. This suggest that the mercury activation is independent of the increase in water permeability caused by the mutations in loop A.

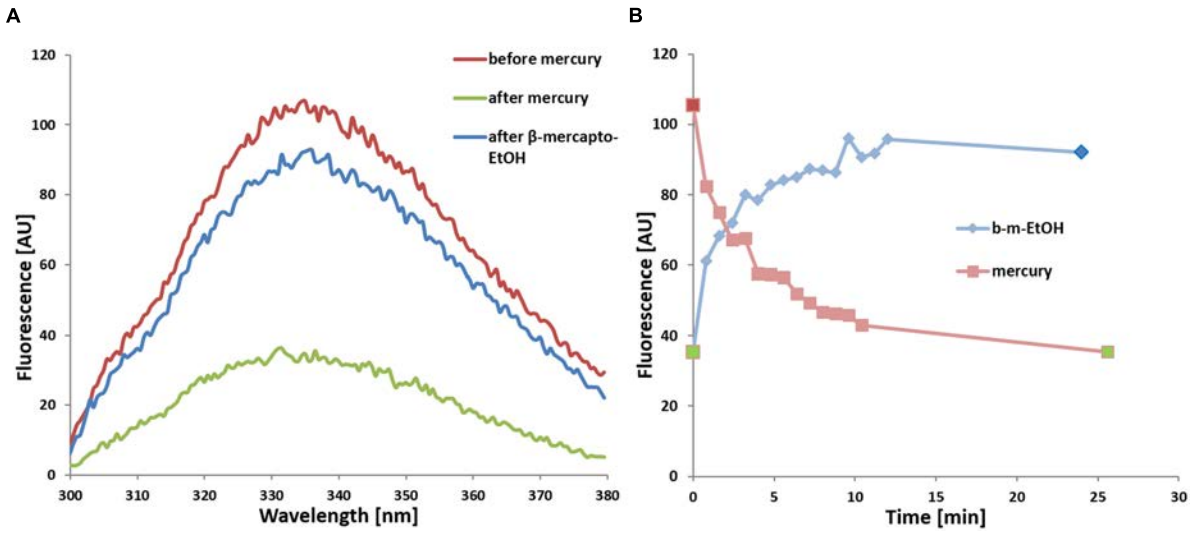

FIGURE 5 | (A) Quenching of tryptophan fluorescence of WT *So*PIP2;1 upon addition of 200 μM mercury (green) and subsequent reversal by addition of 1 mM β-mercaptoethanol (blue) in comparison to untreated protein (red). The fluorescence at 335 nm from excitation at 280 nm is lowered by two thirds. **(B)** Time dependence of fluorescence quenching upon addition of 200 μM $HgCl_2$ (light red) and recovering of fluorescence upon subsequent addition of 1 mM β-mercaptoethanol to the same sample (b-m-EtOH, light blue). The individual maximum of every spectrum are plotted, where each spectrum was recorded at a scanning speed of 100 nm/min (48 s per spectrum + 1 s delay). The spectra in **(A)** correspond to the three time points marked in the same color in **(B)**: before addition of $HgCl_2$ (red), after 25 min incubation with $HgCl_2$ but before addition of β-mercaptoethanol (green; replotted at time zero), and at the endpoint after the incubation with β-mercaptoethanol (blue).

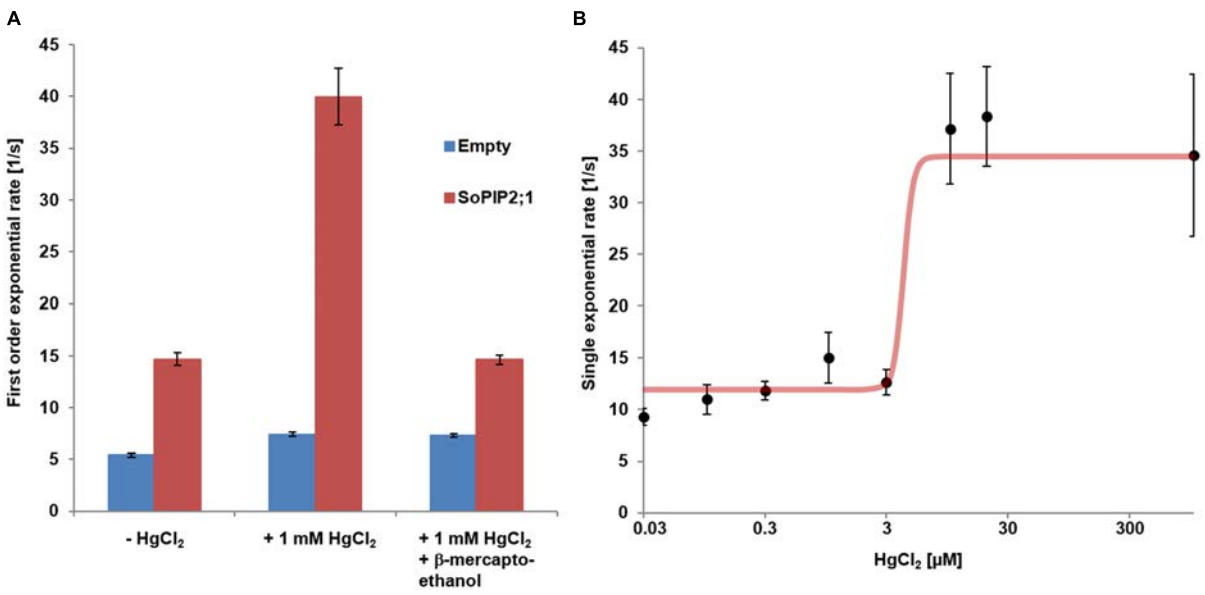

FIGURE 6 | Mercury activation of WT *So*PIP2;1. (A) Reversibility of mercury activation first order exponential rates of water conductivity from stopped-flow experiments. Mean rates (±SD) are presented for proteo-liposomes (red) and control liposome (blue). Activation of proteo-liposomes treated with mercury can be reversed by subsequent incubation with 2 mM β-mercaptoethanol. Statistics for comparisons of the rate constants are reported in Supplementary Table 3 and numerical values for mean rates and SD are found in Supplementary Table 4. **(B)** Dose response curve of mercury activation. The curve presents a Hill coefficient around 11 and an EC_{50} for mercury of 4.2 μM.

DISCUSSION

This work was originally initiated to describe intermonomeric interactions and their effects. The effect of reducing agents on the oligomeric pattern in SDS-PAGE indicated the existence of disulfide bonds that stabilize protein dimers. This was also concluded in studies mutating corresponding cysteines in the tetrameric center of various PIP2s from

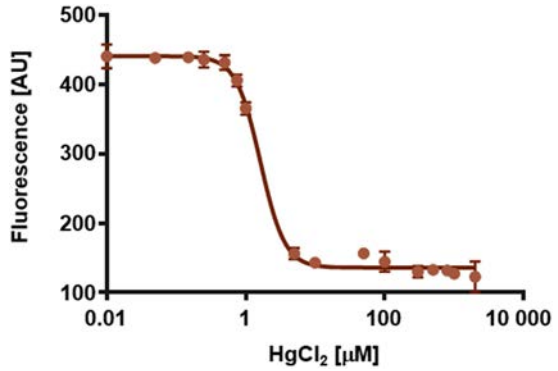

FIGURE 7 | Quenching of the intrinsic tryptophan fluorescence of *So*PIP2;1 at 335 nm as function of the logarithm of the $HgCl_2$ concentration. The calculated EC_{50} is 1.6 µM and the Hill slope is −2.5. Averages of three replicates and standard errors are plotted.

maize (Bienert et al., 2012). Additional to the more detailed analysis of disulfide bridges in the tetrameric center, we discovered that our preparation of *So*PIP2;1 was not maximally permeable under our standard conditions. It should be noted that the obtained p_f-values here (1.6–8.0 [10^{-14}cm^{3}s^{-1}]) are in the same range as has been estimated for other AQPs using *Xenopus* oocytes (0.2–24 [10^{-14}cm^{3}s^{-1}]; Yang and Verkman, 1997) and correspond to a passage of more than 10^{11} water molecules per second through each monomer of *So*PIP2;1. Although activation of a water specific channel by mercury is unlikely to have a physiological role, the molecular details of its binding and conformational changes may still be relevant for our understanding of physiological gating mechanisms.

Increased Permeability in Mutants and by Mercury

Our results suggest that the mechanism for activation by mercury is independent of the enhancement of water permeability caused by the mutations in the A loop. A simple mechanistic explanation of this would be that permeation through the monomeric pore is increased in the mutants and this is amplified by mercury by stabilization of the gate in an open conformation. However, looking at the structure it is not obvious how a mutation of cysteine 69 could achieve this, but it cannot be excluded that the release of loop A is resulting in a relaxation at the selectivity filter and thereby a higher permeability. If instead also the central pore of the mutant proteins permeates water, how would that be enhanced by mercury binding? Possibly in the same way mercury may support the open conformation of loop D at the monomeric pore; the C-terminal end is removed from its position in the inter-monomeric space. If the highest energy barrier for water permeation through the central pore is caused by interactions between the four C-termini, a destabilization of the C-terminal regions would increase the water leakage through this hypothetical pore. One should keep in mind that these C-terminal interactions are not structurally supported as the last modeled amino acid residues in the closed structures are still too far from the center. Thus a possible contribution of the central pore to the increased permeability remains speculative.

Tryptophan Fluorescence

The observation that both activation and quenching of tryptophan fluorescence can be triggered by the same ligand, mercury, may suggest that these two effects are not independent but caused by structural rearrangements initiated from the same binding site. So where is the mercury binding and which conformational changes lead to a fluorescence drop of 2/3? If all six tryptophans of the monomer have the same quantum yield, at least four of them must be quenched. That involves a huge structural change of the protein or putatively a rearrangement of the micelle. Restructuring the micelle of a membrane protein is thought to denature the protein, which is unlikely here, as quenching (**Figure 5**) and increase in activity (**Figure 6A**) are both reversible, and no denaturation was indicated in CD measurements or by precipitating protein (data not shown). Fluorescence intensity of tryptophans can vary greatly depending on their environment (Lakowicz, 2006). Therefore, it appears more likely that one or two tryptophans with high quantum yields, located in a hydrophobic/hydrophilic interface, are responsible for the observed quenching of fluorescence by mercury. According to analyses of structural parameters tryptophans can be classified into five spectral-structural classes (Shen et al., 2008). The observed emission maximum at 335 nm would suggest that Class I and possibly Class II tryptophans dominate the fluorescence spectrum of *So*PIP2;1. This automatic analysis of PDB-files is most likely not applicable for tryptophans that are expected to interact with detergents in a micelle, since the micelle is not included in the structure file. However, it should be relevant for buried residues, like tryptophan 79 situated at the center of the tetramer (**Figure 8**). Based on the closed tetrameric structure (4JC6, omitting detergents or metal atoms) this residue belongs to Class S with an expected emission maximum range between 321 and 325 nm, and is therefore not likely to contribute much to the intensity at 335 nm.

As speculated above the mercury activation may be achieved by stabilizing an open conformation and interestingly the positions of tryptophans 35 and 38 differ in the open and closed structure (Törnroth-Horsefield et al., 2006). In the closed structure tryptophan 35 is potentially in a hydrophobic-polar interface and close to the C-terminus of the next monomer. In the open structure of *So*PIP2;1 tryptophan 35 is repositioned and in addition this conformation is expected to have released the C-terminus, which could have an effect on the environment of tryptophan 35 and therefore quench its fluorescence.

Mercury Binding Site

In a mutational study of *So*PIP2;1 by Frick et al. (2013) it was found that mercury activation is independent of the presence

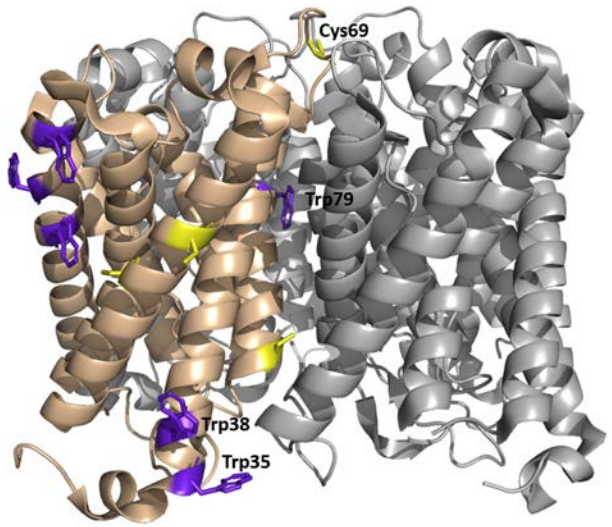

FIGURE 8 | Tetrameric structure of WT *So*PIP2;1 in a closed conformation (PDB ID 1Z98) showing positions of tryptophan and cysteine residues. Each monomer exposes six tryptophans on its outside (purple); four of them (left in the picture) are expected to be in a non-polar environment (detergent micelle in buffer or a lipid membrane), one (tryptophan 79) is positioned in the tetrameric center and only tryptophan 35 is exposed to mobile waters, sitting at the beginning of helix 1 and close to the end of helix 6 and the C-terminus of the next monomer. Four cysteines are present in each monomer, two (left in the picture) are situated close to the tetramer equator, one is positioned in the monomer interface close to the cytosolic side, and cysteine 69 is highly accessible at the periplasmic side of the tetrameric center.

of cysteines. They were able to determine a structure at 2.15 Å with bound mercury and cadmium, in a closed conformation. Additional to the expected binding to cysteines and the known Ca^{2+} site, a new metal binding site was reported. It is described as a second binding site for cadmium, but given the comparable size of the cations and similar preference for hexagonal coordination, one could imagine that also mercury has a potential to bind. The metal seen at this site interacts with a carbonyl (A267) from the C-terminal region (**Figure 9A**). The carbonyl of A267 is actually occupying the same space as the carbonyl of A266 in the first closed structure of *So*PIP2;1 (Törnroth-Horsefield et al., 2006), and consequently there is a different position and orientation of preceding residues up to the end of helix 6. This distinctive change in the structure does not change the averaged static view on the C-terminal regions, which overall are located at the interfaces of the monomers in a closed conformation. Still, the binding strength might be reduced and thereby lower the probability to find this conformation in solution. The conformation of the protein when incubated in β-mercaptoethanol after binding mercury does not change within seconds (**Figure 5B**). We expect that mercury binding or chelating is much faster. Thus, the observed time dependence could be a result of the restructuring of the C-terminal end. If the activation is caused by destabilization of the C-terminal stretch, the effect could be reduced in situations where it is already destabilized for other reasons. This is observed, when comparing the permeability of an untagged *So*PIP2;1 WT and the permeability of the same isoform that ends with a c-myc epitope followed by a hexa-his-tag. The basal (i.e., not fully activated) permeability is higher for the tagged protein, seemingly because the closed conformation of the unphosphorylated C-terminal end is less stabilized (data not shown). It should not go unnoted that similar conclusions were drawn before (Nyblom, 2008, Ph.D. thesis, paper III, page 5). When incubated with mercury the specific water permeability, of both the tagged and untagged protein, levels out at approximately the same permeability values. Conclusively, destabilization by binding of mercury overlaps the destabilization caused by the tag, suggesting that the gate is close to its maximum opening probability in the mercury activated state. Frick et al. (2013) suggested an indirect activation of *So*PIP2;1 via a mercury induced change in membrane properties. This possibility cannot be ruled out, but the relatively low EC_{50} of about 4 μM, which is about 10-fold lower than the IC_{50} for *Hs*AQP5 in proteoliposomes with the same lipid composition (Horsefield et al., 2008), and the correlation with the quenching

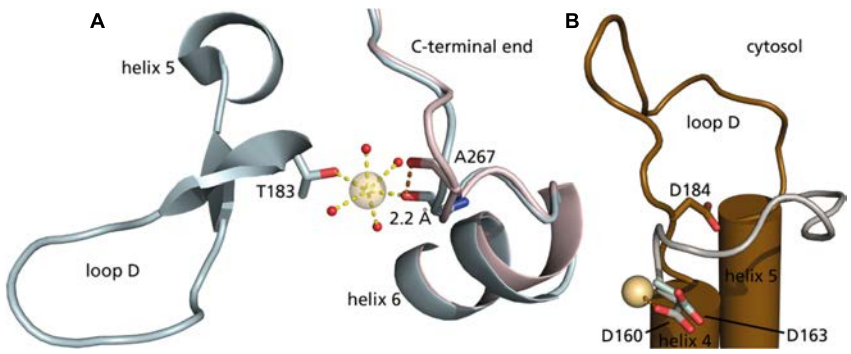

FIGURE 9 | The second metal binding site in *So*PIP2;1. (A) Cytoplasmic view on two closed structures of *So*PIP2;1, with mercury (PDB ID 4JC6) in blue and without mercury (PDB ID 1Z98) in pink. Alanine 267 is shifted 2.2 Å to coordinate the additional heavy metal site. The heavy atom is further coordinated in this structure by threonine 183 at the beginning of loop D and four water molecules (oxygens in red). **(B)** Comparison of conserved aspartate in the open structure of *So*PIP2;1 (D184, brown, one monomer of PDB ID 2B5F) with aspartates of *At*TIP2;1 (D163, light green, 5I32) and *Bt*AQP1 (D160, gray, 1J4N). The carboxyl group of D160 from the aligned bovine structure is close (2.7 Å) to the heavy metal binding site in 4JC6.

of fluorescence in micelles, would argue for a direct binding to and activation of *So*PIP2;1.

Here, we describe the activation by mercury as a result of moving serine 274 away to leave space for leucine 197 in an open position, to promote the conformation. However, could mercury further stabilize the open conformation? As mercury is positively charged, we looked for a negatively charged residue in the vicinity. There is an aspartate in loop D, which is conserved among water-specific AQPs from both plants and animals. This residue approaches the binding site in the open conformation (**Figure 9B**), but the distance is still too far. Comparison to other water-specific AQPs suggests that the aspartate could come close enough to bind mercury and thereby stabilize the D-loop in an open position. Although the aspartate corresponding to aspartate 184 in *So*PIP2;1 is well conserved not only among PIPs, there is considerable sequence variation at the position aligned to alanine 267 of SoPIP2;1 even within the PIP2 group, making it difficult discern if the proposed activation mechanism is valid for other PIPs. However, the fact that it is the back bone carbonyl of this residue that contributes to the metal binding site, and the general observation that structure is more conserved than sequence, argues that the binding site and the suggested mechanism may be relevant also for other PIP2s of terrestrial plants. It should be noted that the plant plasma membrane has a different lipid composition and is much more complex than the liposomes of *E. coli* lipids used here. Hence, the relevance of the demonstrated mercury activation remains to be shown in a physiological context where indirect effects by mercury via interacting lipids or proteins may override a direct activation.

Is There a Central Pore?

The functionality of the protein is determined by stabilization of certain conformational states and thereby dependent on the availability of certain interacting residues, not only within a monomer, but also with neighboring monomers. This has already been described for many proteins and underlines that proteins evolve based on their final oligomeric structure. This brings us back to cysteine 69, which is found to be strongly conserved among PIPs and covalently links the monomers but does not add much thermodynamic stability. Interaction studies with PIPs in maize demonstrated that expression rate and localization is also independent of disulfide bond formation (Bienert et al., 2012). Taking only our own results into account, one could suggest the prevention of water leakage through the tetrameric center, but this is inconclusive with the mutational study of maize PIPs measured in oocytes. As the utilized maize PIP2 is very similar to *So*PIP2;1, the most prominent difference between these studies is the protein environment. As several AQP structures, including *So*PIP2;1, have presented a detergent or a lipid molecule in the tetrameric center (Jiang et al., 2006; Horsefield et al., 2008; Frick et al., 2013), one could assume the presence of a lipid molecule at these sites in the native environment to avoid water or even proton leakage. In this study, the protein was heterologously expressed and extracted from the hydrophobic environment by a detergent. These detergent molecules are capable of removing most or all of the lipid molecules bound to the protein. Additionally, the protein–lipid mixture was thoroughly dialyzed to reconstitute this protein in liposomes, potentially removing all detergent molecules. Thus cysteine 69 mutants could leak water through a central pore. As other AQP isoforms without this cysteine have also evolved to be proton tight, there is probably a different reason for the high degree of conservation. We therefore agree with Bienert et al. (2012) that disulfide bonds between monomers result in a higher kinetic stability and thereby stabilize the oligomeric state of the protein, which may comprise certain functions *in planta*.

CONCLUSION

In agreement with studies on maize PIPs we show that disulfide bridges stabilize the oligomeric state of SoPIP2;1, but contrary to results on maize PIPs we find that mutations preventing the disulfide bridge increase the permeability. Furthermore, the permeability of both WT and mutant protein can be enhanced by mercury and based on quenching of the intrinsic tryptophan fluorescence by mercury we speculate on a binding site, possibly responsible for both effects of this heavy metal. Mercury has been regarded as general inhibitor for AQPs and therefore used to classify observed *in vivo* phenomena as being "AQP dependent." The sole possibility that some AQPs under certain circumstances can be activated by mercury puts these conclusions into a new perspective. Mercury is not a physiological relevant ligand to regulate protein function, but presents a tool to study functional properties of the gating mechanism of PIPs and thereby potentially revealing new opportunities to modulate water homeostasis in plants.

MATERIALS AND METHODS

Overexpression and Purification of Cysteine Mutants of *So*PIP2;1

Cysteine mutants of *So*PIP2;1 were generated by using Quickchange site directed mutagenesis kit (Stratagene), using the plasmid pPICZB-*So*PIP2;1 (WT) with C-terminal His-tag as a template (Karlsson et al., 2003). Mutations were confirmed by DNA sequencing (Eurofins MWG operon). Mutants were overexpressed in methylotropic yeast *Pichia pastoris* as previously described (Karlsson et al., 2003) for WT *So*PIP2;1 purification. Similar procedure was followed for membrane preparation and purification of mutated proteins as described previously (Karlsson et al., 2003) with a minor change; the detergent used in the present study is *n*-Octyl-β-D-Glucopyranoside (OG; Affymetrix, O311).

Electrophoresis

The purified *So*PIP2;1 (WT) was incubated at room temperature for varying time periods, with different concentration of dithiothreitol (DTT) or β-mercaptoethanol to reduce the dimeric form into monomers. After incubation with reducing agent the sample loading buffer (125 mM Tris-HCl, pH 6.8, 20% glycerol, 4% SDS) was mixed with protein sample and further

incubated for 10 min at room temperature. To monitored the effect of reducing agent concentration and incubation time, the oligomeric forms of the protein were resolved by SDS-PAGE (12%) and visualized by staining with coomassie brilliant blue R250 (Laemmli, 1970).

In order to compare the SDS-PAGE profile of the WT and mutant proteins (**Figure 3**), the protein was directly mixed with sample loading buffer (as mentioned above) supplemented with 10% β-mercaptoethanol and incubated for 10 min at room temperature, before resolving on SDS-PAGE (12%).

Circular Dichroism (CD) Spectroscopy

Far-UV CD spectra were measured for the WT *So*PIP2;1 and the mutants using a Jasco J-720 spectrometer (Jasco, Tokyo, Japan). Spectra were recorded at 25–95°C (with 5°C interval) between 250 nm and 190 nm at 20 nm/min as an average of three scans with a response time 8 s and a data pitch of 0.1 nm. Baselines were collected in the same manner on the buffer solution, and spectra were baseline corrected (Galka et al., 2008; Plasencia et al., 2011).

Mean residue ellipticity (MRE, $[\theta]_M \times 10^{-3}$ deg cm^2 dmol^{-1}) was calculated by using Eq. (1).

$$[\theta]_M = M \times \theta/(10 \times l \times c \times n) \quad (1)$$

where M is the molecular weight of protein (e.g., 32512 g/mol), θ is the measured ellipticity in millidegrees, l is the cell path length, c is the concentration in [g/l], and n is the number of residues (303).

The MRE at 222 nm was plotted over temperature. For curve fitting, following Boltzmann sigmoidal equation was used:

$$Y_{obs} = Y_{native} - \frac{Y_{denatured} - Y_{native}}{1 + e^{T_{1/2} - \frac{T}{m}}} \quad (2)$$

Where Y_{obs} is the MRE, $T_{1/2}$ is the temperature at which MRE is halfway between native and denatured state, m is the slope of the curve. Data was analyzed using Prism (Graphpad software, Inc.).

Reconstitution into Liposomes

E. coli POLAR lipids (Avanti) provided in chloroform were dried with N_2 for 4 h and kept at −20°C until use. For reconstitution the lipids were solubilized with 10% OG in dialyze buffer (20 mM Tris pH 8, 100 mM NaCl, 0.003% NaN_2, 2 mM DTT) for concentration of 4 mg/mL and aliquoted. Proteins were added and solution was mixed thoroughly. Lipid–protein mix was diluted with dialyze buffer to 2 mg/mL lipids and 66 μg/mL proteins (LPR30) and dialyzed using a membrane with 6–8 kDa cut-off (Spectrum Laboratories) against dialyze buffer for 7 days at room temperature.

Water Conductivity

Liposomes were extruded 11 times with a pore size of 200 nm (Avestin) and their resulting average radius was determined by dynamic light scattering DLS (Malvern Zetasizer). Samples were diluted with dialyze buffer (with or without mercury) to 0.2 mg/mL lipids. To show that activation of the protein is reversible, a sample incubated for 30 min with 1 mM $HgCl_2$, 2 mM β-mercaptoethanol was added and incubated at least 30 min further prior to the activity assay. Water transport activity was measured by stopped-flow with a hyper-osmolar gradient of 100 mM sorbitol using Hi-Tech stopped-flow device at a volume of 150 μL per shot. Rise in scattering upon shape change due to water transport out of the vesicles was observed at 90° angle at a wavelength of 500 nm. Unless mentioned otherwise, single exponential functions were fitted to 10 to 17 individual curves by the software Kinetic Studio (TgK Scientific Limited 2010). Total water permeability P_f is used to calculate individual p_f-values by multiplying relative P_f [P_f (proteoliposome) – P_f (control liposomes)] with the surface area of the liposome and dividing with the number of monomers per vesicle.

$$P_f = k \cdot \frac{V_0}{A \cdot V_w \cdot c_{out}} \quad (3)$$

$$p_f = \frac{(P_f - P_{f,\ control}) \cdot A}{\#monomers} \quad (4)$$

Protein concentration was analyzed by Western-blot using tetra-His antibody, and vesicle concentration was calculated assuming no lipid loss during dialysis and an area of 0.52 nm^2 per lipid molecule (for a monolayer). To construct a dose response curve of mercury activation, single exponential rates from 10 to 16 stopped-flow measurements were averaged per samples exposed to different mercury concentration; each average is presented with their standard deviations. Curve fitting was done employing a Hill-function.

Statistical Analyses

The significance was analyzed in Prism (Graphpad software, Inc.), using the unpaired *t*-test with Welch's correction and two-tailed *P*-values.

Tryptophan Fluorescence

Fluorescence was measured with His-tag purified and desalted protein in Buffer A supported by 0.8% OG. Monochromatic light at a wavelength of 280 nm was used for excitation while scans were done from 300 to 380 nm at a speed of 100 nm/min and a data pitch of 0.5 nm. Fifteen scans were accumulated to reduce noise. For kinetic experiments, mercury chloride to a final concentration of 200 μM was added and briefly mixed before starting scans. First, single records were done with a delay of 1 s, resulting in one plot every 49 s. The averages of five data points were used to determine height of the curve maximum. After incubating for 25 min, another accumulated spectrum was recorded. Sequentially, β-mercaptoethanol to a final concentration of 1 mM was added to reverse the binding, followed by the same measurement procedure as before.

For dose-response experiments, the sample was pre-incubated with mercury chloride at room temperature for 15 min before

recording the fluorescence between 310 and 400 nm. Three scans were accumulated to reduce the noise and the measurement was repeated tree times. The emission data at 335 nm were fitted with four parameters to sigmoidal dose response equation using Prism version 6.00 (GraphPad Software, La Jolla, CA, USA) to estimate the EC_{50} value.

AUTHOR CONTRIBUTIONS

AK and SS contributed equally to this work, did all the technical work, and analyzed the data. PK and UJ conceived the project. AK drafted the manuscript and all authors contributed to writing of the final article.

FUNDING

This work was supported by the Swedish Research Council.

ACKNOWLEDGMENT

We thank Adine Karlsson for technical assistance and Dr S. Raza Haq for help with statistical analyses.

SUPPLEMENTARY MATERIAL

The Supplementary Material for this article can be found online at: http://journal.frontiersin.org/article/10.3389/fpls.2016.01249

REFERENCES

Abascal, F., Irisarri, I., and Zardoya, R. (2014). Diversity and evolution of membrane intrinsic proteins. *Biochim. Biophys. Acta* 1840, 1468–1481. doi: 10.1016/j.bbagen.2013.12.001

Alexandersson, E., Danielson, J. A., Råde, J., Moparthi, V. K., Fontes, M., Kjellbom, P., et al. (2010). Transcriptional regulation of aquaporins in accessions of *Arabidopsis* in response to drought stress. *Plant J.* 61, 650–660. doi: 10.1111/j.1365-313X.2009.04087.x

Alexandersson, E., Fraysse, L., Sjövall-Larsen, S., Gustavsson, S., Fellert, M., Karlsson, M., et al. (2005). Whole gene family expression and drought stress regulation of aquaporins. *Plant Mol. Biol.* 59, 469–484. doi: 10.1007/s11103-005-0352-1

Bienert, G. P., Cavez, D., Besserer, A., Berny, M. C., Gilis, D., Rooman, M., et al. (2012). A conserved cysteine residue is involved in disulfide bond formation between plant plasma membrane aquaporin monomers. *Biochem. J.* 445, 101–111. doi: 10.1042/bj20111704

Clarke, J., and Fersht, A. R. (1993). Engineered disulfide bonds as probes of the folding pathway of barnase: increasing the stability of proteins against the rate of denaturation. *Biochemistry* 32, 4322–4329. doi: 10.1021/bi00067a022

Danielson, J. A. H., and Johanson, U. (2010). "Phylogeny of Major Intrinsic Proteins," in *Mips and Their Role in the Exchange of Metalloids*, eds T. P. Jahn and G. P. Bienert (New York, NY: Springer), 19–32.

Frick, A., Järvå, M., Ekvall, M., Uzdavinys, P., Nyblom, M., and Törnroth-Horsefield, S. (2013). Mercury increases water permeability of a plant aquaporin through a non-cysteine-related mechanism. *Biochem. J.* 454, 491–499. doi: 10.1042/BJ20130377

Fu, D., Libson, A., Miercke, L. J., Weitzman, C., Nollert, P., Krucinski, J., et al. (2000). Structure of a glycerol-conducting channel and the basis for its selectivity. *Science* 290, 481–486. doi: 10.1126/science.290.5491.481

Galka, J. J., Baturin, S. J., Manley, D. M., Kehler, A. J., and O'neil, J. D. (2008). Stability of the glycerol facilitator in detergent solutions. *Biochemistry* 47, 3513–3524. doi: 10.1021/bi7021409

Horsefield, R., Nordén, K., Fellert, M., Backmark, A., Törnroth-Horsefield, S., Terwisscha van Scheltinga, A. C., et al. (2008). High-resolution x-ray structure of human aquaporin 5. *Proc. Natl. Acad. Sci. U.S.A.* 105, 13327–13332. doi: 10.1073/pnas.0801466105

Hukin, D., Doering-Saad, C., Thomas, C. R., and Pritchard, J. (2002). Sensitivity of cell hydraulic conductivity to mercury is coincident with symplasmic isolation and expression of plasmalemma aquaporin genes in growing maize roots. *Planta* 215, 1047–1056. doi: 10.1007/s00425-002-0841-2

Jiang, J., Daniels, B. V., and Fu, D. (2006). Crystal structure of AqpZ tetramer reveals two distinct Arg-189 conformations associated with water permeation through the narrowest constriction of the water-conducting channel. *J. Biol. Chem.* 281, 454–460. doi: 10.1074/jbc.M508926200

Johanson, U., Karlsson, M., Johansson, I., Gustavsson, S., Sjövall, S., Fraysse, L., et al. (2001). The complete set of genes encoding major intrinsic proteins in *Arabidopsis* provides a framework for a new nomenclature for major intrinsic proteins in plants. *Plant Physiol.* 126, 1358–1369. doi: 10.1104/pp.126.4.1358

Johansson, I., Karlsson, M., Shukla, V. K., Chrispeels, M. J., Larsson, C., and Kjellbom, P. (1998). Water transport activity of the plasma membrane aquaporin PM28A is regulated by phosphorylation. *Plant Cell* 10, 451–459. doi: 10.1105/tpc.10.3.451

Johansson, I., Larsson, C., Ek, B., and Kjellbom, P. (1996). The major integral proteins of spinach leaf plasma membranes are putative aquaporins and are phosphorylated in response to Ca^{2+} and apoplastic water potential. *Plant Cell* 8, 1181–1191. doi: 10.1105/tpc.8.7.1181

Karlsson, M., Fotiadis, D., Sjövall, S., Johansson, I., Hedfalk, K., Engel, A., et al. (2003). Reconstitution of water channel function of an aquaporin overexpressed and purified from *Pichia pastoris*. *FEBS Lett.* 537, 68–72. doi: 10.1016/S0014-5793(03)00082-6

Kirscht, A., Kaptan, S. S., Bienert, G. P., Chaumont, F., Nissen, P., de Groot, B. L., et al. (2016). Crystal structure of an ammonia-permeable aquaporin. *PLoS Biol.* 14:e1002411. doi: 10.1371/journal.pbio.1002411

Kukulski, W., Schenk, A. D., Johanson, U., Braun, T., de Groot, B. L., Fotiadis, D., et al. (2005). The 5A structure of heterologously expressed plant aquaporin SoPIP2;1. *J. Mol. Biol.* 350, 611–616. doi: 10.1016/j.jmb.2005.05.001

Laemmli, U. K. (1970). Cleavage of structural proteins during the assembly of the head of bacteriophage T4. *Nature* 227, 680–685. doi: 10.1038/227680a0

Lakowicz, J. R. (ed.) (2006). *Principles of Fluorescence Spectroscopy*. Berlin: Springer.

Nyblom, M. (2008). *Water Transport Regulation: Biochemical and Structural Analyses of Eukaryotic Aquaporins*. Ph.D. thesis, Chalmers University of Technology, Gothenburg.

Nyblom, M., Frick, A., Wang, Y., Ekvall, M., Hallgren, K., Hedfalk, K., et al. (2009). Structural and functional analysis of SoPIP2;1 mutants adds insight into plant aquaporin gating. *J. Mol. Biol.* 387, 653–668. doi: 10.1016/j.jmb.2009.01.065

Plasencia, I., Survery, S., Ibragimova, S., Hansen, J. S., Kjellbom, P., Helix-Nielsen, C., et al. (2011). Structure and stability of the spinach aquaporin SoPIP2;1 in detergent micelles and lipid membranes. *PLoS ONE* 6:e14674. doi: 10.1371/journal.pone.0014674

Preston, G. M., Jung, J. S., Guggino, W. B., and Agre, P. (1993). The mercury-sensitive residue at cysteine 189 in the CHIP28 water channel. *J. Biol. Chem.* 268, 17–20.

Shen, C., Menon, R., Das, D., Bansal, N., Nahar, N., Guduru, N., et al. (2008). The protein fluorescence and structural toolkit: database and programs for the analysis of protein fluorescence and structural data. *Proteins* 71, 1744–1754. doi: 10.1002/prot.21857

Sui, H., Han, B. G., Lee, J. K., Walian, P., and Jap, B. K. (2001). Structural basis of water-specific transport through the AQP1 water channel. *Nature* 414, 872–878. doi: 10.1038/414872a

Törnroth-Horsefield, S., Wang, Y., Hedfalk, K., Johanson, U., Karlsson, M., Tajkhorshid, E., et al. (2006). Structural mechanism of plant aquaporin gating. *Nature* 439, 688–694. doi: 10.1038/nature04316

Yang, B., and Verkman, A. S. (1997). Water and glycerol permeabilities of aquaporins 1-5 and MIP determined quantitatively by expression of epitope-tagged constructs in *Xenopus* oocytes. *J. Biol. Chem.* 272, 16140–16146. doi: 10.1074/jbc.272.26.16140

Conflict of Interest Statement: The authors declare that the research was conducted in the absence of any commercial or financial relationships that could be construed as a potential conflict of interest.

frontiers

Supplementary Material

Increased Permeability of the Aquaporin *So*PIP2;1 by Mercury and Mutations in Loop A

Andreas Kirscht†, Sabeen Survery†, Per Kjellbom and Urban Johanson *

† Shared first authors

*** Correspondence:** Urban.Johanson@biochemistry.lu.se

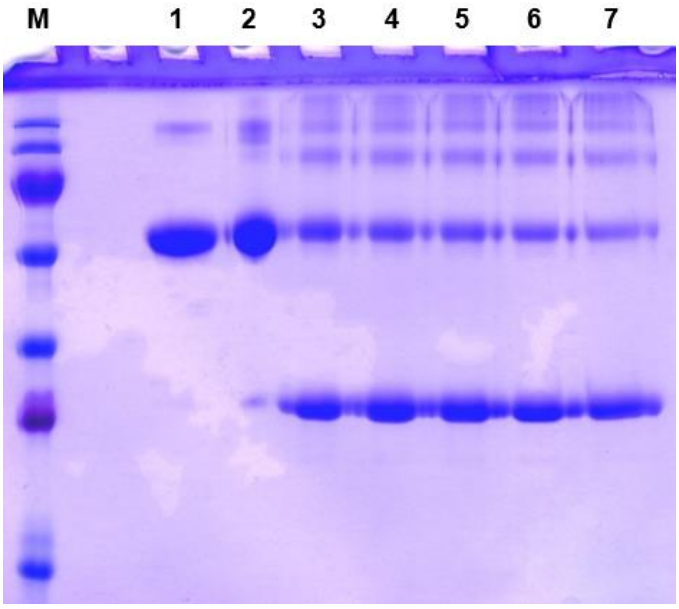

Supplementary Figure 1. Reduction *So*PIP2;1 by DTT with 8 M urea. Coomassie-stained SDS-PAGE gel with 8 M urea showing samples in PBS and 1% OG diluted 20-fold in buffer, water and varying concentrations of DTT with 8 M urea. All samples were incubated at room temperature for one hour. The dimeric band is weaker relative the monomeric band, but is not completely abolished even at 300 mM DTT and 8 M urea. 1 = SoPIP2;1 dissolved in PBS (1% OG), 2 = SoPIP2;1 dissolved in water, 3 = 100 mM DTT and 8M urea, 4 = 150 mM DTT and 8M urea, 5 = 200 mM DTT and 8M urea, 6 = 250 mM DTT and 8M urea, 7 = 300 mM DTT and 8M urea. Equal amounts of protein were loaded in all lanes. M = molecular weight marker (from top 250, 130, 100 and 70 not separated, 55, 35, 25, 15 and 10 kDa).

Supplementary Table 1. Single exponential rates for traces presented in Figure 4A used to calculate p_f values presented in Figure 4B.

Sample	Average rate (s^{-1})	Standard error of the mean (s^{-1})	p_f (10^{-14} cm^3 s^{-1})	Standard deviation (10^{-14} cm^3 s^{-1})
Empty liposomes	6.47	0.02		
*So*PIP2;1	14.61	0.12	1.61	0.09
*So*PIP2;1 + $HgCl_2$	39.26	0.92	3.41	0.24
C69S	22.07	0.17	2.22	0.10
C69S + $HgCl_2$	27.93	0.37	6.02	0.69
C69A	28.30	0.26	3.64	0.23
C69A + $HgCl_2$	35.32	0.48	8.02	0.60

Supplementary Table 2. *P* values for pairwise comparisons of data presented in Fig. 4B, unpaired t-test with Welch's correction.

Sample	*So*PIP2;1	*So*PIP2;1 + $HgCl_2$	C69S	C69S + $HgCl_2$	C69A	C69A + $HgCl_2$
*So*PIP2;1		<0.0001	0.0003	0.0001	<0.0001	<0.0001
*So*PIP2;1 + $HgCl_2$			0.0007	0.0043	**0.4984**	<0.0001
C69S				0.0003	0.0001	<0.0001
C69S + $HgCl_2$					0.0075	0.0424
C69A						<0.0001
C69A + $HgCl_2$						

Supplementary Table 3. *P* values for pairwise comparisons of data presented in Fig. 6A, using unpaired t-test with Welch's correction.

Sample	Empty liposomes	Empty + $HgCl_2$	Empty + $HgCl_2$ + β-mercapto ethanol	*So*PIP2;1	*So*PIP2;1 + $HgCl_2$	*So*PIP2;1 + $HgCl_2$ + β-mercapto ethanol
Empty liposomes		<0.0001	<0.0001	<0.0001	<0.0001	<0.0001
Empty + $HgCl_2$			**0.1361**	<0.0001	<0.0001	<0.0001
Empty + $HgCl_2$ + β-mercapto ethanol				<0.0001	<0.0001	<0.0001
*So*PIP2;1					<0.0001	**>0.9999**
*So*PIP2;1 + $HgCl_2$						<0.0001

Supplementary Table 4. Numerical values for values presented in Fig. 6A

Sample	Average rate (s^{-1})	Standard deviation (s^{-1})
Empty liposomes	5.37	0.05
Empty + $HgCl_2$	7.39	0.04
Empty + $HgCl_2$ + β-mercapto ethanol	7.29	0.05
*So*PIP2;1	14.69	0.61
*So*PIP2;1 + $HgCl_2$	39.99	2.69
*So*PIP2;1 + $HgCl_2$ + β-mercapto ethanol	14.61	0.45